Experimental Investigation of Vortex Solitons Transition and New Previously Unapproachable Kelvin Equilibria

Nima Farhang Aghyari

A thesis

in

The Department

of

Mechanical, Industrial and Aerospace Engineering

Presented in Partial Fulfillment of the Requirements

For the Degree of Master of Applied Science in Mechanical Engineering

Concordia University

Montréal, Québec, Canada

April 2020

© Nima Farhang Aghyari, 2020

CONCORDIA UNIVERSITY
School of Graduate Studies

This is to certify that the thesis prepared By:

NIMA FARHANG AGHYARI

Entitled: Experimental Investigation of Vortex Solitons Transition and New Previously Unapproachable Kelvin Equilibria

and submitted in partial fulfillment of the requirements for the degree of
Master of Applied Science in Mechanical Engineering

complies with the regulations of the University and meets the accepted standards with respect to originality and quality.

Signed by the final examining committee:

Dr. Youmin Zahang . Chair

Dr. Athienitis Andreas . Examiner

Dr. Biran Vermeire . Examiner

Dr. Georgios H. Vatistas . Thesis Supervisor

Approved by: Martin D. Pugh, Chair .
Department of Mechanical and Industrial Engineering

Amir Asif, Dean
Faculty of Engineering and Computer science

Date: April 2020

Abstract

Experimental Investigation of Vortex Solitons Transition
and New Previously Unapproachable Kelvin Equilibria

Nima Farhang Aghyari

A series of exploratory tests were conducted in a cylindrical vessel with a revolving disk at the bottom to investigate the behavior of solitary waves in oil vortices. The formation, transition, stability, symmetrically or asymmetrically rotation of stationary waves were explored via post image processing through MATLAB. Fast Fourier Transformation function was applied to investigate the performance of the solitary waves in the vortex pattern.

The Spindle oil with kinematic viscosity of 22.7 cSt was used as the working fluid. The experiments were conducted in a relatively shallow liquid situation with a 10 mm initial liquid height above the rotating disk.

An abrupt disk velocity change was applied to explore the bifurcation or existence of multiple patterns under the same boundary conditions. Its influence on the formation, transition, and behavior of solitons had also been investigated. Eventually, the angular velocity range for the existence of solitons had been identified.

New Kelvin equilibrium states and also groups of the stationary waves were revealed. A demonstration of 1, 2, 3, 4, 11, 12, and 13 solitons rotating symmetrically around the pattern were also identified. Moreover, the possibility of asymmetrical rotation for solitons and the existence of multiple packets of solitary waves group is presented. The ratio between disk velocity and solitons' frequency is also calculated and compared.

The Weber number was taken to analyze the results which showed the stability of solitons' frequency and disk speed ratio at about 0.558 having a very low standard deviation.

Acknowledgment

Chiefly, I thank the almighty God for giving me the chance of living in this era and also supporting me mentally and physically with his divine energy to complete this thesis.

Accidents in life affect people's way of living, yet incidents make them evolve and think outside of the box. I cannot be grateful enough to the universe for creating one of the most prominent incidents of my life, meeting Professor Vatistas. When I decided to change my field of study from the master of engineering to the thesis-based study, applying for research had been very critical. Although Professor Vatistas had already made his mind to go for semi-retirement and would not like to agree to take new students, he accepted me under his supervision. He was deeply aware of how not depriving of an eager science enthusiast student's hopes would be; because he had faced the same situation during his studies when he was a student. My gratitude knows no bounds for the given opportunity. Perhaps no one will recognize how vital it has been for me, but I most certainly do.

I am very thankful to Dr. Hamid Ait Abderrahmane for his unconditional assistance. Though he was not officially my co-supervisor, he treated me as a brother and brought confidence in me with his unique knowledge and priceless understanding regarding MATLAB image processing codes and analytical sections. Additionally, I do appreciate Dr. Hoi Dick Ng for his associations apropos the high-speed camera.

Moreover, I am incredibly grateful to the members of my examination committee for taking their valuable time to examine and read my thesis.

There are a lot of awakened people whom I am grateful for their support; Especially Sant Baljit Singh, Mr. Parviz Shahbazi, Maulana Rumi, Attar, Hafez, and Buckethead who guided me spiritually through the obstacles I faced during this path. Without them, this thesis would not be steered in the right direction.

This achievement should not have been possible without the devotion and dedication of my friends, particularly, Kunal, Amir, Hamed, Hooman, and Sarah who showed their borderless support and continuous encouragement.

A million thanks to my beautiful parents, whom I cannot imagine what I would do without their invaluable love. I do not have the words to thank them enough. I will never forget from where I had started this journey and I owe them big time.

Finally, my very profound gratitude goes to Concordia University for providing me the unfailing supports and funds during my study.

If the tip (point) of every hair of mine [may] gain a tongue (power to speak), [yet] the gratitude due to Thee are inexpressible. – Rumi [1]

Contents

List of Figures

List of Tables

Page

List of Equations

Nomenclature

f_n	Function	
FFT	Fast Fourier Transformation	
fps	frame per second	
Fr	Frequency	$[\frac{1}{s}]$
Fs_3	Frequency of three solitons	$[\frac{1}{s}]$
g	acceleration due to gravity	$[\frac{m}{s^2}]$
L	Length	$[m]$
M	Mass	$[Kg]$
PDE	Partial Differential Equation	
R_d	Disk radius	$[m]$
T	Time	$[s]$
u	Soliton velocity	$[\frac{m}{s}]$

Greek letters

h_0	Initial height of the fluid	$[\boldsymbol{m}]$
ν	kinematic viscosity	$[\frac{m^2}{s}]$
ω_d	Disk angular velocity	$[\frac{1}{s}]$
ω_p	Pattern angular velocity	$[\frac{1}{s}]$
ω_s	Soliton angular velocity	$[\frac{1}{s}]$

$\omega_{s_{11}}$	Frequency of each soliton in a group of eleven	$[\frac{1}{s}]$
$\omega_{s_{12}}$	Frequency of each soliton in a group of twelve	$[\frac{1}{s}]$
$\omega_{s_{13}}$	Frequency of each soliton in a group of thirteen	$[\frac{1}{s}]$
ω_{s_1}	One soliton frequency	$[\frac{1}{s}]$
ω_{s_2}	Frequency of each soliton in a group of two	$[\frac{1}{s}]$
ω_{s_3}	Frequency of each soliton in a group of three	$[\frac{1}{s}]$
ρ	Density	$[\frac{Kg}{m^3}]$
σ	Surface tension	$[\frac{Kg}{s^2}]$

Dimensionless elements

Fr	Froude number	$[\frac{{\omega_d}^2 R_d}{g}]$
K	Wavenumber	$[dimensionless]$
N	Kelvin equilibrium state number	$[dimensionless]$
Re	Reynolds number	$[\frac{\nu}{h_0 R_d \omega_d}]$
We	Weber number	$[\frac{\rho(R_d\omega_d)^2 h_0}{\sigma}]$

1 Literature review

1.1 Kelvin equilibrium states

In 1880, William Thomson, also known as Lord Kelvin, postulated the presence of waves inside the core of a columnar vortex [4]. Utilizing the inviscid equations of motion, he suggested that the vortex core is disturbed by waves of various numbers [5]. In an attempt to develop his idea of vortex atoms [6] he claimed that atoms are vortices in ether (a rarefied noble fluid) and examined their stability [6]. Although the Michelson-Morley's [7] experiment, the discovery of the subatomic electron in 1897 [8] and Einstein's special relativity [9] against the presence of luminiferous ether pushed the idea to the backburner for a protracted period of time; it was the inception for further experiments in combustion, geophysics, and low-temperature physics [10, 11] that revived the interest in this subject. Also, some parts of the vortex atom theory led to the development of new branches in mathematical topology [12].

Previously, experiments were conducted to investigate the existence of Kelvin Equilibrium in a Plexiglas cylinder via a spinning disk. The disk immersed in water near the bottom was rotating with constant speed in a counter-clockwise direction [10]. Some Kelvin stationary states with polygonal cores appeared for a specific range of disk speeds [8, 13]. It was identified that initial water levels correlated with the patterns, which were in the form of Rankine's state shapes. The mentioned shapes appeared to be stable; even after they were disturbed or destroyed by the insertion of a rod into the vortex, they returned to their former shape [10]. Also, it was discovered that there were spectra of stable and transitional states in both stationary and equilibrium modes, in which a small increment of the rotational disk speed did not have a change into the next stationary state. It was observed that there were mixed state shapes. Their frequency was proportional to the disk speed. The bandwidth of both the equilibrium and mixed regions decreased with the wavenumber [8]. It was noticed that the mixed modes were time-dependent, and their interval of persistence displayed an inverse relationship with the wavenumber. Besides, it was found that there is a direct

relationship between the velocity phase and disk rotational speed [11].

Vatistas et al. [10] presented for the first time that draining a liquid from the tank, after the water level reached a certain height, a solitary wave emerged. Nevertheless, more controlled experiments with accurately quantified processes were needed. Apart from relatively low viscosity fluids, Vatistas et al. [11] conducted other experiments using fluids with intermediate and high viscosity. It was discovered that the transition regions did not materialize in intermediate viscosity oils, and the transformation from one equilibrium state to the other was taking place suddenly and unexpectedly. It was noticed that the core of a vortex in highly viscous liquids was stable, having a circular shape [11]. It was exposed that different states evolved during the ascending order in comparison to the descending. Greater initial liquid levels were found to push the associated states to higher frequencies. Notwithstanding the previous, disk speed spin-up schedules other than a quasi-static, produced different equilibrium states [8].

As indicated earlier, Vatistas et al. [8, 10] found that in low viscosity fluids (water), the wavenumbers increased in consecutive order with the increment of disk rotational speed. For relatively low viscosity fluids, there were six stable stationary states. Cores with wavenumbers more than six were not stable.

In order to have an extensive view of the fluid mechanism' during the slow transition, Vatistas et al. [11] conducted more experiments with water as the working fluid. The same apparatus as the one mentioned in the previous experiments, i.e. a fixed cylindrical container with a flat rotational disk near its bottom rotating in a counter-clockwise direction, was used to conduct the tests. The wave speeds were recorded accurately via a stroboscope. They observed the behaviors of the vortex core in a low viscosity fluid. To predict the development of core shape for the two neighboring equilibrium states, they carried out a linear stability analysis assuming a combined Rankin's forced-free vortex that yielded satisfactory results.

To generalize their observations, Vatistas et al. [13] conducted experiments with different rotating disks and initial liquid heights to capture the wave activity in nearly inviscid liquid vortices. The experimental apparatus instrumentation and procedure was the same as indicated earlier [8, 10, 11]. To make a sharp distinction between Kelvin's stationary polygons [4], they deduced the flow parameters into the dimensionless numbers by applying the Buckingham's π-theorem [14]. Consequently, they came to the conclusion that the pattern to disk frequency ratio and the interval of stationary states and mixed region dependent on the dimensionless initial height, Froude and Reynolds numbers. Accordingly, using the π-groups in their experimental measurements, showed that with higher initial heights or revolving disk sizes, had no other effect than to shift the spectra of the equilibrium states [13].

Vatistas et al. [15] continued their investigation on water vortices produced inside a stationary cylinder via the assistance of image processing instead of visually inspecting utilizing a stroboscope. They performed their experiments with different disks and also three distinct initial heights. Two marks were juxtaposed on the disk to measure the velocity of the revolving disk through image processing. In addition, they also found that the disk frequency to the pattern ratio depends on both wave and Froude numbers. It was confirmed with the increment of the wavenumber, the Froude number decreases. They identified those mentioned patterns were not sensitive to initial conditions. The stability of polygons (Kelvin's equilibria patterns) was verified when they were perturbed or even entirely ruined by applying an outer solid rod into the liquid. It was discovered that after a short period of time the patterns came into sight in their original form.

1.2 Solitary waves

In August 1834, a naval architect and Scottish engineer named John Scott Russel had one of the most extraordinary observations in the history of fluid hydrodynamics. A boat was pulled by a pair of horses in the canal of Edinburgh in Glasgow in Scotland. When stopped, he noticed a water wave created in the canal with a constant velocity. While on horseback, he chased the waterfront for a couple of miles and realized that the wave was maintaining its original shape [16]. That is how the story of solitary waves began. Russel later called this unique and marvelous phenomenon the Wave of Translation [17].

For more than half of a century after Russel's discovery, the scientific community was skeptical of such waves. Although several scientists such as Bossinesque (1871) [18] and Rayleigh (1874) [19] stated the possibilities of solitary waves, there was a feeble interest to consider solitary waves in the field of nonlinear waves [20]. The argument was sustained until 1885 when the Dutch professor Diederik Korteweg and his doctoral student Gustav de Vries came up with a mathematical formulation based on firm physical arguments for shallow inviscid fluids. They derived a partial differential equation (PDE), which now bears their names under KdV equation [16]. This equation (Such as Eq.1) admitted the existence of solitary waves that Russell had been observing and modeling. It also put an end to the mentioned dispute and controversy about solitary waves [21].

$$\left(\frac{\partial}{\partial t}u(x,t)\right) \pm 6u(x,t)\left(\frac{\partial}{\partial x}u(x,t)\right) + \left(\frac{\partial^3}{\partial x^3}u(x,t)\right) = 0 \tag{1}$$

A nonlinear wave that preserves its unity is called a solitary wave. Solitary waves possess confined amplitude and spread with constant speed. They disperse with a constant shape with either a single crest or trough. In other words, solitary waves are a particular type of localized gravity sinuosity consisting of a single elevation or depression [16].

Scott Russel discovered serendipitously this type of waves experimentally. He claimed the following characteristics for such waves after his observations in his laboratory:

- Solitary waves conserve their shapes and size.
- Both amplitude of the wave and its velocity are proportional to each other.
- They can break into smaller solitary waves.

He also identified that for some solitary waves, collisions of two or more such waves are alike to perfect elastic collisions [21]. This property led to a new comprehensive numerical study by Zabusky and Kruskal [22] in correspondence with colliding particles. They found that the remarkable quality of solitary waves with stable pulse-like could exist in a system defined by the KdV equation. To describe these elastically colliding waves that they are capable of colliding and maintain their shapes and speeds after the collision. They coined the term 'soliton' for the solitary waves that possess an elastic scattering property [16, 23]. See Figure 1. It should be noted that since the amplitude of solitary waves on water surface changes a little bit after a collision or passing through, they are identified as near-solitons. Therefore, they leave oscillatory residuals behind them [24].

Based on the solutions of the KdV equation, the non-dispersive characteristic of the solitons arises since the non-linearities, balance the effects of dispersion in the medium. Subsequently, there should be a precise degree of non-linearity for the inception of solitons in the system. As mentioned above, a limited non-dispersive solution of classical field theory notes a soliton. So, in order to have a non-dispersive solution, a nonlinear term must appear in theory to cancel the dispersion [23, 25].

As depicted in Figure 1, two solitary waves with different velocities merge and again separate conserving their original shapes and speed. This feature distinguishes a solitary wave from a soliton. Solitons will not alter after a collision with other solitons. However, solitary waves may lose energy after a collision and interact with each other inelastically [26].

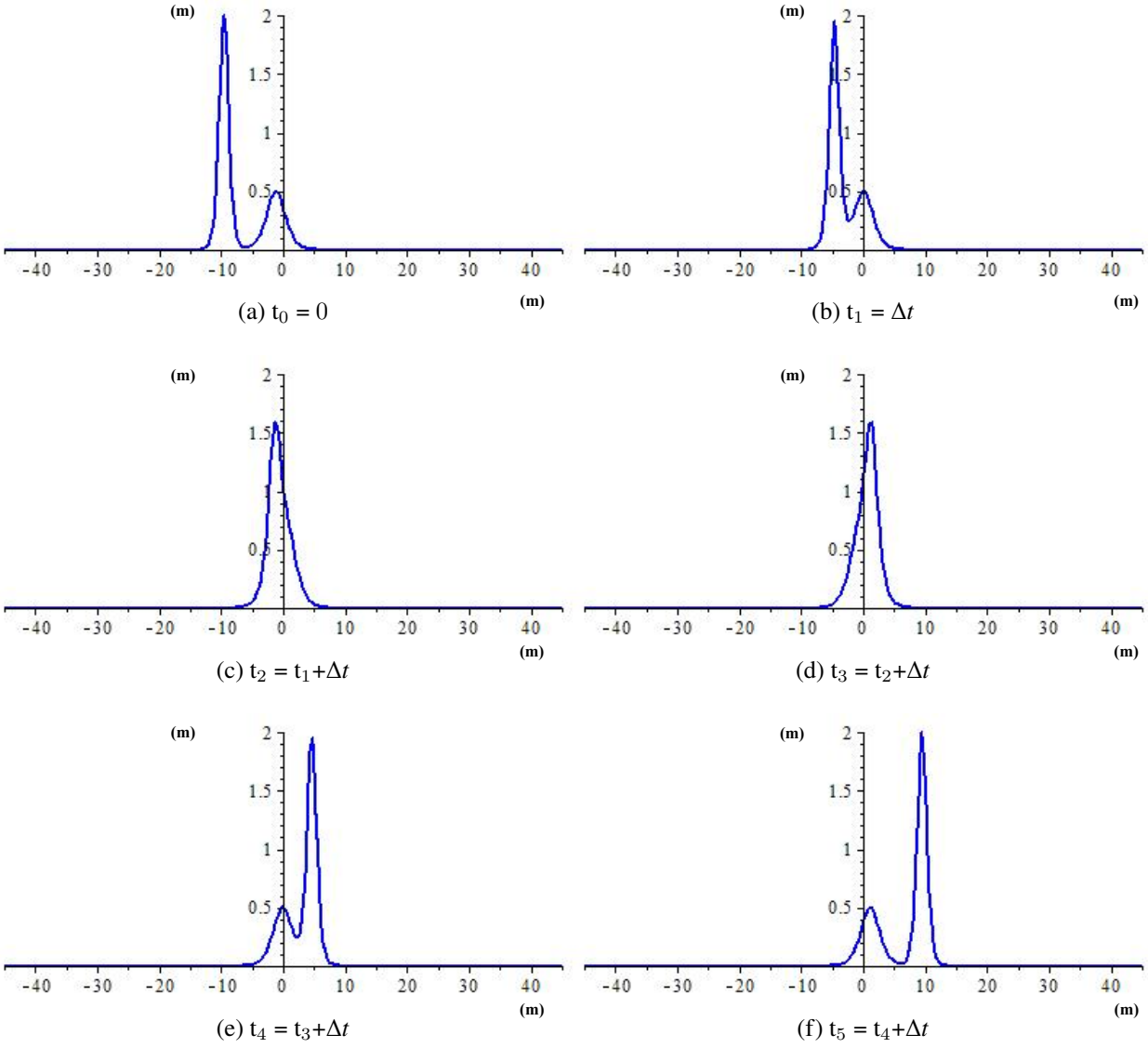

Figure 1: Collision of two simulated solitons [2]

2 Introduction

2.1 Overview of solitons

A solitary wave is a nonlinear swell that maintains its unity. Solitary waves possess confined amplitude and move with constant speed. They disperse having a constant shape of either a single crest or trough. In other words, solitary waves are a particular type of localized gravity sinuosity consisting of a single elevation or depression [16]. After collision with each other they continue their movement without an appreciable energy loss.

As mentioned before, the exact amount of non-linearity in the system may lead to the formation of solitary waves. In the previous account [3], to check the stability in the current equilibrium state, a solid rod was inserted into the vortex. It was discovered that a perturbation in the fluid may trigger the development or formation of solitons. In this study, the effect of abrupt disk velocity change has been explored and discussed instead of disturbing the fluid.

2.2 Dimensional Analysis

To obtain the relationship between the dimensionless variables and analyzing them; usually, two methods; Rayleigh's technique and Buckingham's π- theorem, are employed. In this thesis, the latter used to form the group of the dimensionless variables. In the last method i.e. the Π theorem states that if in a problem, n variables contain m primary dimensions (such as M, L, T), there will be (n-m) dimensionless groups. The preference of choosing the mentioned method is because of its simplicity [14, 27].

In past exploratory experiments of water and different oils with different viscosities, Abderrahmane et al. [28] and Soltanian [3], discovered that the dispersion velocity ratio ($\frac{\omega_p}{\omega_d}$) for water is $\frac{1}{3}$, and for spindle oil is around $\frac{1}{10}$.

Consider Kelvin equilibrium states to depend on the following variables:

$N = \{\nu, \omega_d, R_d, h_0, \rho, \sigma\}$

$[\nu] = [L^2][T^{-1}]$

$[\omega_d] = [T^{-1}]$

$[R_d] = [L]$

$[h_0] = [L]$

$[\rho] = [M][L^{-3}]$

$[\sigma] = [M][T^{-2}]$

$[N] = 1$

Therefore there are seven independent variables involving three primary dimensions. Based on Buckingham's theorem, four dimensionless numbers (7 minus 3) are required to describe the same phenomenon. It should be noted that N and $\frac{h_0}{R_d}$ are dimensionless. So $\pi_1 = N$ and $\pi_2 = \frac{h_0}{R_d}$. Thus two more dimensionless numbers are needed:

If $[\nu] = L^2T^{-1} \Rightarrow [\nu] = [h_0][R_d][\omega_d] \Rightarrow \frac{[\nu]}{[h_0][R_d][\omega_d]}=1 \Rightarrow \boxed{\pi_3 = Re}$

If $[\rho] = ML^{-3}$ and $[\sigma] = MT^{-2} \Rightarrow \frac{[\rho]}{[\sigma]} =[h_0]^{-1}[R_d]^{-2}[\omega_d]^{-2} \Rightarrow \frac{[\rho][V^*]^2[h_0]}{[\sigma]}=1 \Rightarrow \boxed{\pi_4 = We}$

$^*(V= R_d\omega_d)$

Therefore $N = f_n\{Re, We, \frac{h_0}{R_d}\}$ and if $\frac{h_0}{R_d} = cte$, then:

$$N = f_n\{Re, We\} \tag{2}$$

It is presumed that the velocity of the solitons is dependent on the following parameters:

$\omega_s = \{\nu, \omega_d, R_d, h_0, \rho, \sigma, N, g\}$, $[\omega_s] = [T^{-1}]$

Therefore, there are nine independent variables and three primary dimensions. According to Buckingham theorem, six dimensionless numbers (9 minus 3) are required to state the mentioned problem. As it was found earlier:

$\pi_1 = N$, $\pi_2 = \frac{h_0}{R_d}$, $\pi_3 = Re$, $\pi_4 = We$, and $\pi_5 = \frac{\omega_s}{\omega_d}$.

Hence there will be one more left:

If $[g] = LT^{-2} \Rightarrow [g] = [R_d][\omega_d]^2 \Rightarrow \frac{[\omega_d]^2[R_d]}{[g]} = 1 \Rightarrow [\omega_d]\sqrt{\frac{[R_d]}{[g]}} = 1 \Rightarrow \boxed{\pi_6 = Fr}$

Thus, the functional relationship will be:

$$\frac{\omega_s}{\omega_d} = f_n\{Re, We, Fr, \frac{h_0}{R_d}, N\} \tag{3}$$

Superposition of former results [3] with three different viscosity fluids (Spindle oil, H-22, H-32) and three initial heights (8mm, 10mm, and 12mm) in terms of the ratio of pattern's speed to disk's speed versus Weber number is shown in Figure 2.

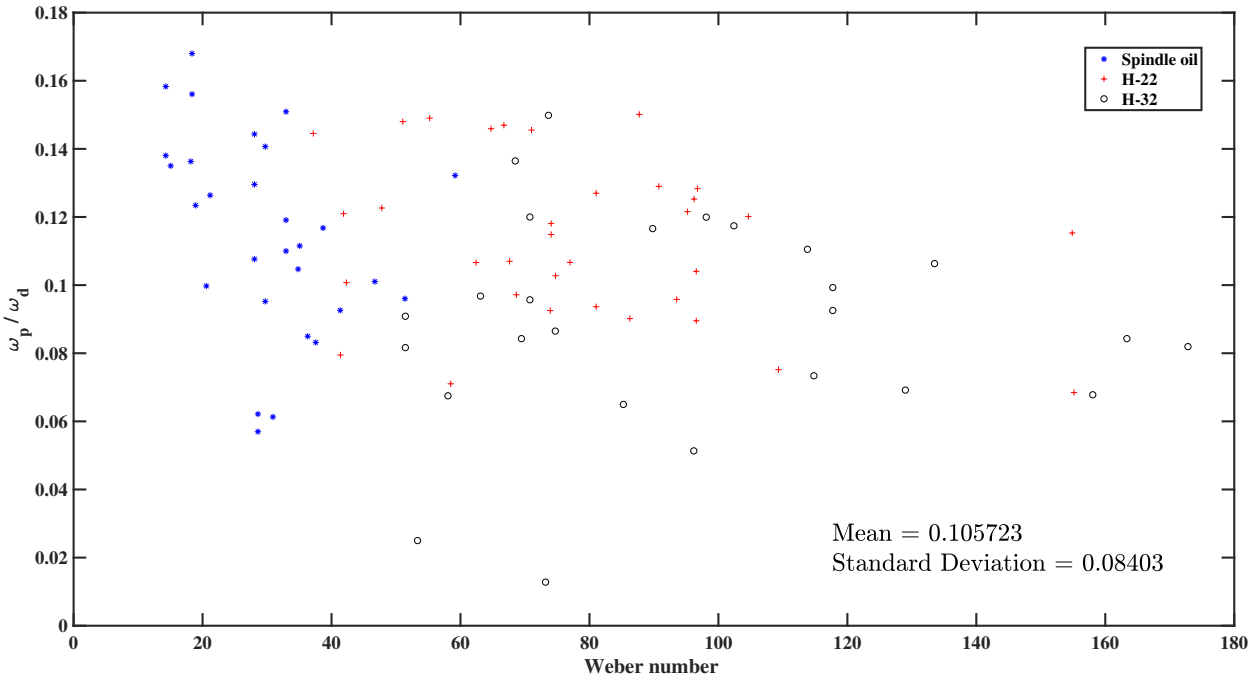

Figure 2: Superposition of ratio of pattern's speed to disk's speed versus Weber number

3 Experiment Setup

3.1 The apparatus description

As indicated earlier, the main purpose of this thesis has been an investigation on solitary waves formation, transition, and development. In order to achieve those, a set of experiments were conducted in the same Plexiglas cylindrical container with a stationary rotating disk on its bottom [3, 8, 10, 11, 13]. The spindle oil was used as a working fluid with an exact 10mm initial height above the disk's surface. The height of the fluid was measured by a ruler and also a vernier caliper. The disk which was employed had almost the same radius as the containing vessel. Thus the revolving disk was covering the mostly entire bottom of the container. ($R_{disk} = 142\ mm$, $R_{tank} = 143\ mm$)

A DC electric motor with a 0.75 Horsepower and the speed range from 0 to 1750 round per minute was employed as the liquid vortex agitator.

The cylindrical vessel was exposed to air from the top and had a small orifice on the bottom side to let the liquid drained through.

Moreover, a one-centimeter line was marked on the disk near its center to calculate the precise rotational speed via image processing which later will be argued.

The equilibria states will be written with a number and a sign after the number. The number expresses the state and the sign indicates the direction of the rotating disk. Plus sign shows that the wave is co-grade and the negative sign will indicate that it is counter-rotating or in essence, the fluid pattern is retrograde.

Spindle oil with the following specification at 23°C was utilized for the experiments:

- The density of ρ = 838.2 $\frac{Kg}{m^3}$
- The surface tension σ = 0.03 $\frac{N}{m}$ or ($\frac{Kg}{s^2}$)

- The kinematic Viscosity ν = 22.69 cSt or ($\frac{m^2}{s}$)

To obtain a series of images with high resolution and the most decent quality, the same lighting system that Soltanian employed [3], was used again. The lighting system included three circular fluorescent bulbs each with 2600 lumens output.

A pco.1200 hs digital high-speed 10bit CMOS camera system was set above the vessel container mounted on a tripod to capture the images of the fluid revolving. It consisted of a compact camera with an external intelligent power supply and the available exposure times range from $1\mu s$ (50 ns optional) to 5 s. The Camware64 software was employed to operate the camera and also to set the exposure time with the best possible resolution for the images and videos. Eventually, the camera could have captured the images up to 636 fps at full frame and 1357 at ROI VGA. Although, because of the 4 GB internal memory Ram, at most, 8432 images could be taken. In other words, the higher the frame per second, the less the capturing time duration.

The nominal specifications of the camera are:

- 636 fps at full resolution (1357 fps at VGA resolution)
- extremely fast image recording - 1 GB/s
- high resolution (1280 × 1024 pixel)
- exposure time range 50 ns - 5 s
- image memory in camera (camRAM up to 4 GB)
- inter-framing time 75 ns
- standard interfaces (IEEE 1394, camera link)

All the experiments were conducted at the Fluid Dynamics Research Laboratory in Concordia University utilizing the apparatus schematically in Figure 3.

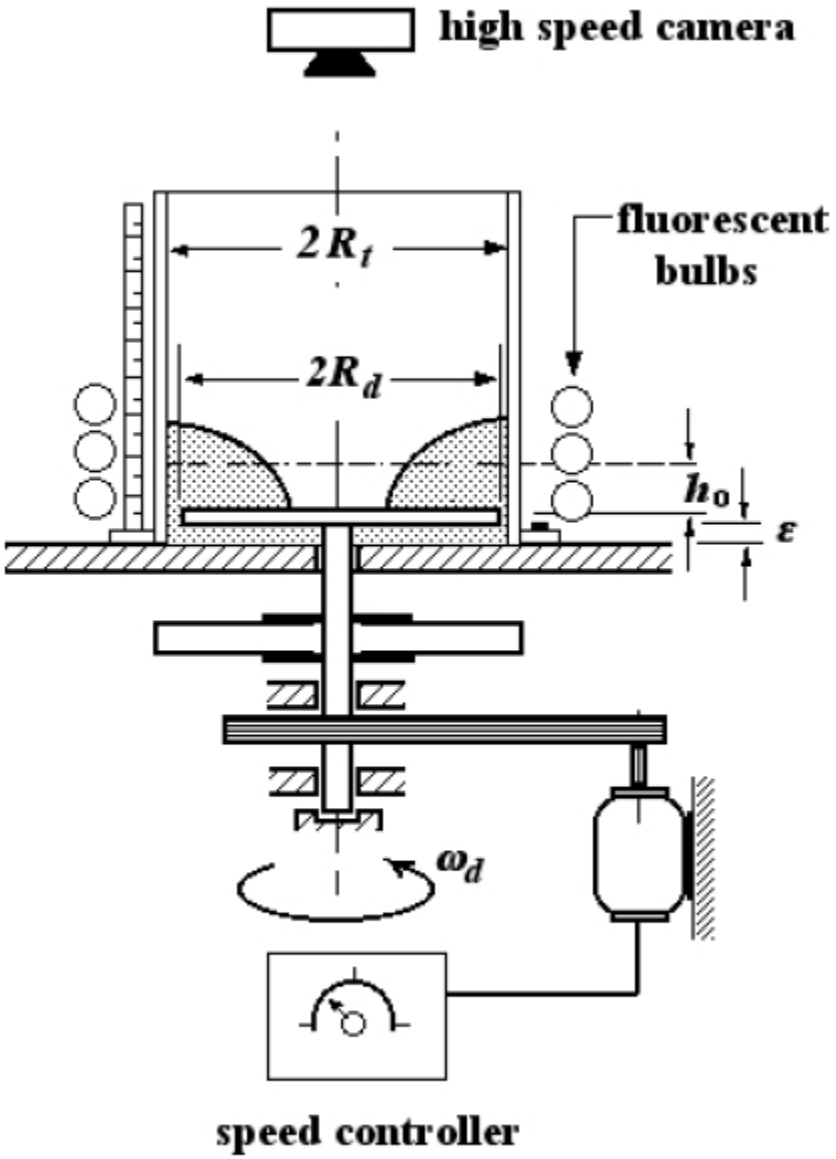

Figure 3: Diagram of the experimental apparatus with $R_d = 142mm$, $R_t = 143mm$ The disk's thickness = 9.525 and the clearance between the disk and the bottom plate (ϵ) = $28mm$. (Courtesy of Soltanian [3]

3.2 Measuring the surface tension

In previous papers, the surface tension was not considered as an essential characteristic, yet in the current thesis, the phenomena were supposed to have a connection to surface tension. Eventually, Weber number (We) is also employed. A surface tension analyzer was employed to obtain surface tension, measuring the phenomena concerning capillary rise or depression. Thus, positive or negative pressure was introduced to persuade capillary depression or rise, respectively. The apparatus consisted of a capillary glass tube and a glass cylinder with a rubber stopper and a tubulation.

At first, a small sample of spindle oil was added to the cylinder. The extended, graduated scale was 0.3 cm above the zero lines. A rubber bulb was attached to the tubulation on the cylinder for drawing or expelling air. Air was expelled into the cylinder, and the sample was pushed out of the top of the capillary three times to wet the whole capillary. After another air expelling for and removing the bulb, the fluid came to equilibrium inside the capillary tube. Then the rubber bulb was again affixed to tubulation to draw air out of the cylinder. After this step, the liquid level inside the capillary tube and cylinder was drawn down, and air bubbles were pulled out of the capillary. The rubber bulb was removed for the last time. Besides, the liquid level inside the capillary tube came to a stable state. At this step, the distance on the graduated scale between the menisci inside the capillary tube and the cylinder was recorded. The difference between the lower and upper meniscus was measured by 0.3 cm. See Figure 4.

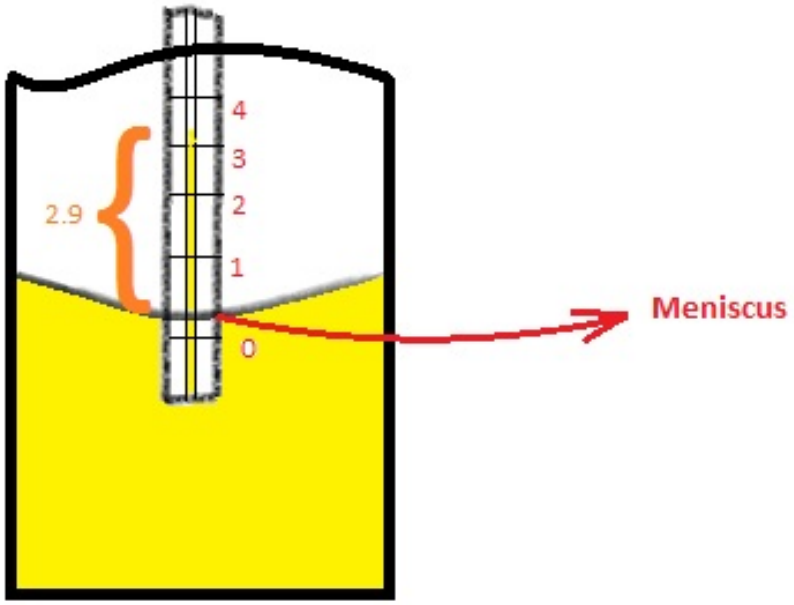

Figure 4: Surface tension analyzer apparatus

The apparatus' manual introduced the following equation to measure the surface tension:

$$\sigma = \frac{r_c \times d \times g \times h}{2} \tag{4}$$

σ = the surface tension ($\frac{dynes}{cm}$)

r_c= the radius of the capillary tube (cm), ($r_c = 0.025cm$ from the apparatus specification)

d = the density of the oil ($\frac{gr}{cm^3}$)

g = the acceleration due to gravity ($\frac{cm}{s^2}$)

h = the distance between menisci (cm)

Based on the spindle oil characteristics (Mobil 6), the density at $15°C$ was available. Nevertheless, the working temperature was $23°C$. Thus, to find the precise surface tension, some calculations are applied. The density at the laboratory temperature is calculated by acquiring the formulas from 'Russia's GOST R 8.610-2004':

$$\rho_{15}\rho_{TP} = \rho_{15}K_T K_P \tag{5}$$

T = Temperature ($°C$) , P = Pressure (MPa)

ρ_{15} = Density of oil at $15°C$ ($\frac{kg}{m^3}$)

ρ_{TP} = Density of oil at target pressure and temperature ($\frac{kg}{m^3}$)

$K_T = e^{-\alpha_{15}(T-15)(1+0.8\alpha_{15}(T-15))}$ = Temperature correction coefficient

$K_P = \frac{1}{(1-10^{-3}\gamma_T P)}$ = Over-pressure correction coefficient

$\alpha_{15} = \frac{K_0+K_1\rho_{15}}{\rho_{15}^2}$ = Coefficient of volumetric expansion at $15°C$ ($°C^{-1}$)

$K_0 = 613.97226, K_1 = 0$

$\gamma_T = 10^{-3}e^{(-1.62080+0.00021592T+\frac{0.87096\times10^6}{\rho_{15}^2}+\frac{4.2092T\times10^3}{\rho_{15}^2})}$ = Compression coefficient (MPa^{-1})

The oil specification mentions the density of the fluid at $15°C = 0.844\frac{gr}{cm^3}$. So with the above calculations: $d_{23} = 0.8382\frac{gr}{cm^3}$. With some correlation based on the latitude (45.499 m) and altitude (57m) of the conducting test, precise acceleration due to the gravity was calculated: g = $980.621\frac{cm}{s^2}$.

Thus, by putting all the variables in Eq.5, we have:

$$\sigma_{spindle\ \ oil} = \frac{0.025\times0.8382\times980.621\times2.9}{2} = 29.796 \approx \boxed{29.8\frac{dynes}{cm}}$$

The surface tension for H-22 and H-32 hydraulic oils with densities $0.856\frac{gr}{cm^3}$ and $0.866\frac{gr}{cm^3}$ respectively, is calculated by following the same procedure:

$$\boxed{\sigma_{H-22} = 30.43\frac{dynes}{cm}}\ ,\ \boxed{\sigma_{H-32} = 30.8\frac{dynes}{cm}}$$

4 Results and discussion

4.1 Image processing

The raw images of the patterns, taken by the high-speed camera, (Figure 3) were analyzed within MATLAB environment. The image was first de-noised using a low Gaussian filter, (Figure 5a). Second the filtered image was segmented or converted into binary image (Figure 5b). Third, using edge detection algorithm, the pattern's contour was extracted from the binary image (Figure 5c), (Figure 5d). Given an arbitrary point on the extracted contour, its radial displacement was followed through time (Figure 5e).

Beside, the negative and positive signs after numbers in patterns indicate the counterclockwise and clockwise rotating state respectively. (i.e., 5^- defines a retrograde pentagon.)

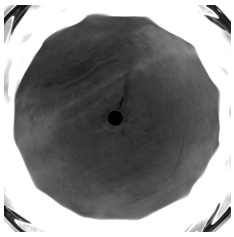

(a) 12 solitons (raw image)

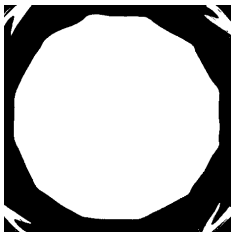

(b) 12 solitons filtered binary image

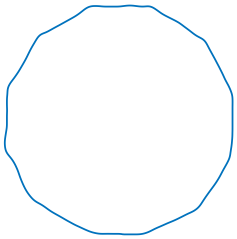

(c) 12 solitons Corresponding contour

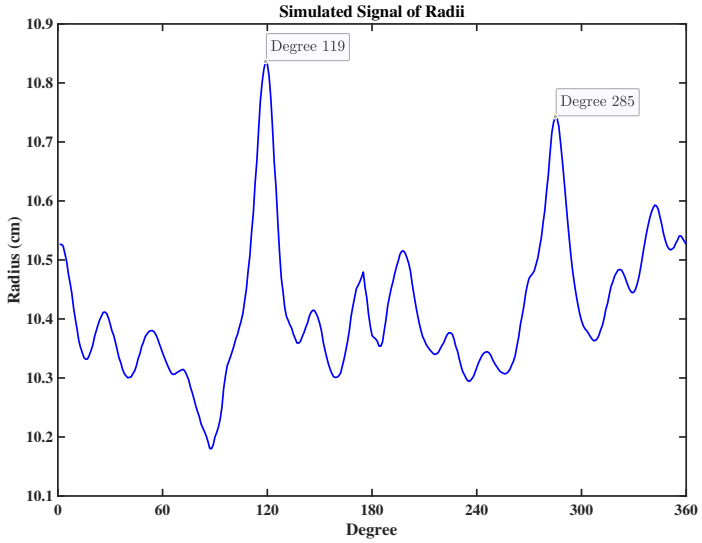

(d) A graph signal for 2 symmetric solitons

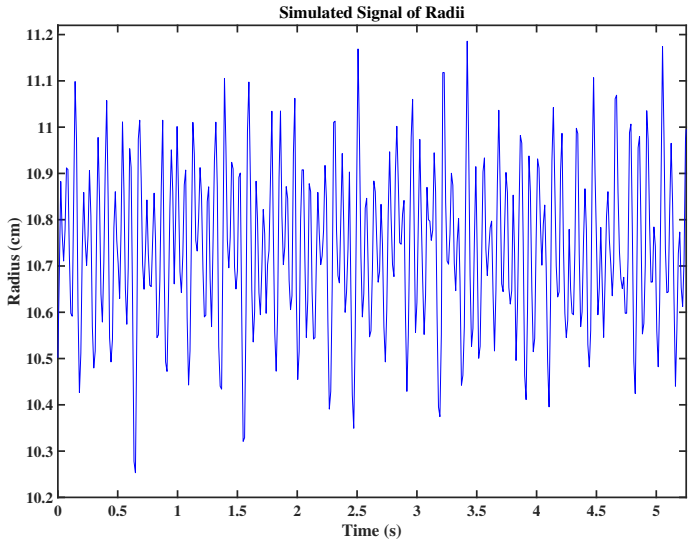

(e) Radius signals for 13 solitons

Figure 5: Image processing procedure (Experiments differ)

The time series depicting the radial displacement is analyzed using Fast Fourier Transformation function algorithm. The obtained power spectrum indicates the frequencies of the dominant modes, associated with high frequencies. The wavenumber was also estimated using the FFT function with a sampling frequency of one degree. The wavenumber (K) is the inversion of wavelength (λ), or $\frac{1}{Degree}$. Then the number of waves within the contour is ($K \times 360$). In most of the cases the dominant mode corresponds to solitary waves.

For instance, Figure 6 depicts the contour dynamics before and after the formation of solitons. Figure 6a indicates that before the formation of the two solitons the contour of the hollow ring is dominated by mode K=1. Figure 6b indicates that the formation of the two solitions is a subharmonic transition. The frequency associated with the two solitons is half of the dominate frequency of the wave dynamics preceding the formation of the two solitons [29].

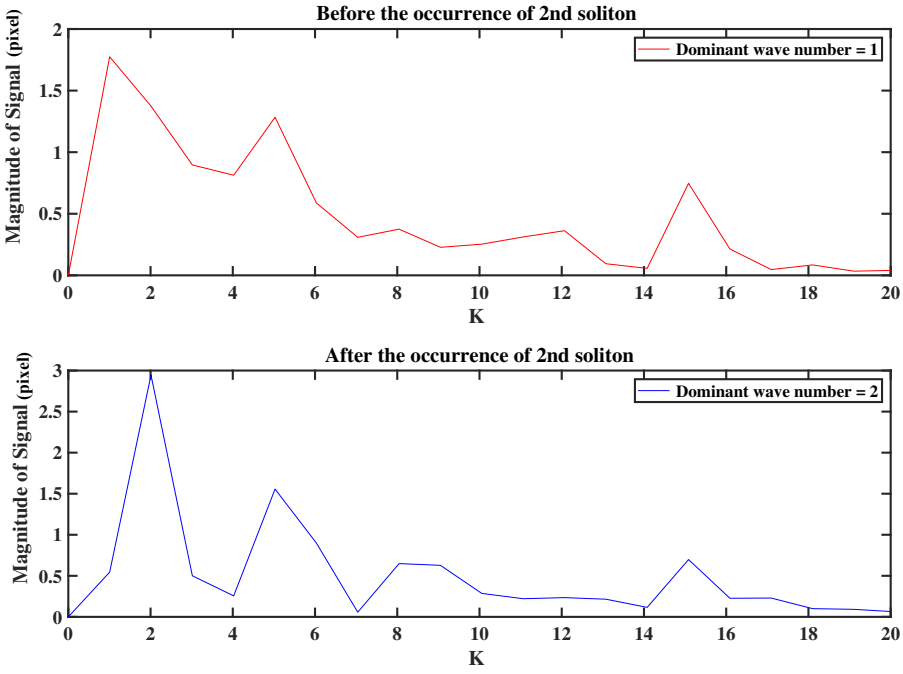

(a) Wave number plot for transition from 1 to 2 solitons

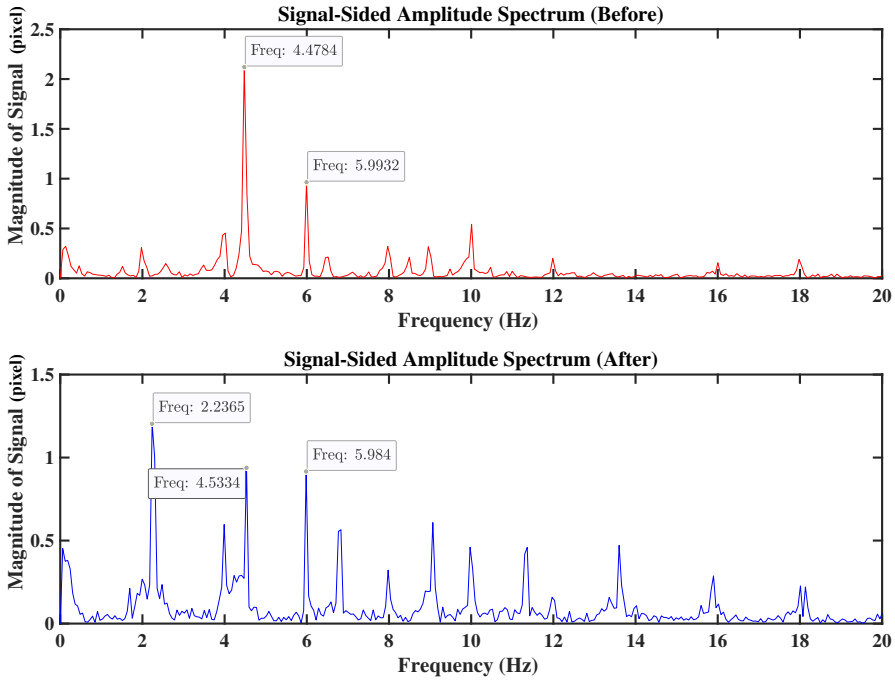

(b) Power spectrum formation of 2 solitons

Figure 6: FFT application procedure (Experiments differ)

In order to discern the dominant frequency over the harmonic signal effects in a power spectrum plot, it is necessary to distinguish the equidistant divisions. As an exemplification, a quasi-state stationary heptagon is explored in Figure 7:

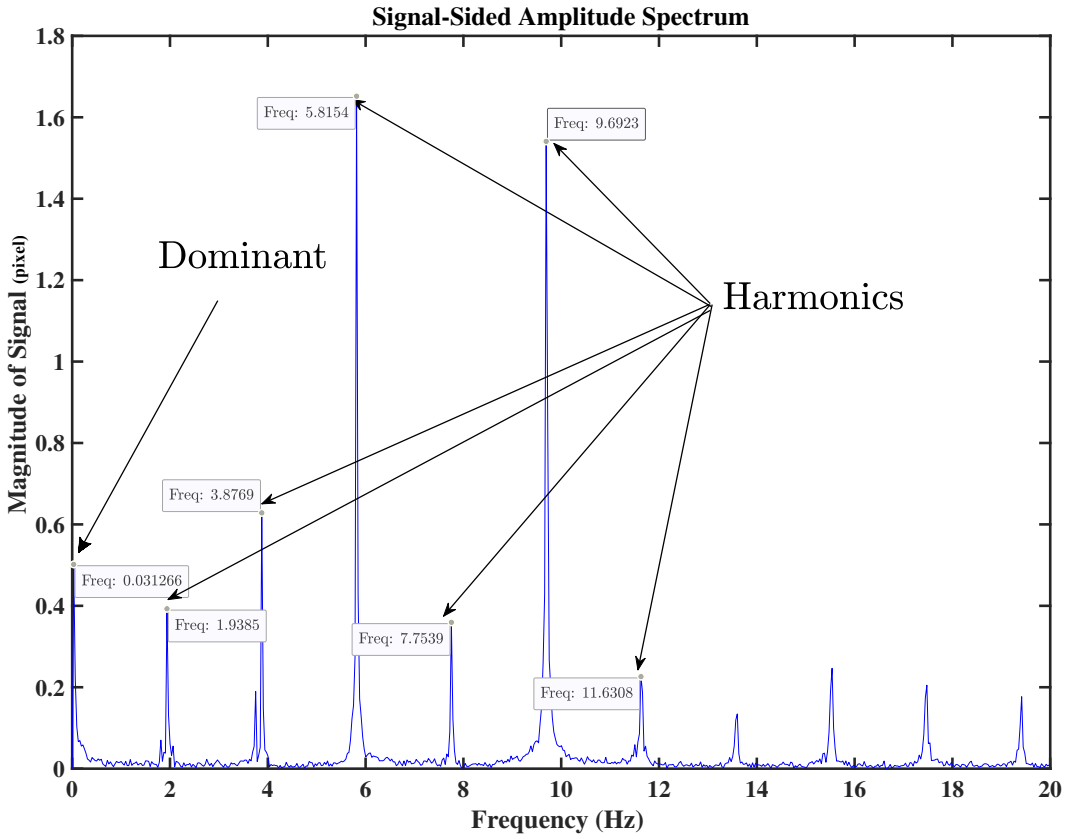

Figure 7: Power spectrum of the stationary heptagon at 117 rpm

As it appears in Figure 7, each corner of the heptagon had the frequency of :

$$\frac{0.031266}{7} = 0.0045\ Hz$$

By inverting the above frequency, the time for an edge of the pattern to undergo a complete revolution will be calculated:

$$\frac{1}{0.0045} = 222.22\ s$$

Therefore, it can be argued that due to the exceptionally long full revolution time, the pattern is stationary.

Furthermore, apart from the dominant frequency, the other peaks represent the harmonic signal effect. Because all the divisions are equidistant:

$$3.8769 - 1.9385 = 5.8154 - 3.8769 = 7.7539 - 5.8154 = 9.6923 - 7.7539 = 11.6308 - 9.6923 = 1.9385\ Hz$$

In the meantime the pattern is stationary, the dominant frequency must be zero; yet, the frequency mentioned above was considered as the dominant frequency to express the procedure of FFT application utilization.

4.2 Findings

These experiments were built on the past experiments on spindle oil as the working fluid with 10 mm initial height [3]. New tests in both ascending and descending sequences were conducted and new Kelvin equilibrium states and solitons were discovered. However, the main focus of the work has been to investigate the wave dynamics within the ring contour that precedes the formation and transition of the solitons. Hence, the evolution of the wave numbers and their corresponding power spectrum are obtained an analyzed. The results are presented in two sequences; before the formation the solition and the transitions towards the solitons. In some transitional regions, due to the complexity and existence of solitary wave states, analysis procedure is distributed in more than two segments. See Figures 29 and 32.

4.2.1 Stationary states

In past experiments, in order to verify the bifurcations at a particular equilibrium state, the fluid was perturbed by inserting a solid rod into the revolving fluid. In the case of possessing a discernible change in the structure of the existing pattern, the conclusion was made that in the same boundary conditions, multiple bifurcations or patterns exist. Yet, in this report, a sudden and instantaneous change in the angular disk speed was explored as another method of disturbance in the fluid. Past experiments on spindle oil were the guide for knowing at which disk velocities solitons appear. Refer to Tables 1 and 2. In these experiments a new quasi-steady heptagon was discovered during the ascending sequence by a precipitous disk change from 80 rpm to 117.2 rpm. See Figure 8.

Two more new quasi-states were discovered in the ascending direction namely a retrograde pentagon at 137 rpm and a hexagon at 151.5 rpm. It should be noted that those same patterns were encountered in the descending direction. This means that these two patterns were stable and did not suffer from hysteresis. The analysis related to these patterns is presented in Figures 9 and 10 respectively. It is worth noticing that these pattern were found by Soltanian [3] in the spin-down sequence.

Table 1: Equilibria spectrum for ascending sequence with $h_0 = 10mm$ (Courtesy of Soltanian)

Disk Velocity (rpm)	**Equilibrium State**	**Camera Frequency (fps)**	**Description**
47.6	Circular	543.05	Shady Circle
62.8	Circular	543.05	Smooth
77.7	2^+	54.427	Stable
86.4	3^+	543.05	Stable
99	Circular	543.05	Wobbling
117.2	Circular	54.427	Two solitary waves around the pattern
125.8	12^+ or 13^+	54.427	Stable-Breathing
154.4	7^+	54.427	Stable
154.4	7^+ or 6^+	50.02	Stable (Bifurcation existed with insertion of an external pod into the fluid.)
161.8	7^+	50.02	Non-symmetric
171.5	7^+	21.85	More Stable than before
193.9	8^+	21.85	Unstable
227.8	Circular	54.427	Chaos

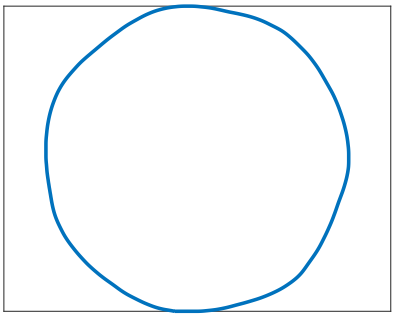

(a) Contour

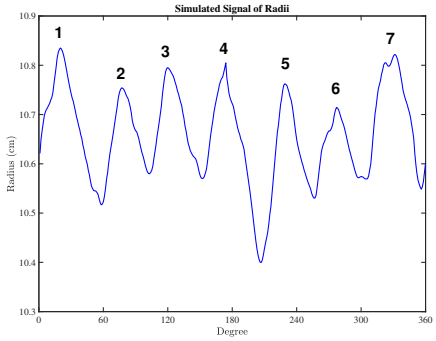

(b) Graph signal

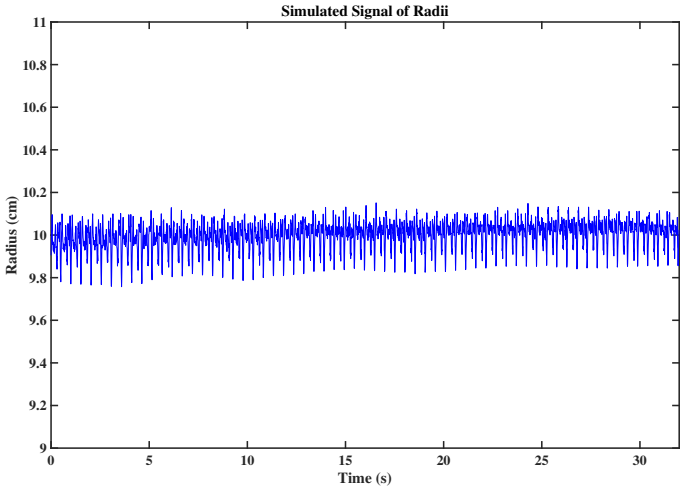

(c) Simulated signal of the radii

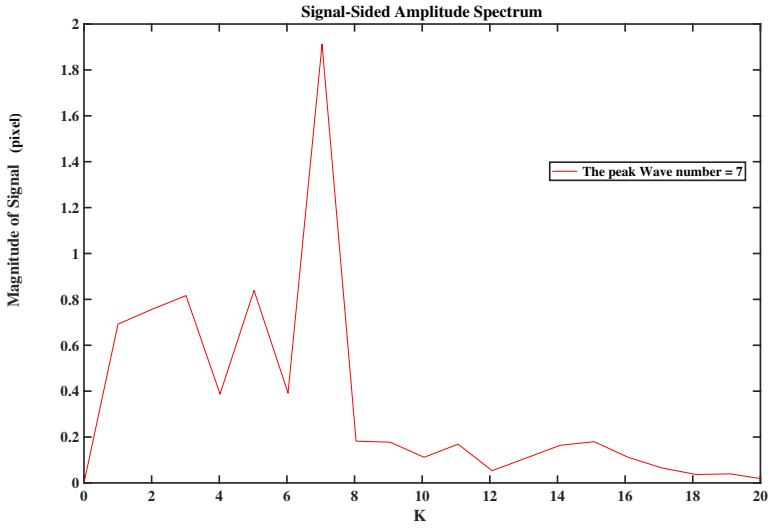

(d) Wave number plot

Figure 8: Image processing procedure for a stable stationary heptagon in ascending sequence with precipitous speed increment from 80 to 118 rpm.

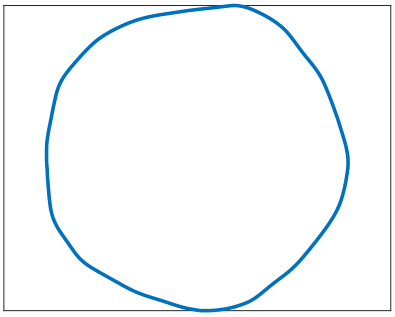

(a) Corresponding contour

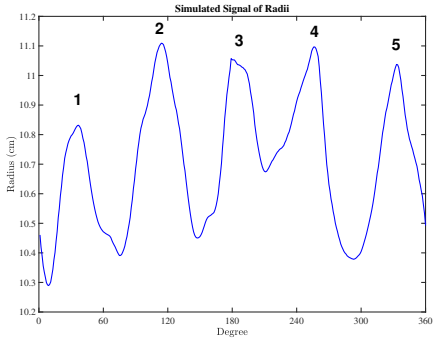

(b) Graph signal

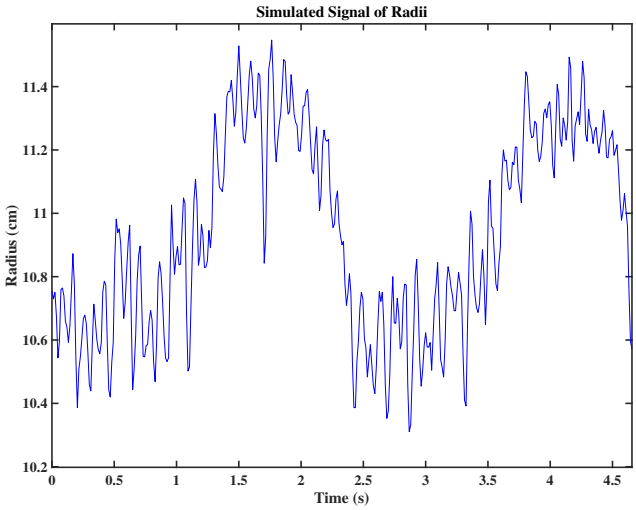

(c) Corresponding radius signals

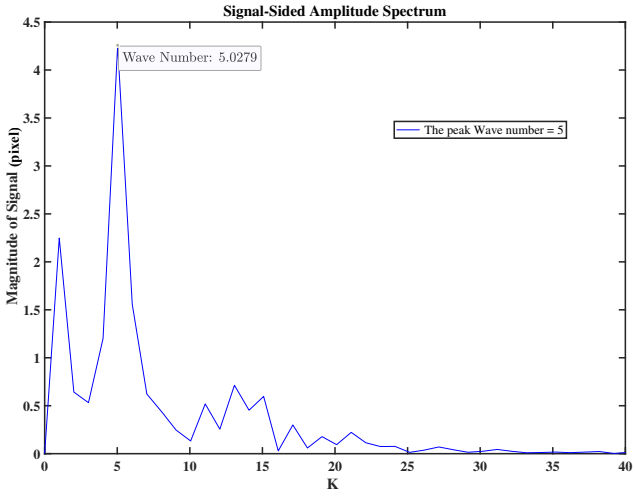

(d) Wave numbers plot

Figure 9: Signal analysis for the retrograde pentagon

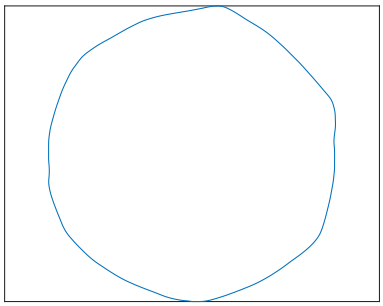

(a) corresponding contour

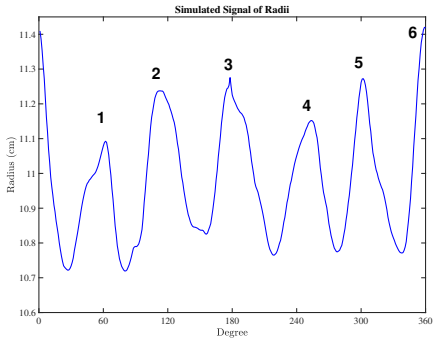

(b) Graph signal

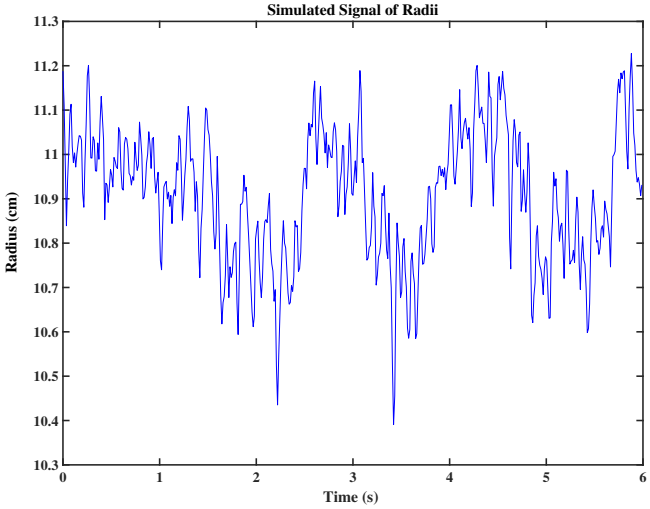

(c) Corresponding radius signals

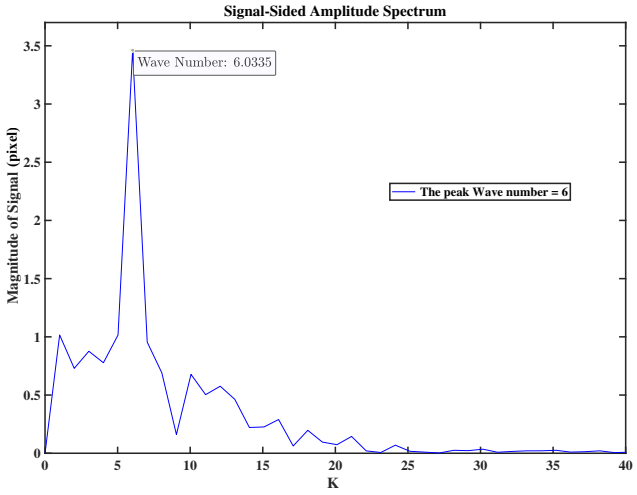

(d) Wave numbers plot

Figure 10: Signal analysis for the quasi state hexagon

4.3 Solitons investigative analysis

In the present experiment, the speeds at which the transition toward solitons occur were identified. After that the disk speed was set just below the mentioned critical speed and suddenly the disk speed was brought up to that point. At this moment the transition was recorded. To identify such critical speed, it was relied on the verified those of the previous work by Slotanian [3] in Tables 1 and 2.

4.3.1 Ascending sequence

The investigation as well as the table 1 suggests that increasing the disk rotational speed quasi-statistically to 117.2 rpm in ascending sequence, leads to the formation of two solitons. This system of two solitons appeared after the transition of a 14^{+} pattern. This transition was preceded by a wobbling of the hollow-core and the apparition of the three standing waves. These were superposed on 14^{+} pattern; See Figure 11a. In Figure 12 the results of the analysis before and after the transition is presented. Before the transition four competing waves existed. A wobbling which correspond to $k = 1$, Standing wave $k = 3$, and two other waves with the wave numbers $k = 5$, and $k = 14$. After the transition, two solitons dominate the spatial spectrum and other peaks are just harmonic of $k = 2$. The power spectrum in Figure 12b indicates a new frequency of 2.23 Hz. This corresponds to the two solitons, which means that these solitons travel at 1.11. The other frequencies 4.33 Hz and 5.98 Hz should correspond to the waves of weak amplitudes of $k = 4$ and $k = 6$ which travel almost at the same speed ($\frac{Fs}{K}$). See Figures 11 and 12

Based on Figure 11d:

Δt between two edges in 14^+ pattern before the formation of the solitons = $17.632 - 17.408 = 0.224s$

$\rightarrow$ Frequency of the pattern (14^+) = $\frac{1}{0.224} = 4.47Hz$. Which is correspondent to the frequency of the pattern in Figure 12b before the formation of the solitons.Since the pattern consists 14 edges, it should be divided by fourteen. Thus, the frequency of the each nod in ascending sequence at 117 rpm is $\frac{4.47}{14} = 0.3193Hz$

Δt between two solitons = $27.608 - 27.168 = 0.44s$

$\rightarrow$ Frequency of the solitons = $\frac{1}{0.44} = 2.27Hz$. Which is correspondent to the frequency of the solitons in Figure 12b after the formation of the solitons. Since there are two solitons rotating, it should be divided by two. Thus, the frequency of the soliton in ascending sequence at 117 rpm is $\frac{2.27}{2} = 1.1364Hz$

The disk speed frequency is $\frac{117_{rpm}}{60_s}$ = 1.95 Hz

So:

$$\boxed{\frac{\omega_{s2}}{\omega_d} = 0.583}, \boxed{\frac{\omega_p}{\omega_d} = 0.164}, \boxed{\frac{\omega_{s2}}{\omega_p} = 3.56}$$

The same procedure is followed for further experiment results to achieve the signal and solitons frequencies, and also their ratios.

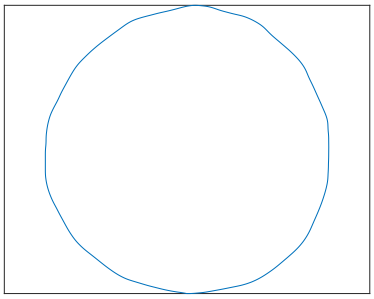

(a) Corresponding contour

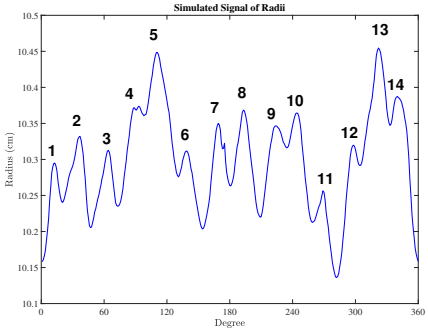

(b) Graph signal

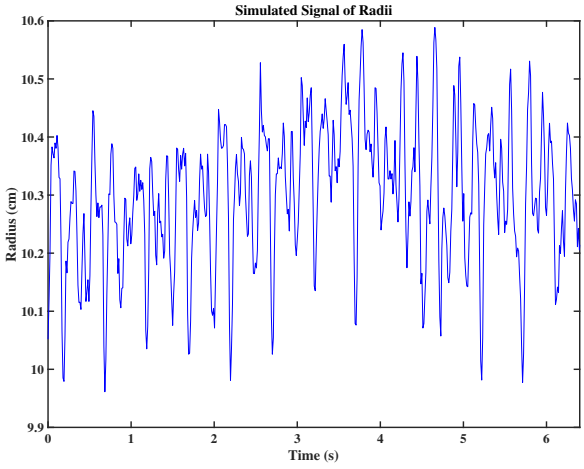

(c) Corresponding radius signals before the formation of solitons

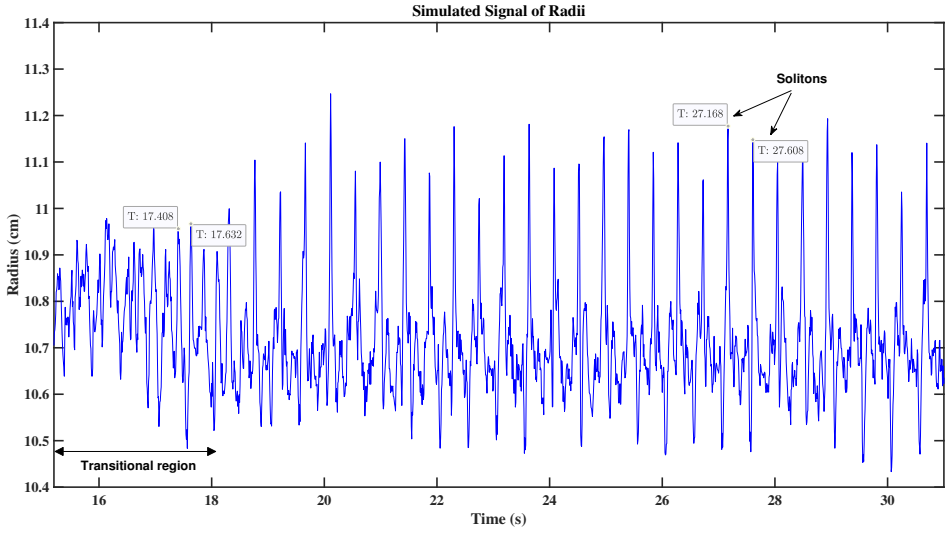

(d) Time period radius signal of solitons

Figure 11: Signal analysis for the 14^{+} equilibrium state at 117 rpm.

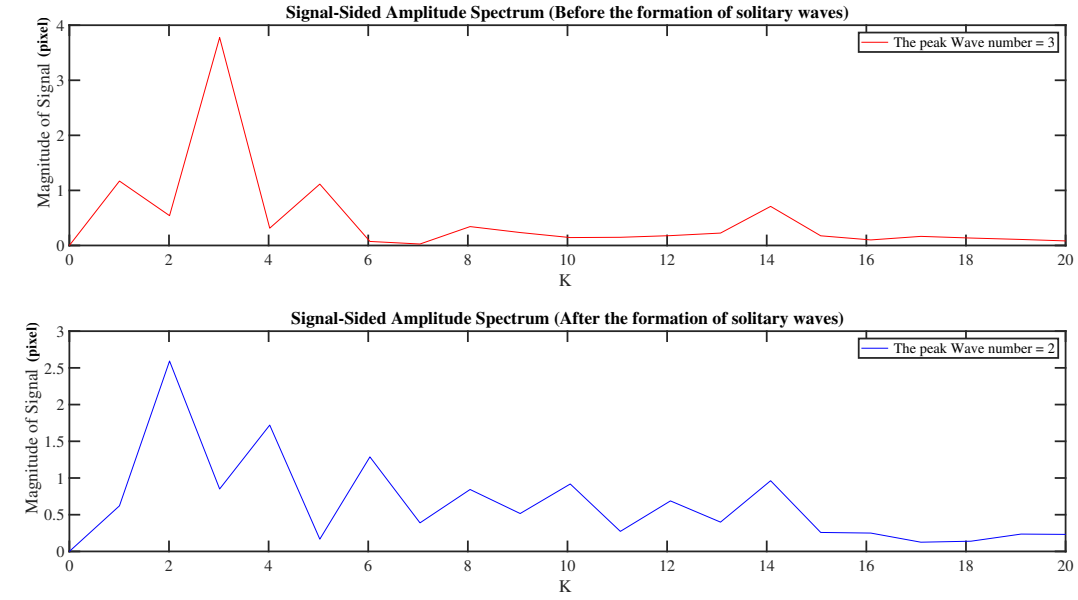

(a) Wave number plot

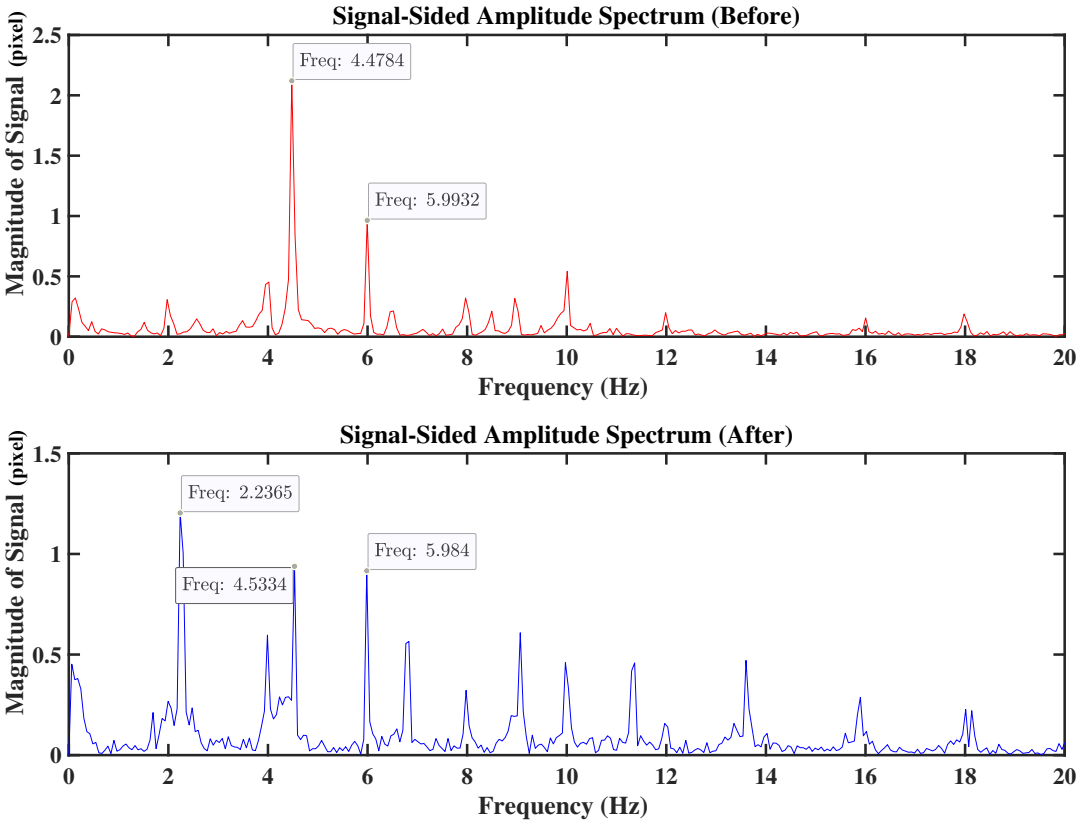

(b) Power spectrum respect to the formation of the solitons

Figure 12: The application of FFT function on 14^{+} equilibrium at 117 rpm in respect to the formation of the solitons.

Another experiment was conducted on a transition from one to two solitary waves. The disk speed was gradually augmented quasi-statically in steps of 5 rpm from rest to 119 rpm. At first, a solitary wave was rotating around the pattern, but after a few seconds, another soliton was formed and two solitons were rotating around the pattern. The Signal analysis for the mentioned experiment is shown in Figures 13 and 14.

In previous papers and experiments [3, 10, 15], symmetrically rotation around the pattern in Kelvin equilibrium states had been introduced as one of the quiddities of solitary waves groups. However, as it appears in Figure 13b and Figure 13d, the second soliton was not rotating symmetrically with another soliton. It can be either presumed that solitons can rotate around a pattern asymmetrically in a Kelvin equilibrium state, or be groups of multiple solitary waves that have their autonomy.

For the current experiment:

$\omega_d = \frac{119_{rpm}}{60_s}$= 1.983 Hz

ω_{s_1} (the frequency of the 1st soliton before the formation of the 2nd soliton) = 1.169 Hz

ω_{s_2} (the frequency of a group 2 solitons) = $\frac{2.3945}{2} = 1.197$Hz

Thus:

$$\boxed{\frac{\omega_{s_1}}{\omega_d} = 0.589}, \boxed{\frac{\omega_{s_2}}{\omega_d} = 0.6}$$

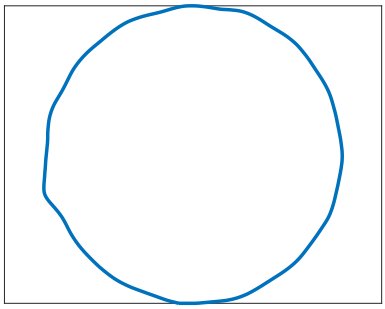

(a) Contour for 1 soliton

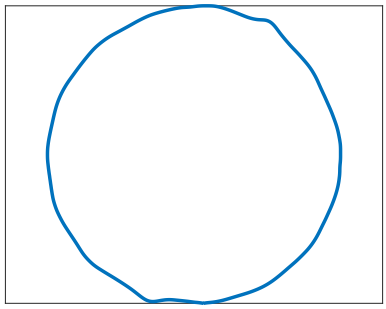

(b) Contour for 2 non-symmetric solitons

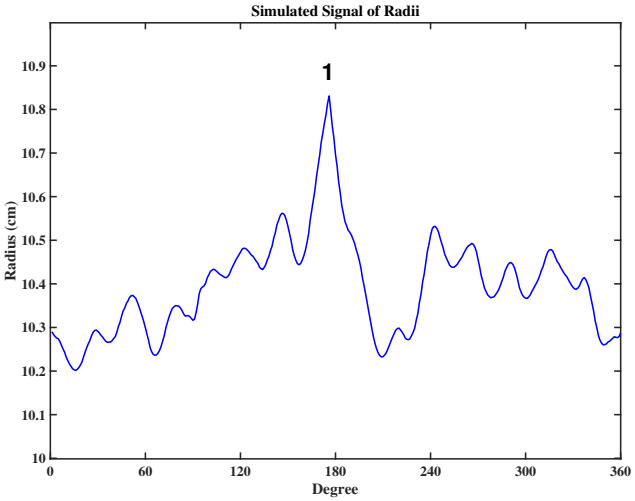

(c) Graph signal for 1 soliton

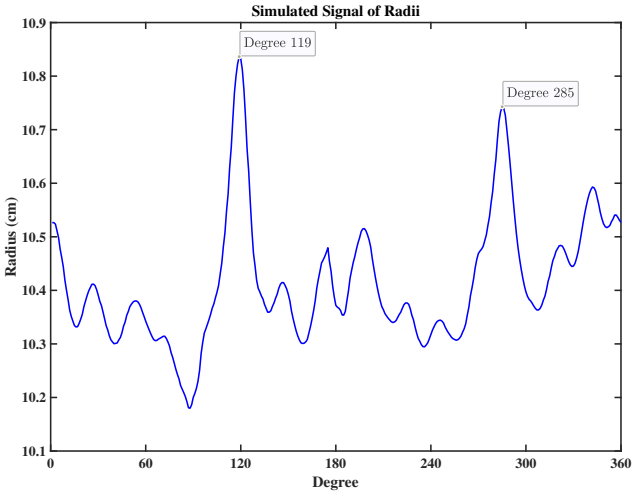

(d) Graph signal for non-symmetric 2 solitons

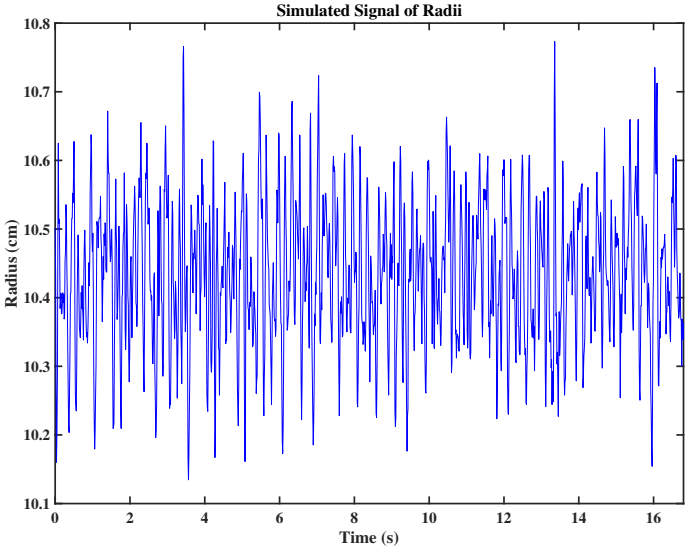

(e) Radius signals containing 1 solitary wave

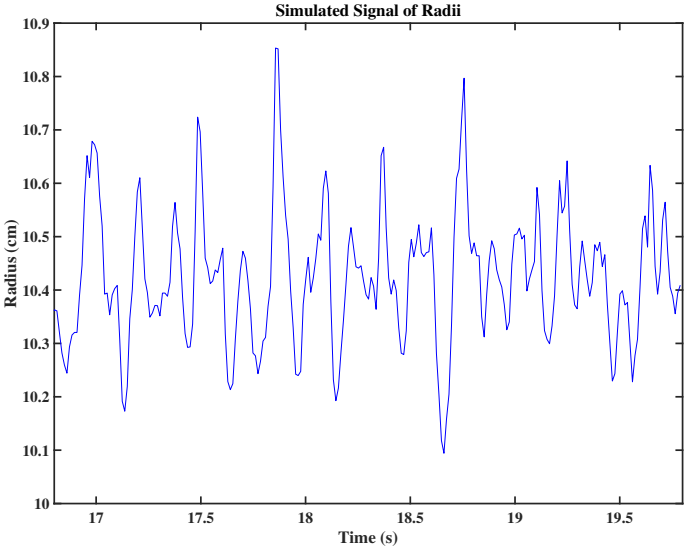

(f) After formation of the second soliton

Figure 13: Signal analysis for transition of 1 soliton to 2nd soliton.

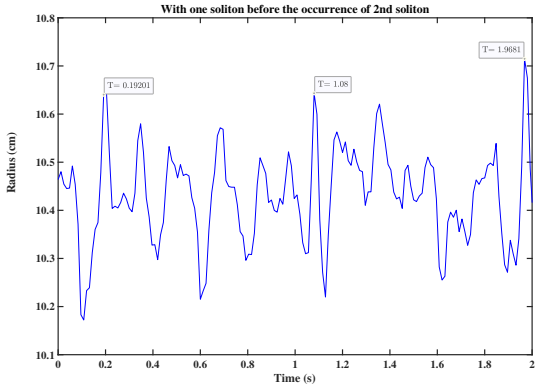

(a) Time period radius signal for one solitary wave

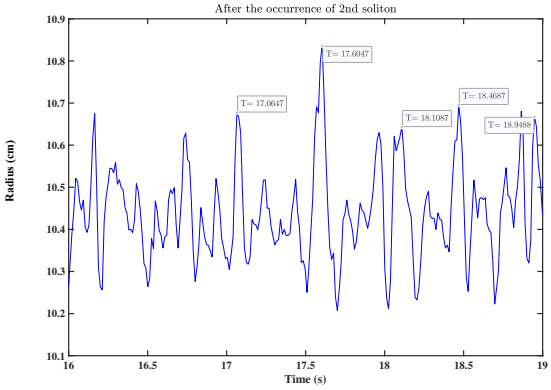

(b) Time period radius signal for two solitary wave

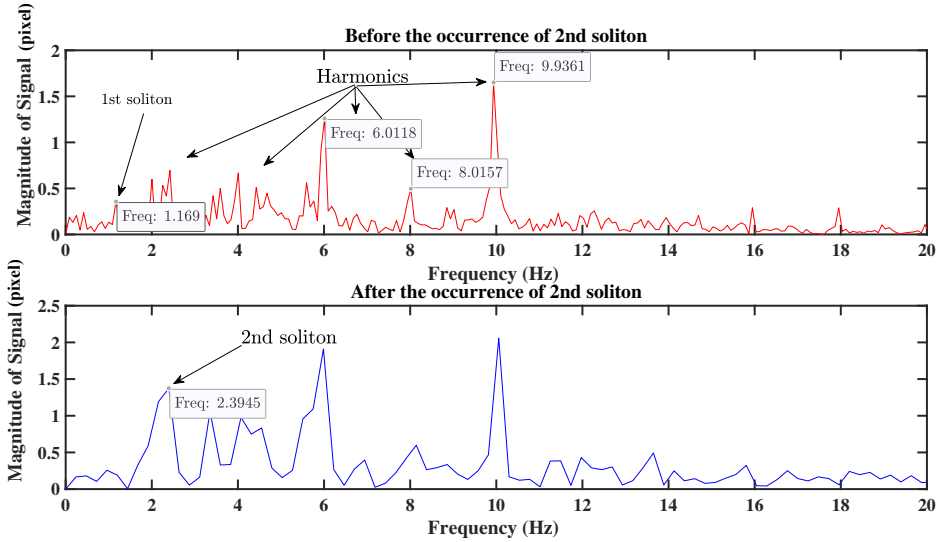

(c) Power spectrum

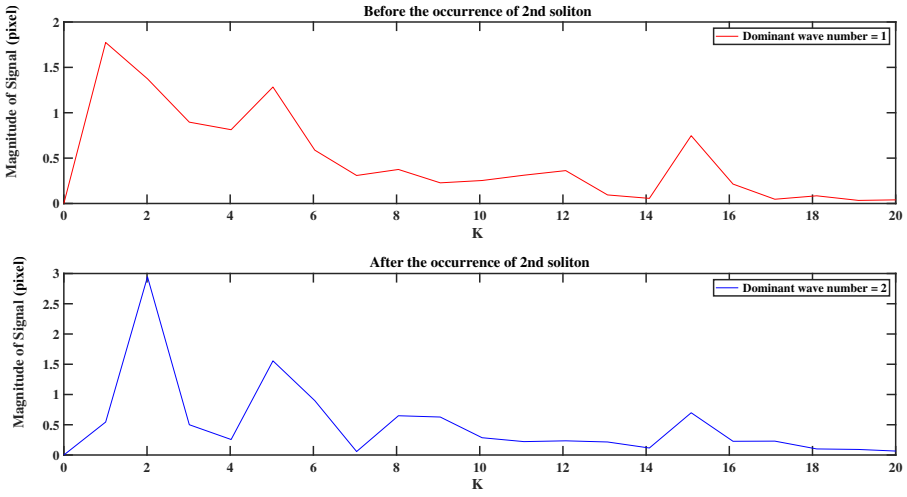

(d) Wave numbers plot

Figure 14: Signal analysis for transition from 1 to 2 solitons at 119 rpm.

In another conducted experiment, the disk speed was augmented from rest to 118 rpm quasi-statically in steps of 10 rpm. Two solitons rotating symmetrically around the pattern were formed. The results of the analysis is presented in Figures 15 and 16.

For the current experiment:

$\omega_d = \frac{119_{rpm}}{60_s}$= 1.983 Hz, $\omega_{s_2} = \frac{2.2248}{2}$= 1.1124 Hz, $\omega_p = \frac{4.5887}{14} = 0.328$Hz. Thus:

$$\boxed{\frac{\omega_{s_2}}{\omega_d} = 0.56}, \boxed{\frac{\omega_p}{\omega_d} = 0.165}, \boxed{\frac{\omega_{s_2}}{\omega_p} = 3.39}$$

Continuing the ascending process, an abrupt disk speed change from 118 rpm to 125 rpm led to a mixed equilibrium state with several solitary waves rotating around the pattern. In this case, signal graphs and simulated signals of radii were not recognizable. Moreover, there were two or more patterns existed at the same time; thus, the power spectrum and FFT application in post images processing MATLAB got complicated. This equilibrium state had one of the most notable heterogeneities and dissimilarity in all other conducted experiments.

The most notable discovery in this test was discerning a group of four solitary waves which is shown in Figure 17.

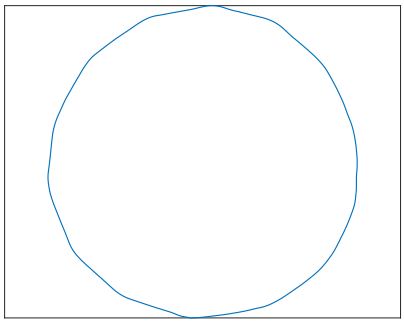

(a) Contour before the formation of the solitons

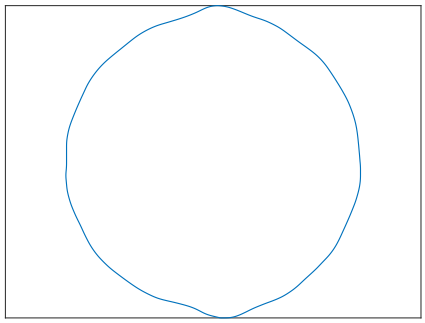

(b) Contour after the formation of the solitons

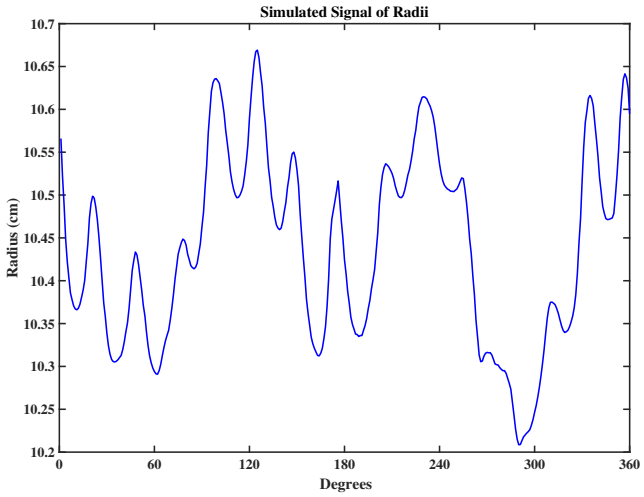

(c) Graph signal before solitons appearance

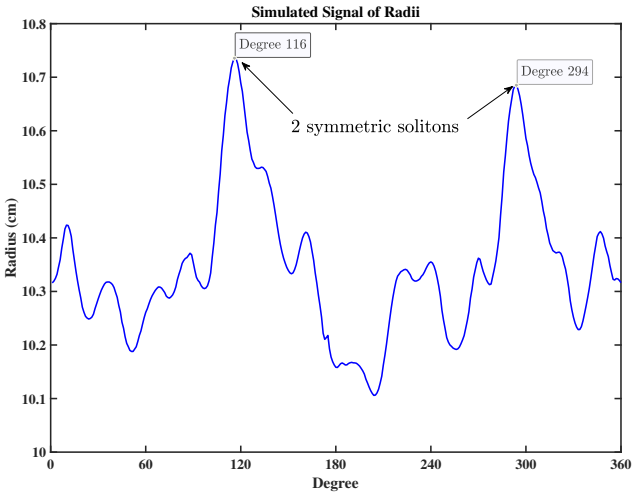

(d) Graph signal for 2 solitons

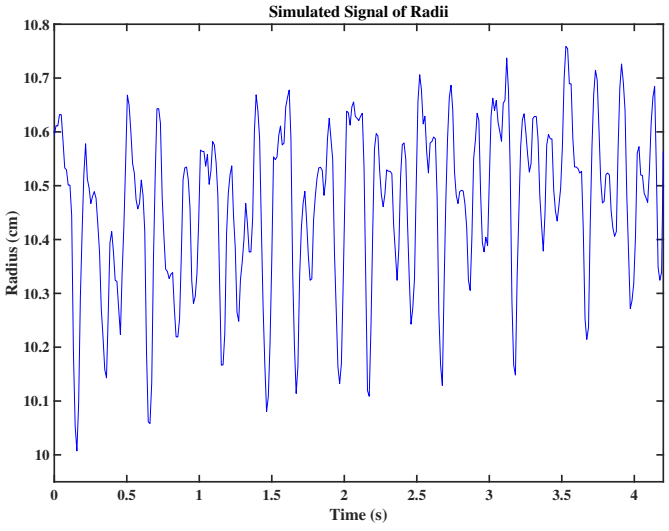

(e) Before the formation of the solitons

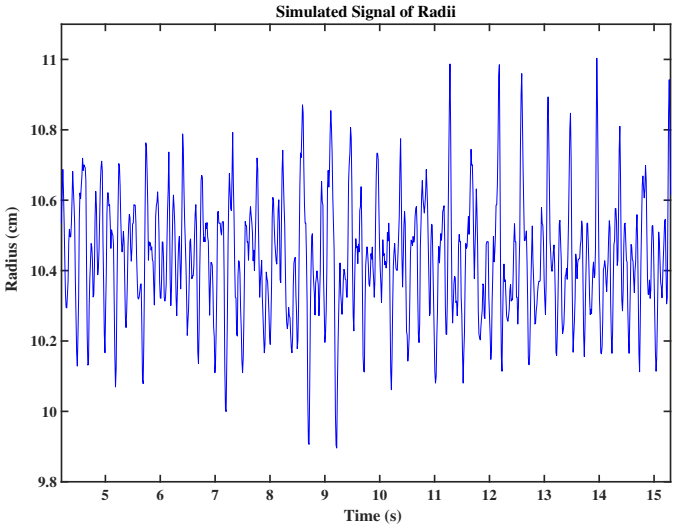

(f) After the formation of the solitons

Figure 15: Signal analysis for formation of 2 symmetric solitons.

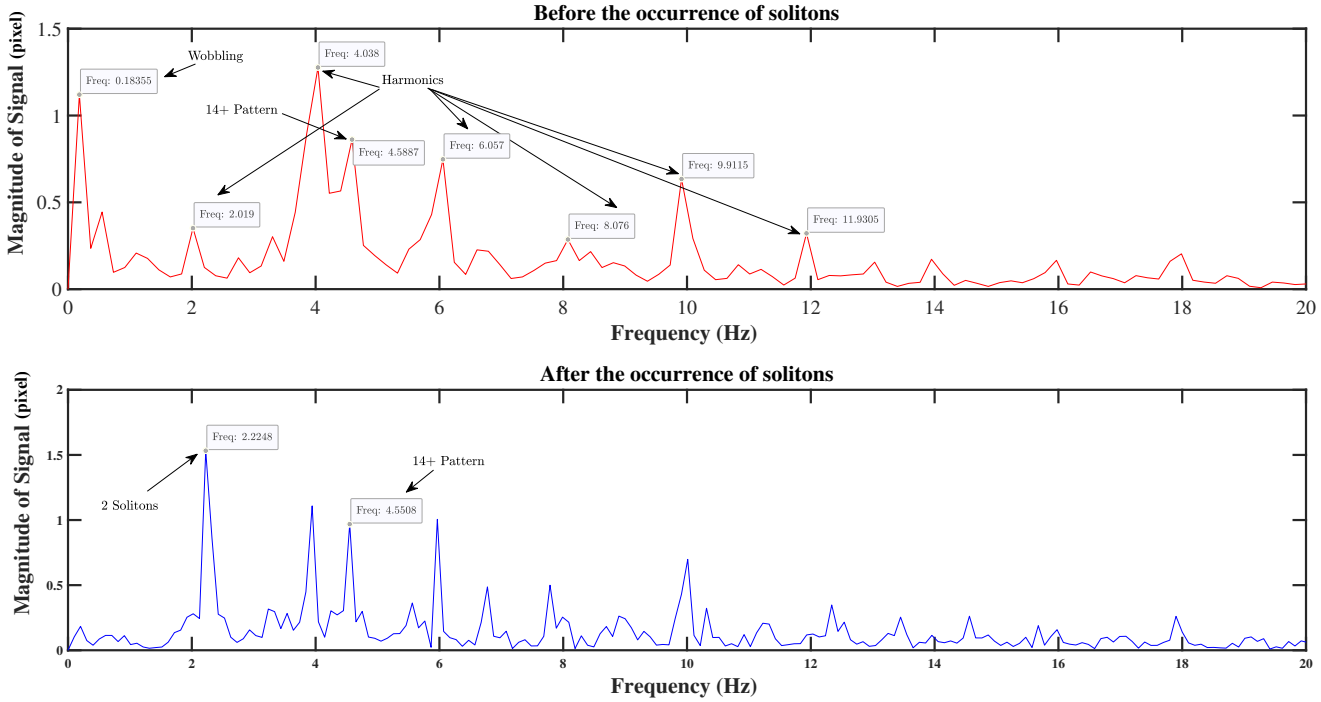

(a) Power spectrum

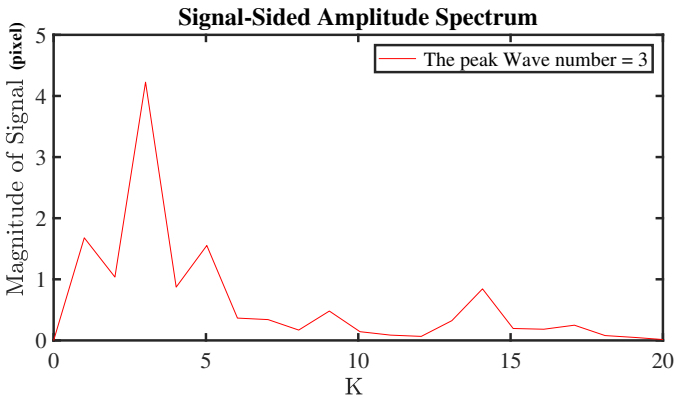

(b) Wave numbers before the solitons (wobbling)

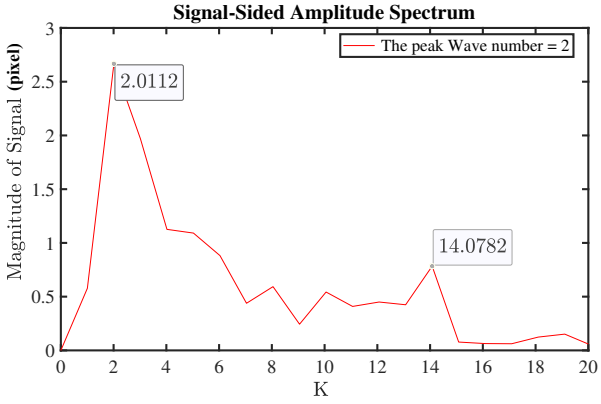

(c) Wave numbers after the formation of solitons

Figure 16: Signal analysis for 2 solitons at 118 rpm.

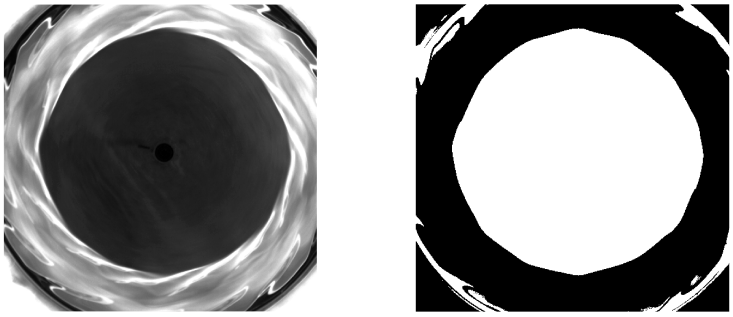

(a) 4 solitons binarizing through MATLAB (left one: raw image)

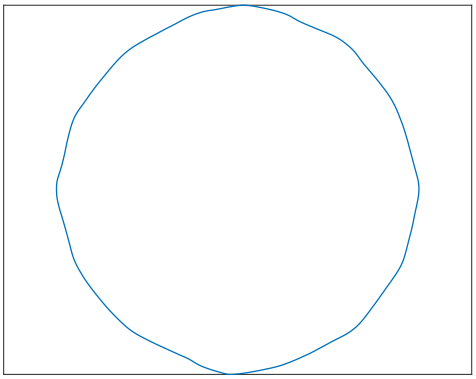

(b) Corresponding contour

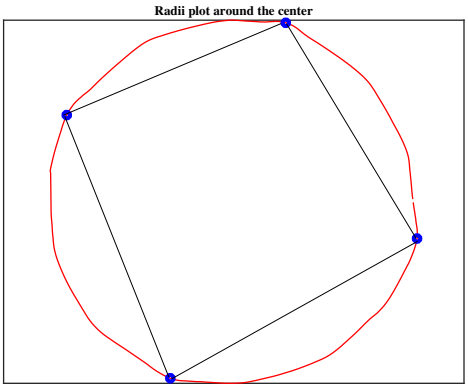

(c) Twisted graph signal around a circle

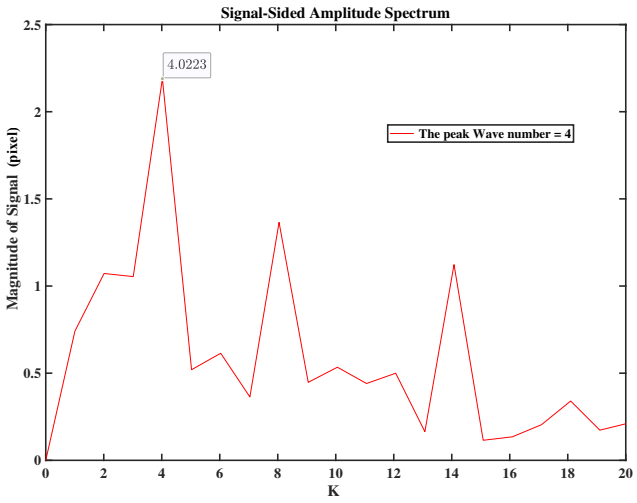

(d) Wave numbers plot

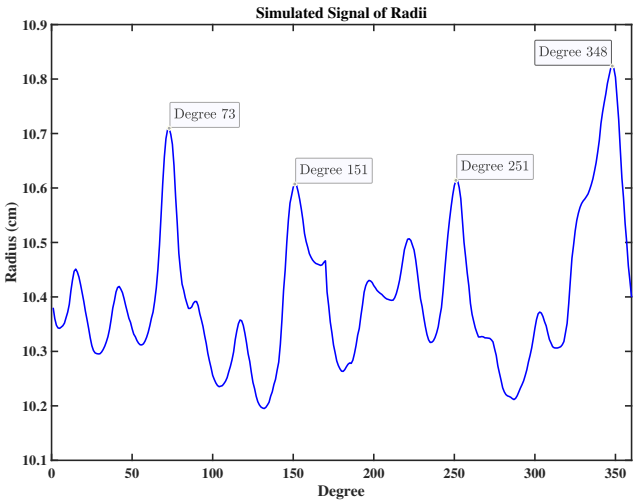

(e) Graph signal for 4 semi-symmetric solitons

Figure 17: Signal analysis for 4 solitons at 125 rpm

Continuing investigating on solitons' behavior, starting from the rest, the disk speed was increased quasi-statically in steps of 5 rpm to 116 rpm. First a 10^+ breathing pattern was observed (Figure 18a). Afterwards, this became a transition 11^+ pattern (Figure 18b), and subsequently a 14^+ equilibrium pattern. (Figure 18c). Then a weak soliton was formed (Figure 18d) followed by the formation of three solitons rotating around the pattern non-symmetrically (Figure 18e). Eventually, two out of the solitons disappeared after about one second. Finally, one stable soliton remained revolving. See Figure 18f. The frequency of the stable soliton is calculated based on its simulated signal of the radii graph (Figure 19e).

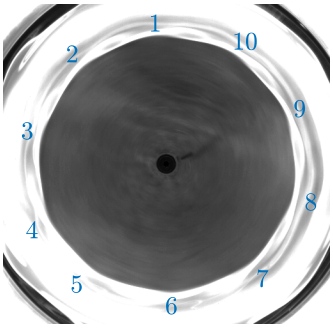

(a) Breathing

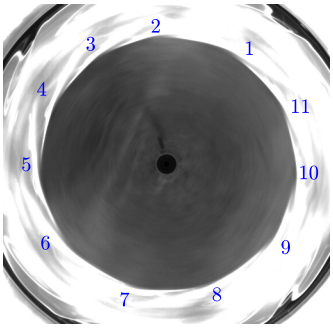

(b) 11^+ pattern (transition region)

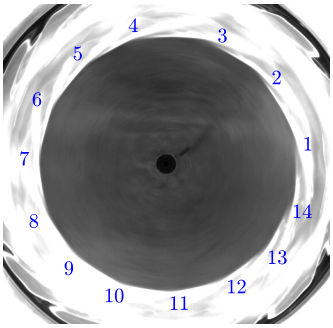

(c) 14^+ pattern

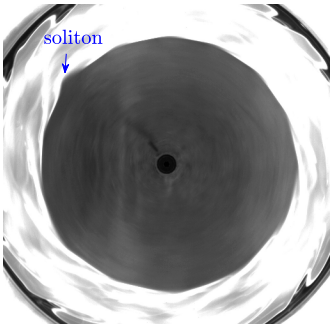

(d) Inception of the 1st soliton

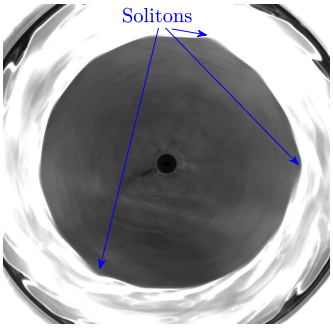

(e) 3 non-symmetric unstable solitons

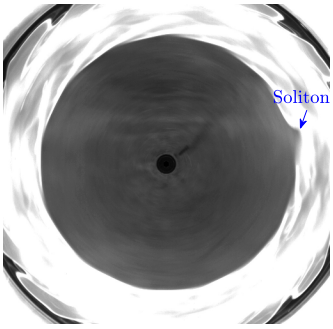

(f) 1 stable soliton (final stage)

Figure 18: Development of the pattern at 116 rpm in ascending sequence

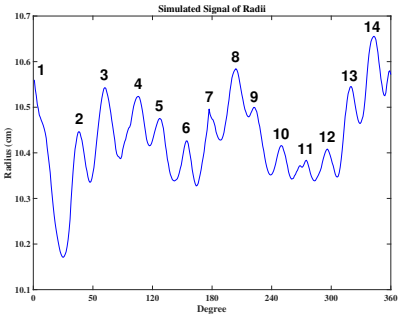

(a) 14^{+} before the formation of soliton(s)

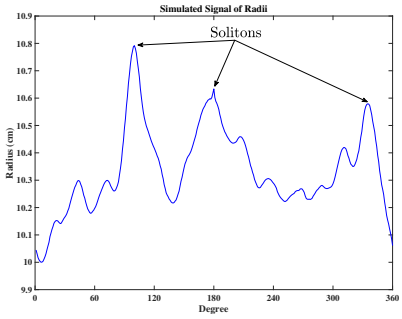

(b) 3 asymmetric unstable solitons

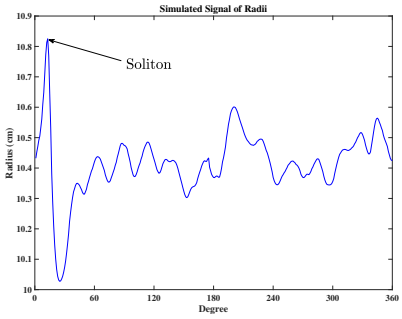

(c) The stable soliton

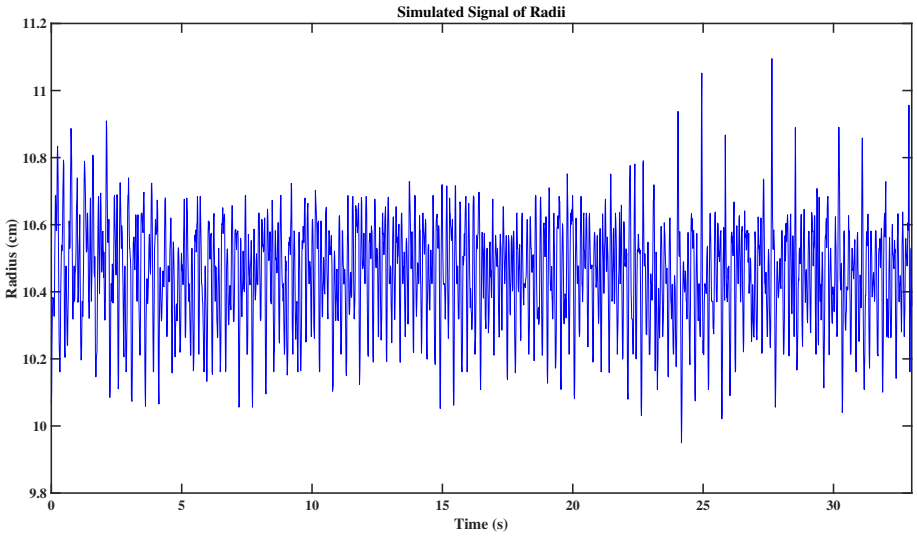

(d) Signal of radii for the whole experiment

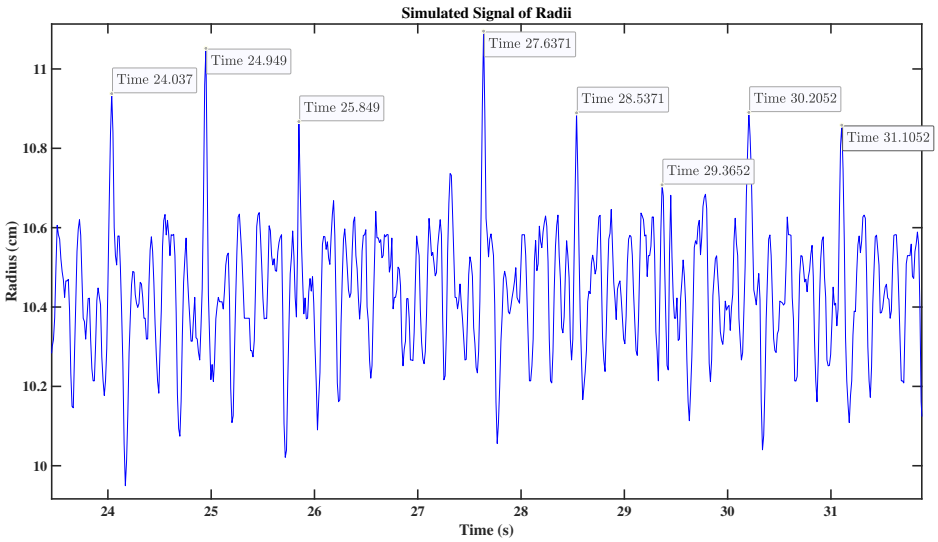

(e) Time period radius signals for the stable soliton

Figure 19: Signal analysis at 116 rpm in ascending sequence

From Figure 19e the differential time for a soliton passing the same point around the disk is the average of:

$31.1052 - 30.2052$, $30.252 - 29.3652$, $29.3652 - 28.5371$, $28.5371 - 27.6371$, $25.849 - 24.949$, $24.949 - 24.037$; Which is 0.888s

So the frequency of the stable soliton will be:

$\omega_s = \frac{1}{0.888_s}$ = 1.13 Hz

$\omega_d = \frac{116.3_{rpm}}{60_s}$ = 1.938 Hz

Thus:

$$\boxed{\frac{\omega_s}{\omega_d} = 0.589}$$

Another test was conducted to investigate the behavior of the flow with an abrupt disk speed change. The disk speed was augmented quasi-statically in steps of 5 rpm with a pause in between starting from the rest to 125 rpm. A precipitous angular velocity increment was applied from 125 rpm to 135 rpm. In this test, the fluid had one of the most complicated behaviors in all the conducted experiments. At 126 rpm, several solitons were revolving around the pattern, which made the Kelvin equilibrium unrecognizable. When the disk speed reached 132 rpm, 13 solitons were consisting of a group of 12 solitons with a weak soliton, formed around the pattern. They stayed rotating even when the pattern reached 135 rpm, yet after passing a few minutes, they vanished and a retrograde pentagon replaced the pattern. Unfortunately, due to the lack of memory in the camera, the transition regions could not be investigated. See Figures 20, 21 and 22.

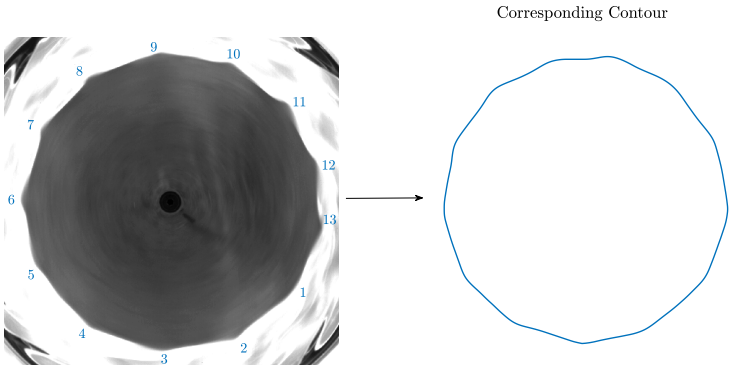

(a) Pattern

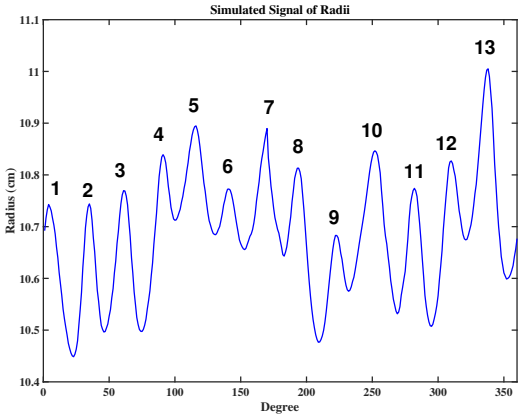

(b) Graph signal

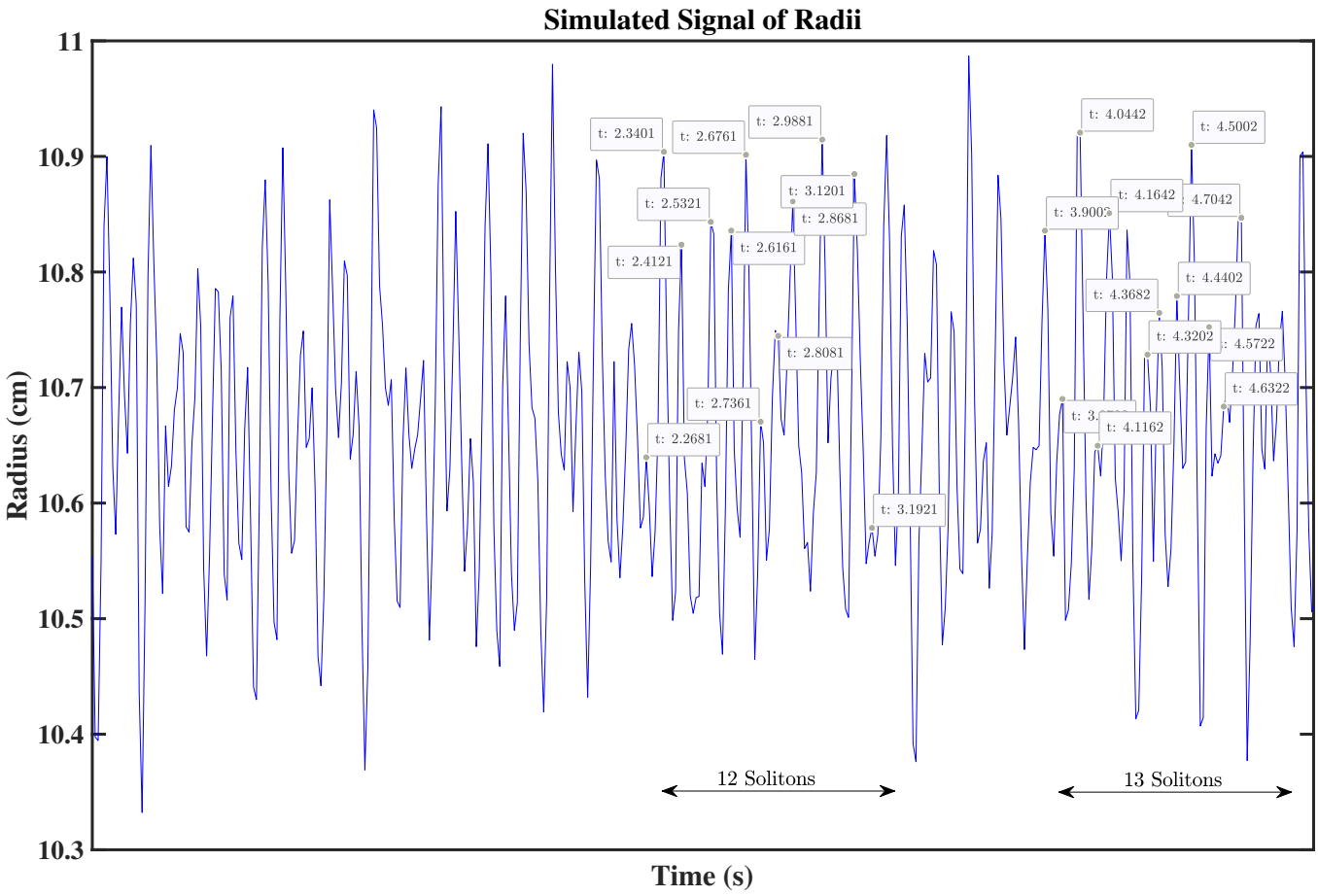

(c) Time period signal for 12 and 13 solitary waves

Figure 20: Signal analysis for 13 solitary waves at 132 rpm in ascending sequence.

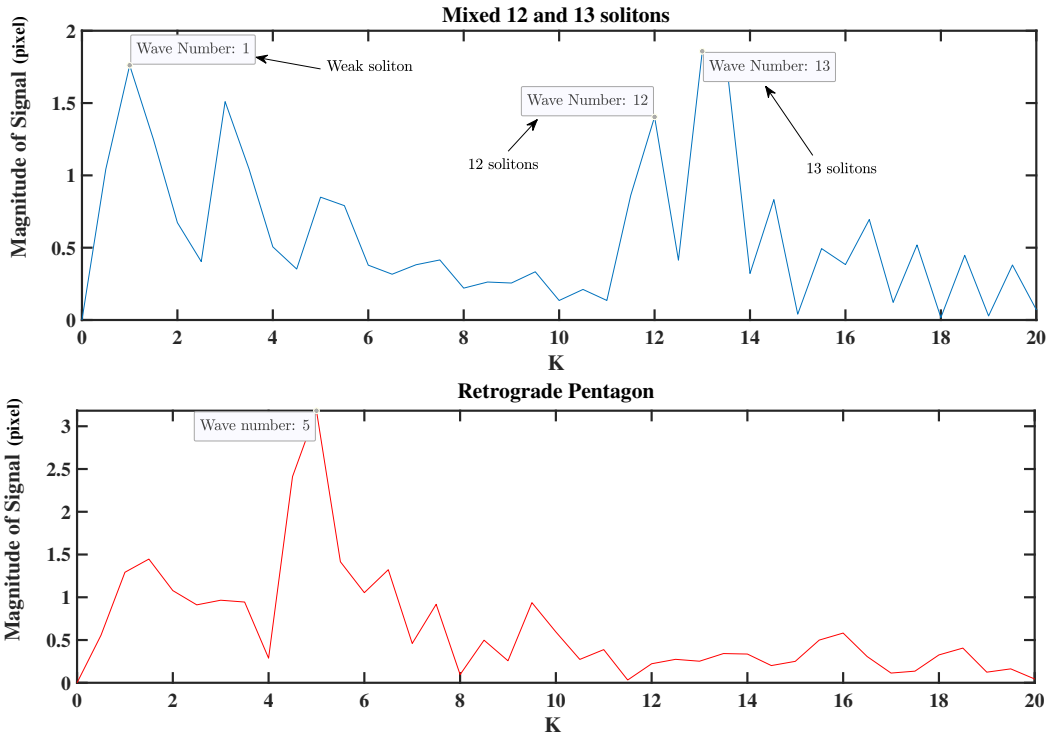

(a) Wave numbers plot

Figure 21: Signal analysis for precipitous speed increase from 125 rpm to 135 rpm with 13 solitons (a group of a weak and 12 strong solitons)

Based on Figure 20 the average differential time between the peaks of radii for 12 solitons and 13 solitons are 0.069s and 0.0637s respectively. The frequencies will be:

$Fs_{12} = \frac{1}{0.069_s} = 14.49$ Hz

$Fs_{13} = \frac{1}{0.0637_s} = 15.69$ Hz

Thus the power spectrum results correspond to the calculated frequencies. Eventually:

$\omega_{s_{13}} = \frac{15.4103}{13} = 1.185$ Hz

$\omega_{s_{12}} = \frac{14.2688}{12} = 1.189$ Hz (It shows the velocity of solitons is the same in both 12 and 13)

$\omega_d = \frac{132_{rpm}}{60_s} = 2.2$ Hz

Thus:

$$\boxed{\frac{\omega_{s12}}{\omega_d} = 0.54}, \boxed{\frac{\omega_{s13}}{\omega_d} = 0.5386}$$

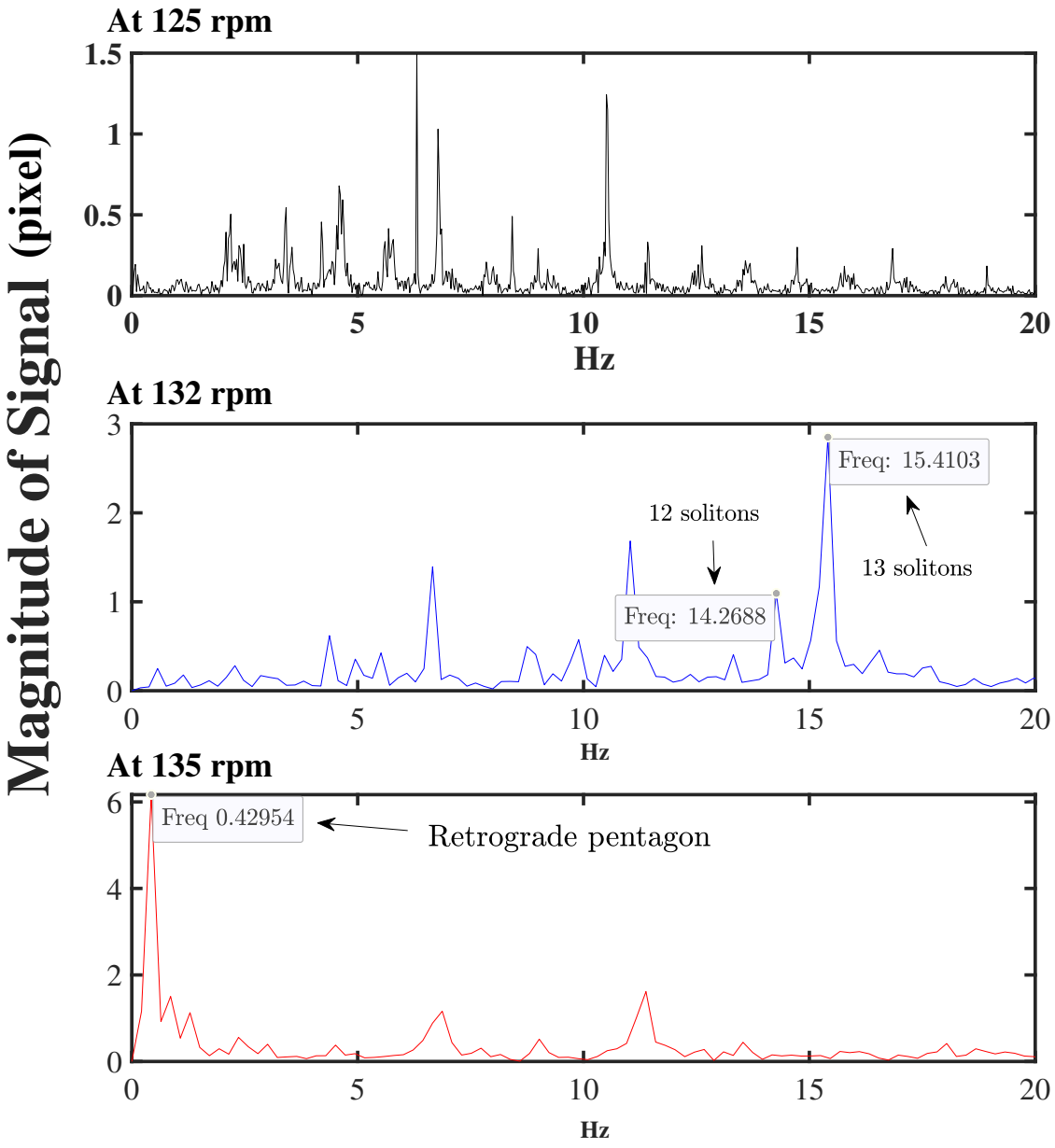

Figure 22: Power spectrum for precipitous speed increase from 125 rpm to 135 rpm in ascending sequence

4.3.2 Descending sequence

To investigate the equilibria spectrum in descending run, chiefly disk was set into the rotation from rest. The disk velocity was augmented quasi-statically with a pause in between up to the chaos region and then, the spin-down flow was started. In this section, the abrupt disk rotational speed decrement had also been utilized. That being said, the effect of an abrupt change in disk's angular velocity was also investigated on the formation of solitary waves. The image processing procedure is also divided into two parts; before and after the formation of solitons.

In previous exploratory experiments conducted on spindle oil with 10 mm initial height and at spin-down sequence [3], the formation of solitons was around 130 rpm to 114 rpm. See Table 2. Yet in this report, new regions consisting of solitons rotating around the pattern were discovered which will be discussed later.

Table 2: Equilibria spectrum for descending sequence with $h_0 = 10mm$ (Courtesy of Soltanian)

Disk Velocity (rpm)	**Equilibrium State**	**Camera Frequency (fps)**	**Description**
181	8^+	54.427	Semi-stable, Non-symmetric
172.4	7^+	21.85	Semi-stable
152	7^+	20.084	Stable
143.3	6^+	50.02	Stable
134.6	5^-	16.067	Smooth and stable with vibration in sides
125.8	16^+ or 17^+ or 18^+	21.85	Unrecognizable due to the three solitary wave
	Unknown	54.427	Unrecognizable due to the six solitary wave
114.3	15^+	54.427	With one solitary wave
107.7	15^+	20.84	Stable and symmetric
104.4	Circular	21.85	Breathing circle
87.3	3^+	543.05	Smooth and stable
65.2	Circular	543.05	Shady
48.2	Circular	543.05	Shady, Squeezed

For the first set of the experiment in the spin-down procedure, the disk speed, starting from rest up to 200 rpm, was increased. After the full development of the fluid at 200 rpm, the disk velocity was decreased in steps of 5 rpm to 157 rpm. A smooth retrograde pentagon (5^{-}) appeared with vibrations in sides. At this point, the angular velocity was reduced instantaneously to 139 rpm which caused the state to dissolve and instead, 13 solitons emerged revolving symmetrically around the pattern. See Figures 23 and 24. By comparing the power spectrum of two states (before and after the formation of solitons), the frequencies of the equilibrium state and solitons were discerned. The other common signal effects in the power spectrum plot are the harmonics, the noises in both patterns and the transition region.

Based on Figure 24a, the frequency of the signals are calculated:

$\omega_{s_{13}} = \frac{15.7162}{13} = 1.209$ Hz , $\omega_d = \frac{139_{rpm}}{60_s} = 2.317$ Hz $\rightarrow \boxed{\frac{\omega_{s_{13}}}{\omega_d} = 0.522}$

Another abrupt decrement in the disk speed from 139 rpm to 125 rpm, caused the transition from 13 to 3 solitons. See Figures 25 and 26.

Based on Figure 26a, the frequency of the signals are calculated:

$\omega_{s_3} = \frac{3.5069}{3} = 1.169$ Hz , $\omega_d = \frac{125_{rpm}}{60_s} = 2.08$ Hz $\rightarrow \boxed{\frac{\omega_{s_3}}{\omega_d} = 0.562}$

The frequency of 3 solitons can be found from the signal plot (Figure 25c):
mean(Δt) = mean($8.0283 - 7.6803, 7.6803 - 7.4763$)= 3.623 Hz; Which corresponds to the above mentioned frequency, with a reasonable precision.

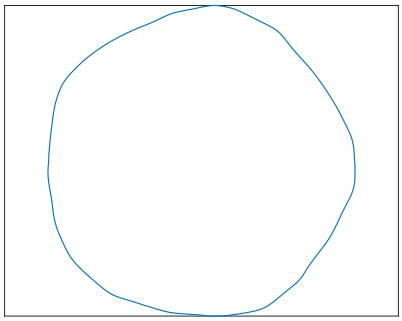

(a) Contour before the formation of the solitons

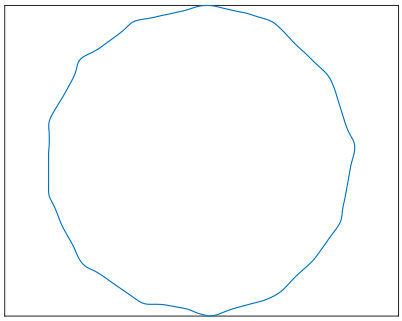

(b) Contour after the formation of 13 solitons

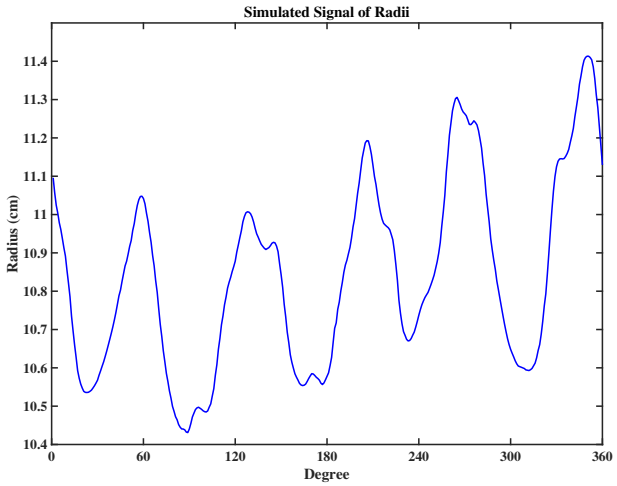

(c) Graph signal for 5^{-} before 13 solitons

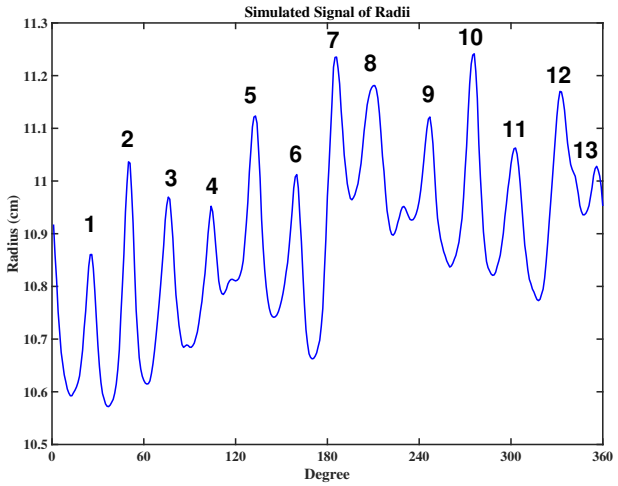

(d) Graph signal for 13 solitons

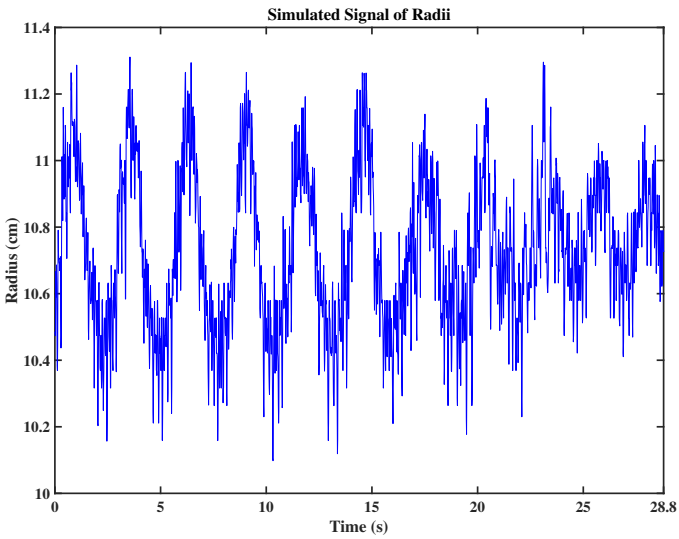

(e) Corresponding signals for 5^{-} before formation of 13 solitons

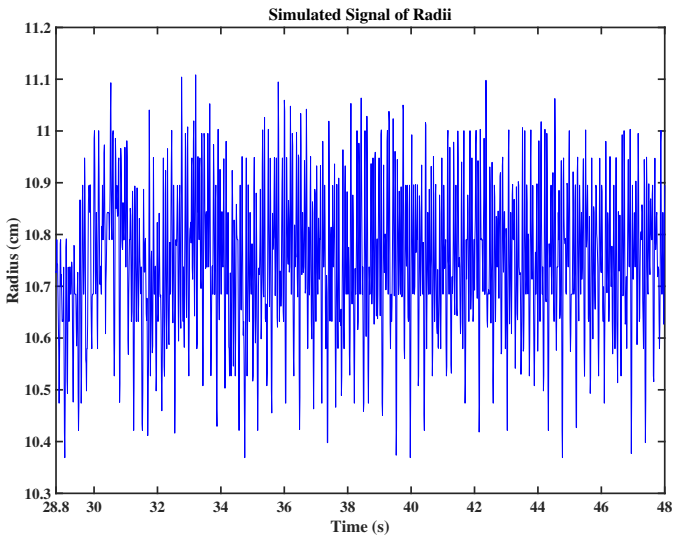

(f) Corresponding signals after formation of 13 solitons

Figure 23: Signal analysis for formation of 13 symmetric solitons at 139 rpm in descending sequence.

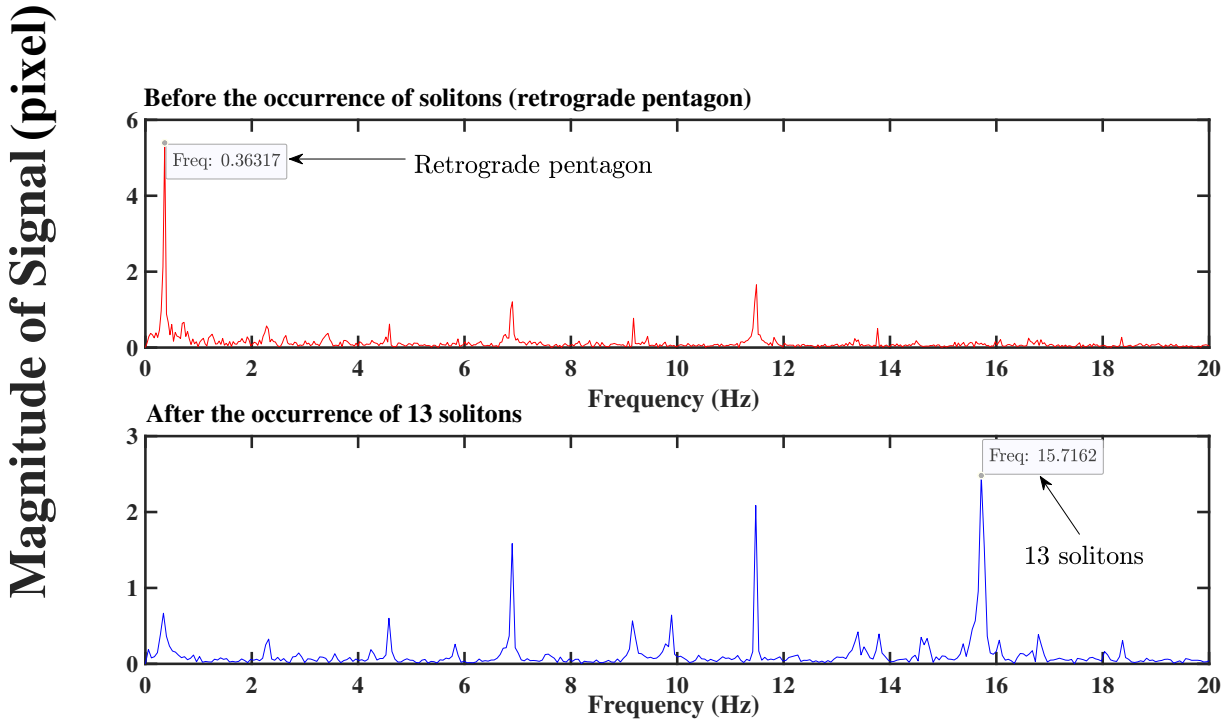

(a) Power spectrum

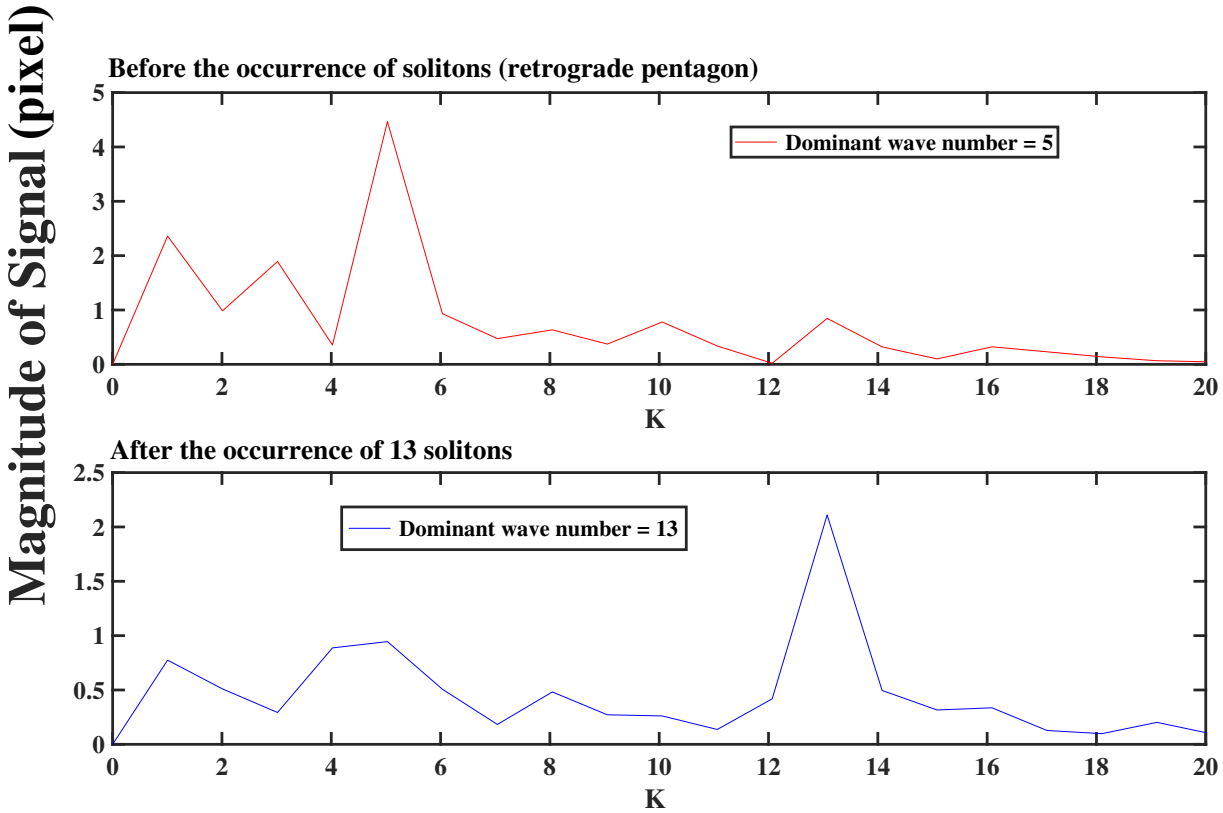

(b) Wave numbers plots

Figure 24: Signal analysis for the formation of 13 solitons at 139 rpm.

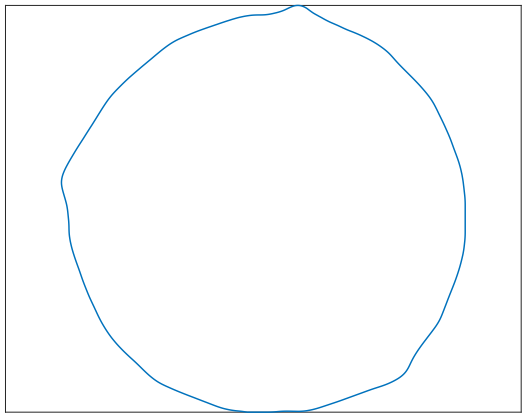

(a) Corresponding contour

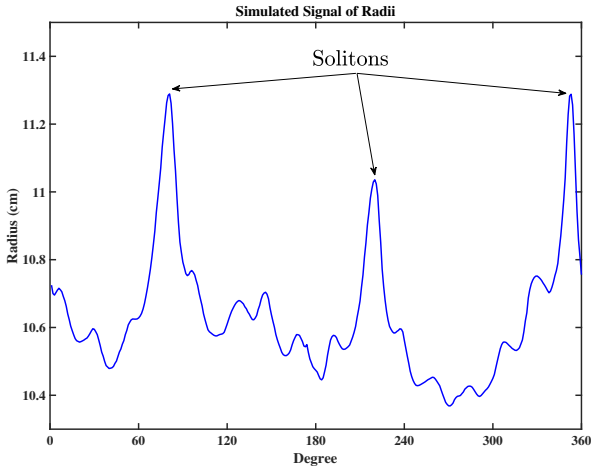

(b) Graph signal for 3 solitons

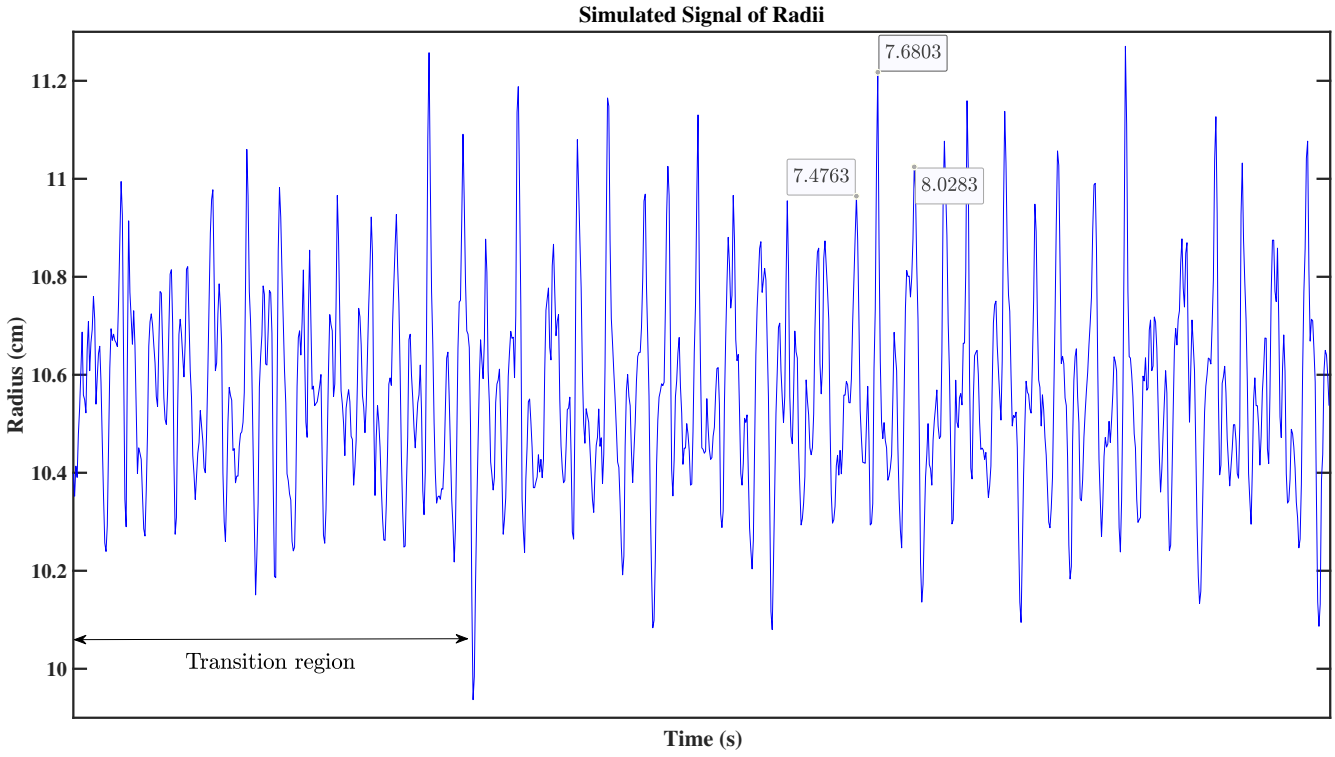

(c) Corresponding signals

Figure 25: Signal analysis after the transition from 13 to 3 solitons at 125 rpm

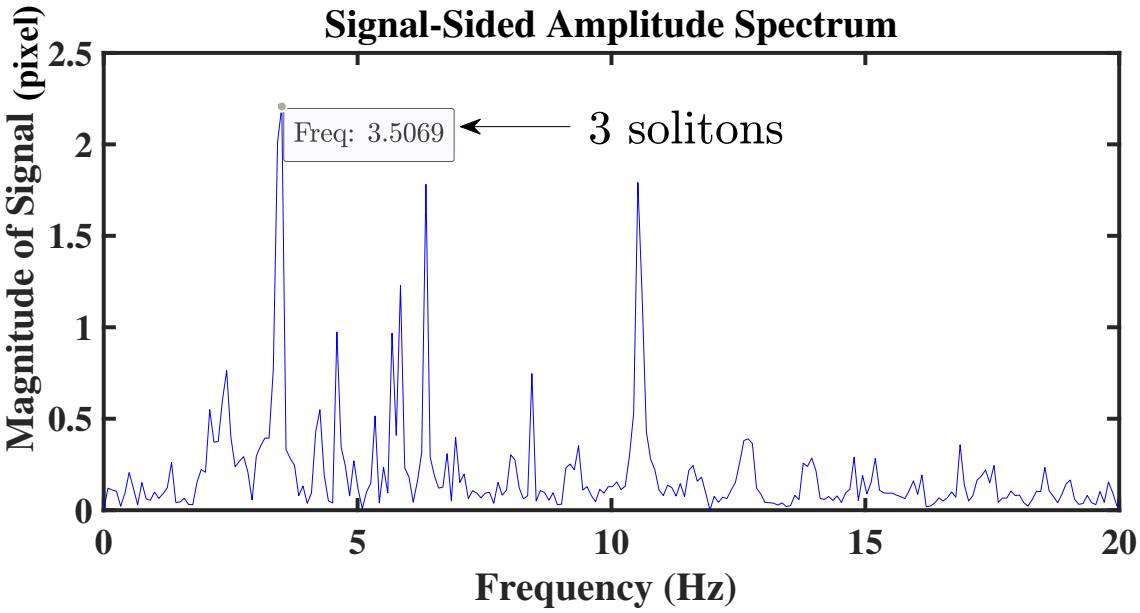

(a) Power spectrum

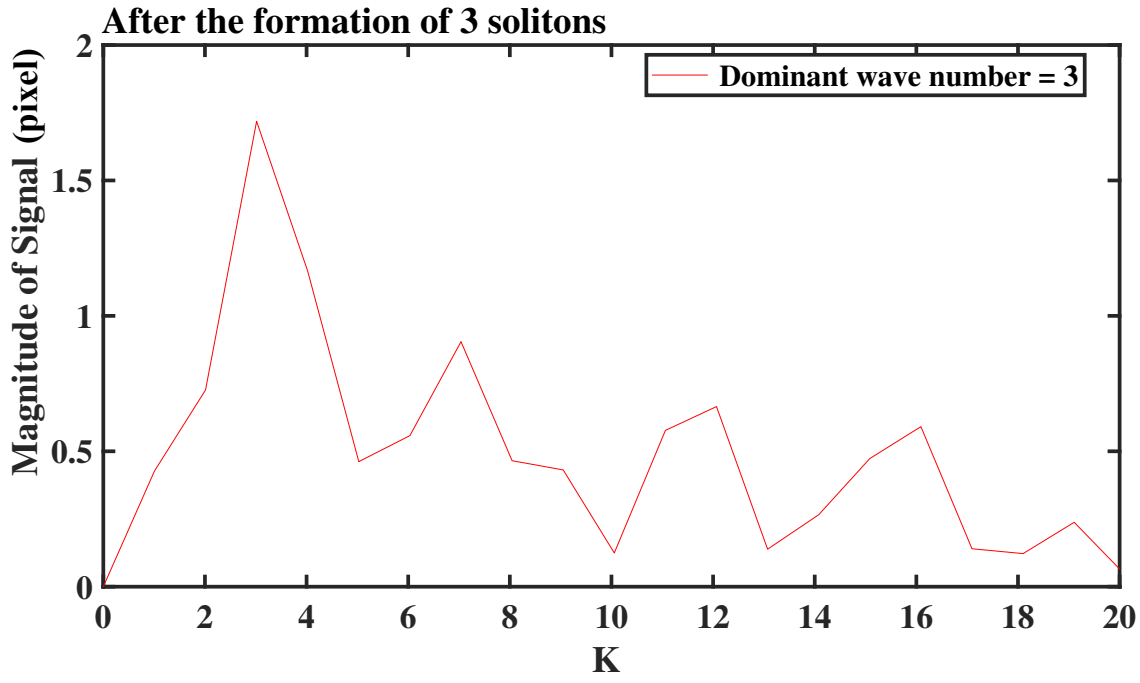

(b) Wave number plot

Figure 26: FFT analysis after the transition from 13 to 3 solitons at 125 rpm

Furthermore, as the disk velocity decreased quasi-statically in steps of 4 rpm to 116.3 rpm (from 125), there existed a 13^{+} pattern, which led to emerging two weak solitons. See Figure 27. Power spectrum and wavenumbers plot were not applicable due to the complexity of the FFT analysis because of the weakness of solitons and smoothness of the edges for the Kelvin equilibrium state pattern.

Another test was conducted to investigate the formation of three symmetric solitons in descending sequence based on Table 2. The disk speed was augmented quasi-statically in steps of 5 rpm with a pause in between starting from the rest to 200 rpm. Then it was decreased to 125 rpm. The pattern was unrecognizable containing several solitons with mixed equilibria state. Three solitons were formed rotating around the pattern symmetrically eventually. See Figure 28. Due to the complexity of the pattern, FFT analysis was not applicable. However, the frequency of the solitons is calculated based on the simulated signals of the radii graph.

Based on Figure 28f the differential time between the peaks of radii for 3 solitons is:

62.8705 - 62.5585 = 62.5585 - 62.2465 = 0.312 s. $\rightarrow Fs_3 = \frac{1}{0.312_s}$ = 3.205 Hz.
$\rightarrow \omega_{s_3} = \frac{3.205}{3}$ = 1.07 Hz , $\omega_d = \frac{125_{rpm}}{60_s}$ = 2.08 Hz. Thus:

$$\boxed{\frac{\omega_{s_3}}{\omega_d} = 0.514}$$

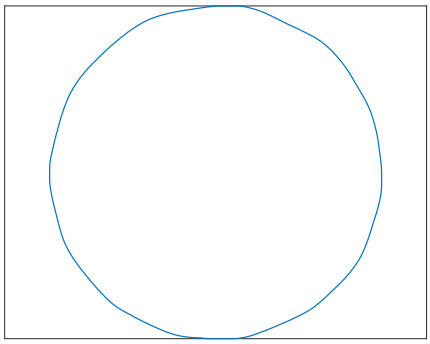

(a) 13^+ contour

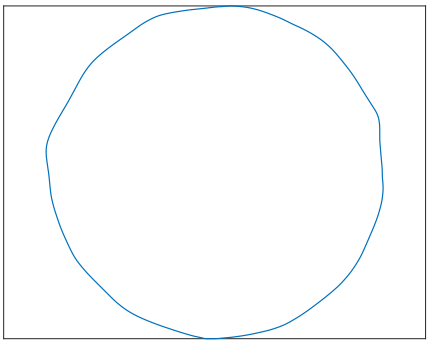

(b) 2 solitons contour

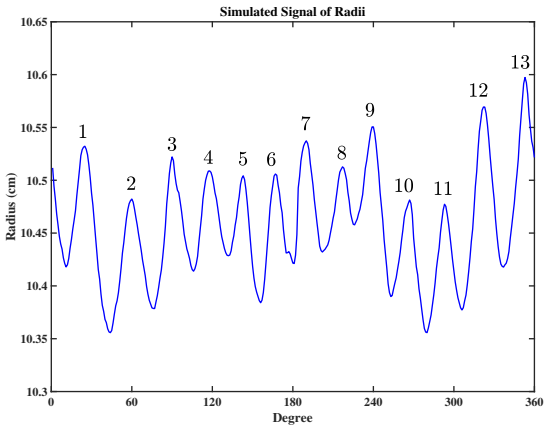

(c) Graph signal for 13^+ pattern

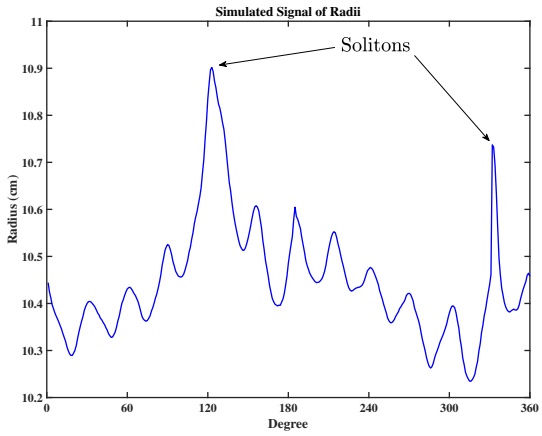

(d) Graph signal for 2 non-symmetric solitons

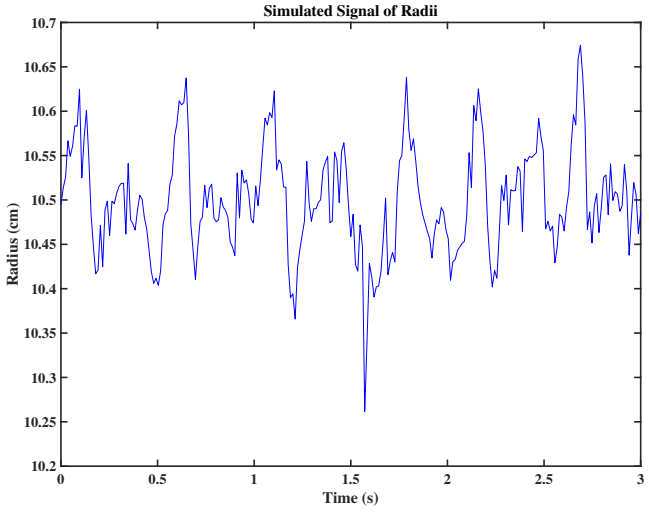

(e) 13^+ pattern radius signals

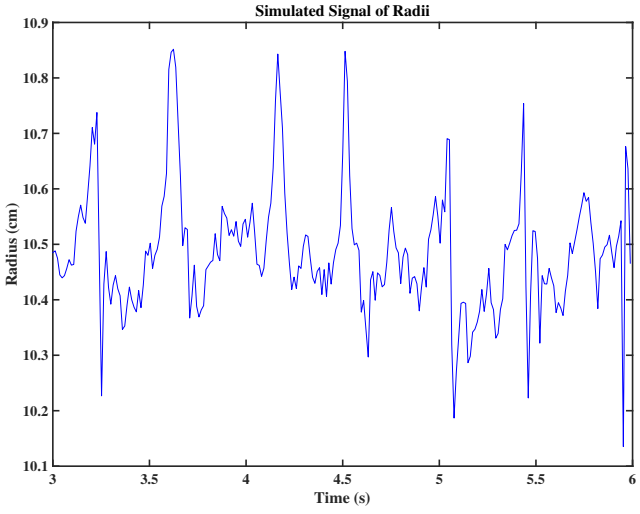

(f) 2 solitons radius signals

Figure 27: Signal analysis for the formation of 2 solitons at 116 rpm.

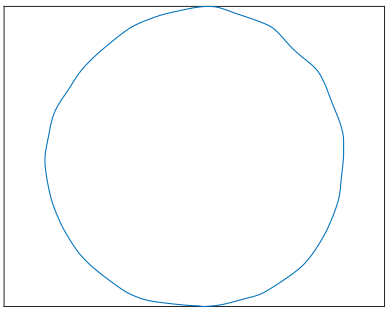

(a) Unrecognizable pattern before 3 solitons

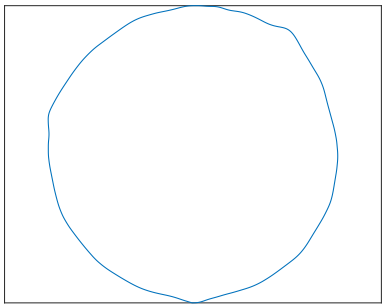

(b) 3 solitons corresponding contour

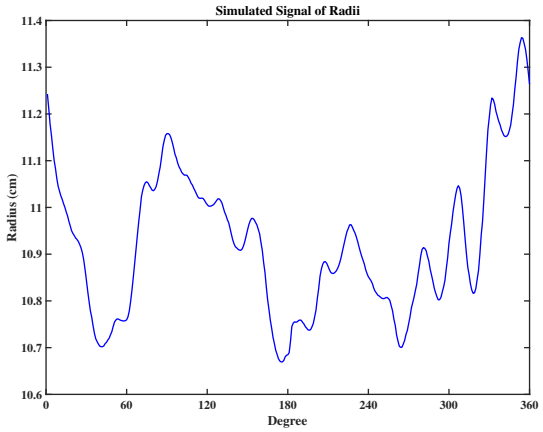

(c) Graph signal for unrecognizable pattern

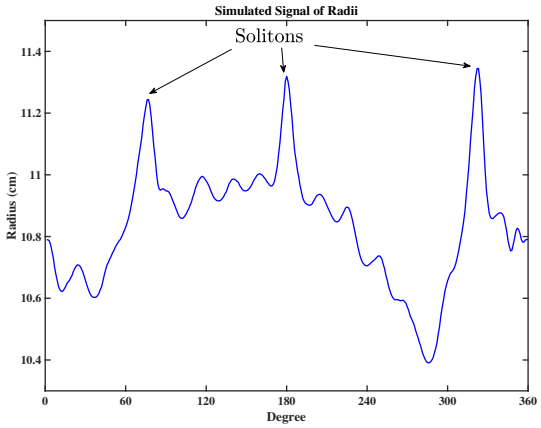

(d) Graph signal for 3 symmetric solitons

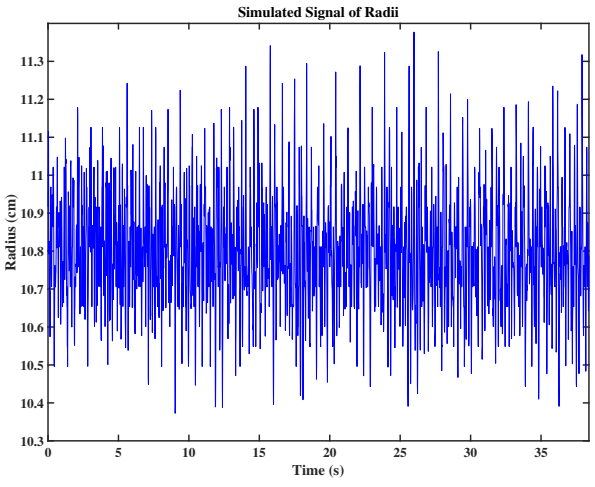

(e) Before the formation of solitons

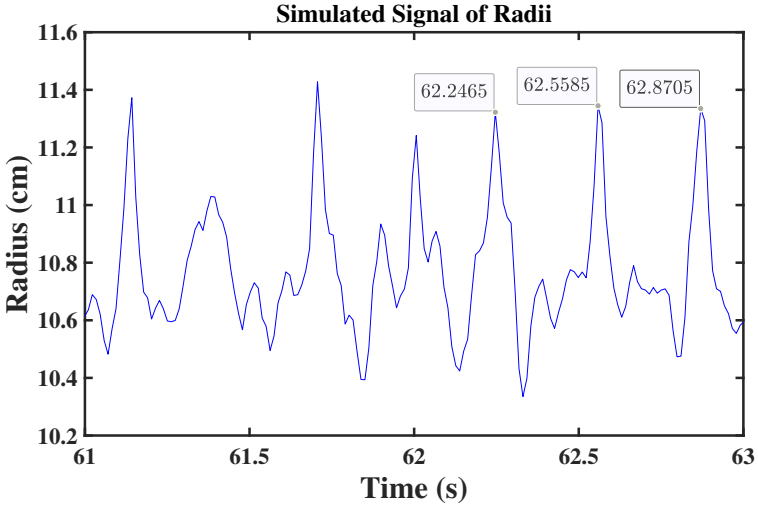

(f) After the formation of solitons

Figure 28: Signal analysis for the formation of 3 solitons at 125 rpm.

To explore the influence of an abrupt decrement disk velocity change on the solitons' behavior; another experiment was conducted. Increasing the disk speed to 200 rpm from rest and then decreasing in steps of 5 rpm to 140 rpm led the fluid containing 12 solitons rotating around the pattern. With an abrupt angular velocity change to 125 rpm, the solitons started disappearing and two unstable symmetric solitons replaced them for a minimal time; approximately 2 seconds. An unrecognizable pattern then replaced two solitons due to several solitary waves. Finally, three symmetric solitons appeared revolving around the pattern. See Figure 29.

Based on Figure 30, the frequencies of the solitons are calculated:

$\omega_{s_{12}} = \frac{13.6555}{12}$ = 1.138 Hz , $\omega_{s_2} = \frac{2.5}{2}$ = 1.25 Hz , $\omega_{s_3} = \frac{3.4645}{3}$ = 1.155 Hz , $\omega_d = \frac{125_{rpm}}{60_s}$ = 2.083 Hz.
Thus:

$$\boxed{\frac{\omega_{s_{12}}}{\omega_d} = 0.546}\ ,\ \boxed{\frac{\omega_{s_2}}{\omega_d} = 0.6}\ ,\ \boxed{\frac{\omega_{s_3}}{\omega_d} = 0.554}\ ,$$

The frequency of solitons can be found from the signal plots (Figures 29g, 29h, 29i) which correspond to the obtained frequencies from power spectrum plots, with a reasonable precision:

mean($\Delta t_{s_{12}}$) = mean($1.008 - 0.92, 0.92 - 0.848, 0.848 - 0.792, 0.792 - 0.712, 0.712 - 0.64$) =
0.0736 s $\rightarrow Fs_{12} = \frac{1}{0.0736_s}$ = 13.587 Hz.
Δt_{s_2} = $16.096 - 15.688$ = 0.408 s
$\rightarrow Fs_2 = \frac{1}{0.408_s}$ = 2.45 Hz.
mean(Δt_{s_3}) = mean($51.032 - 50.752, 50.752 - 50.448$) = 0.292 s
$\rightarrow Fs_3 = \frac{1}{0.292_s}$ = 3.424 Hz.

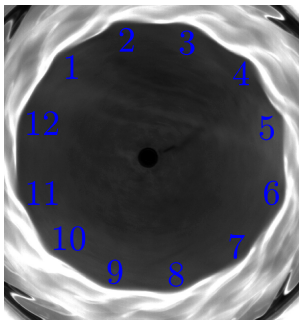

(a) 12 symmetric solitons

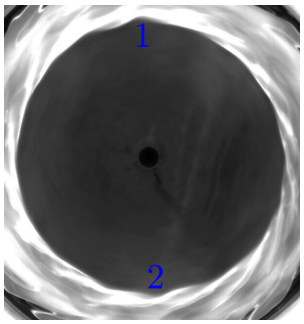

(b) 2 symmetric solitons (transition)

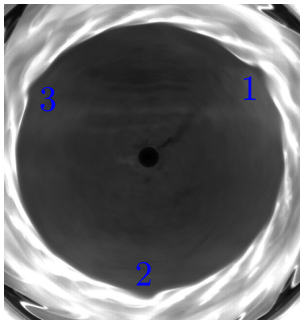

(c) 3 symmetric solitons

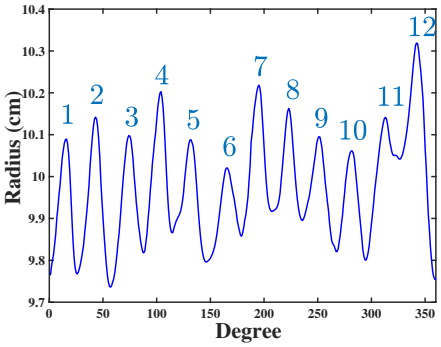

(d) Graph signal for 12 symmetric solitons

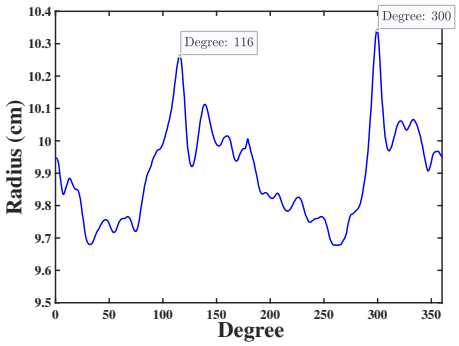

(e) Graph signal for transient 2 symmetric solitons

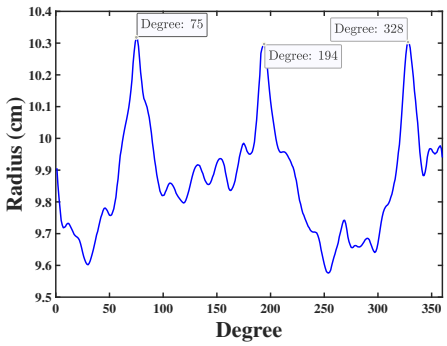

(f) Graph signal for 3 symmetric solitons

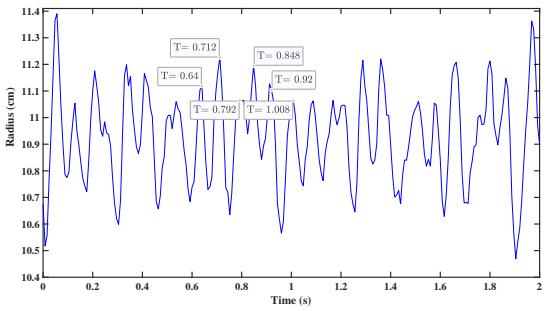

(g) Time period for 12 symmetric solitons

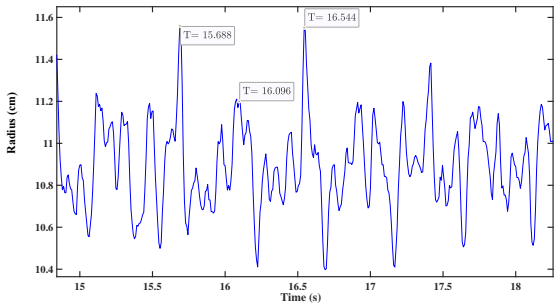

(h) Time period for 2 symmetric solitons

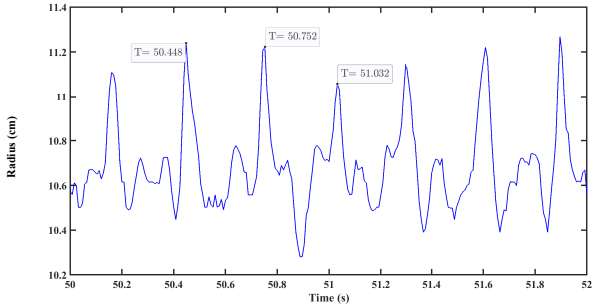

(i) Time period for 3 symmetric solitons

Figure 29: Pattern's development after an abrupt change from 140 to 125 rpm

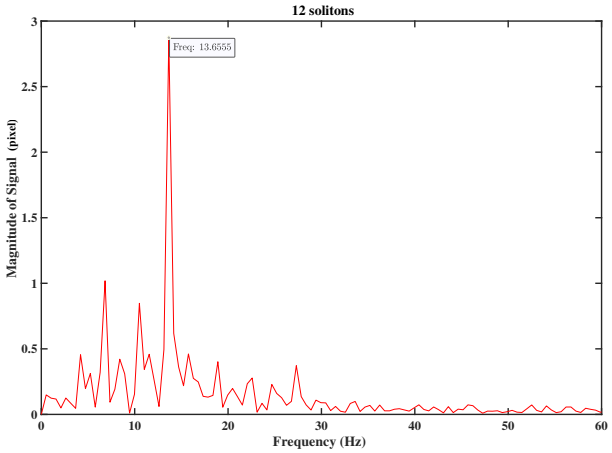

(a) Power spectrum, till 12 solitons fade away

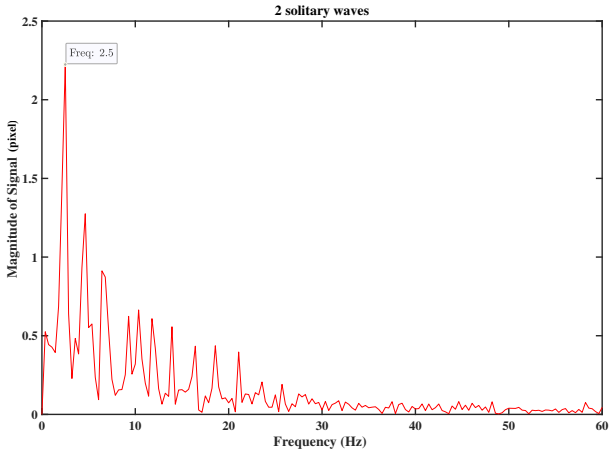

(b) Power spectrum for the evolution of 2 solitary waves (2.8 s transition region)

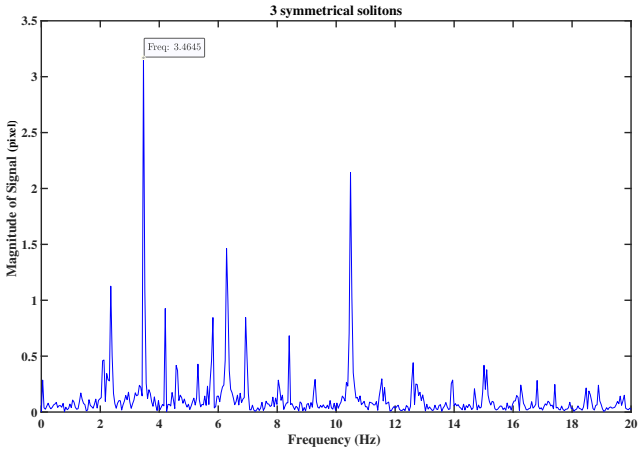

(c) Power spectrum for 3 symmetrical solitons

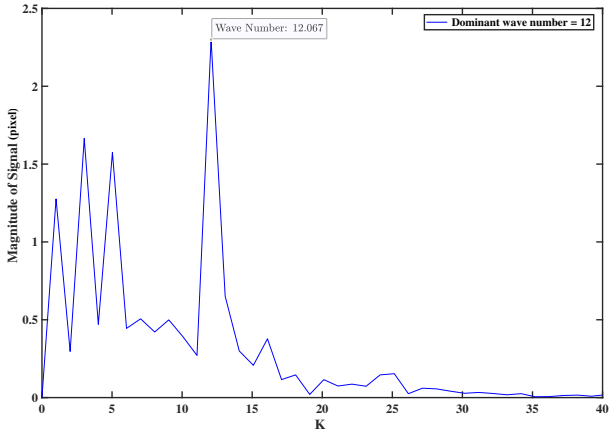

(d) Wavenumber for 12 solitons

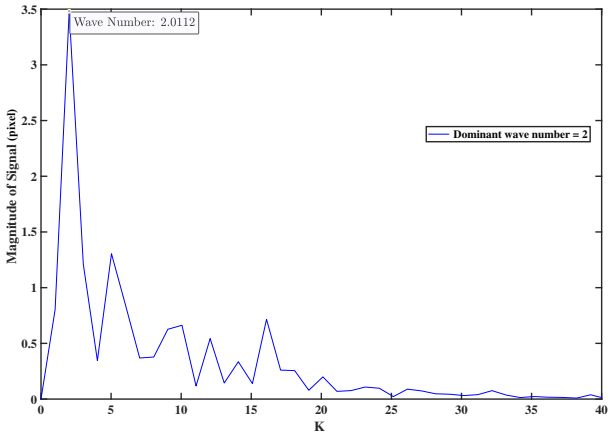

(e) Wavenumber for 2 symmetrical solitons

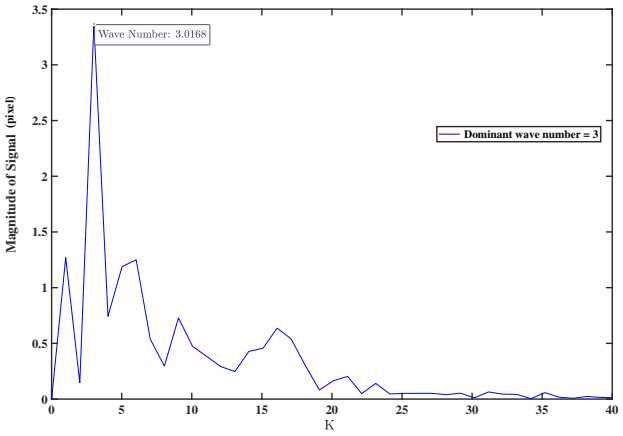

(f) Wavenumber for 3 symmetrical solitons

Figure 30: FFT analysis for an abrupt change from 140 to 125 rpm

In order to suggest a new method of investigating Kelvin equilibrium state, after the former test, the disk speed was again augmented instantaneously from 125 to 143 rpm, which led to the formation of 12 solitons from 2 solitons with the 11 solitons transition region. See Figures 31 and 32.

Based on Figure 32c and 32d the frequencies of the solitons are calculated:

$\omega_{s_{11}} = \frac{13.6207}{11} = 1.238$ Hz , $\omega_{s_{12}} = \frac{14.8678}{12} = 1.239$ Hz , $\omega_d = \frac{143_{rpm}}{60_s} = 2.383$ Hz. Thus:

$$\boxed{\frac{\omega_{s_{11}}}{\omega_d} = 0.52} \quad , \quad \boxed{\frac{\omega_{s_{12}}}{\omega_d} = 0.52}$$

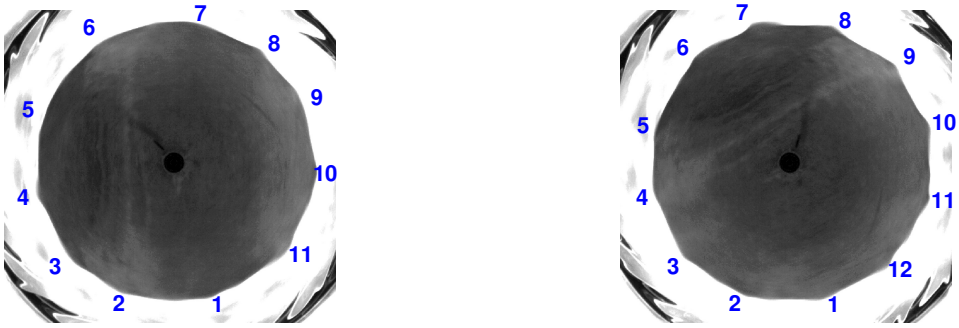

(a) 11 solitons (transient region)

(b) 12 solitons

Figure 31: Pattern's development after another abrupt change from 125 to 143 rpm

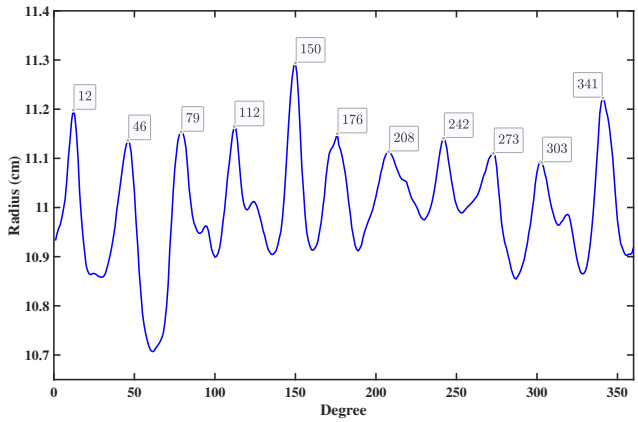

(a) Graph signals 11 symmetric solitons

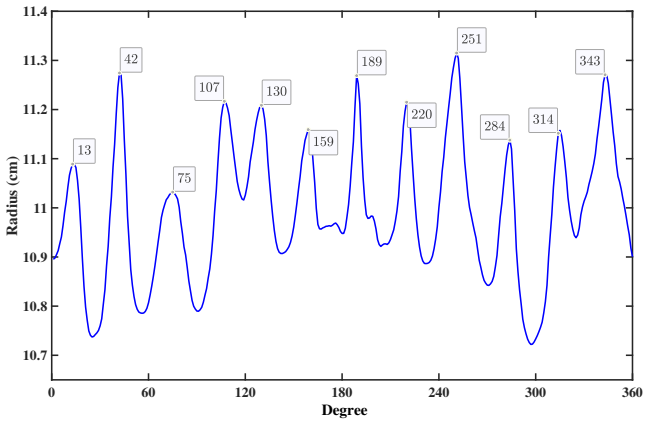

(b) Graph signals for 12 symmetric solitons

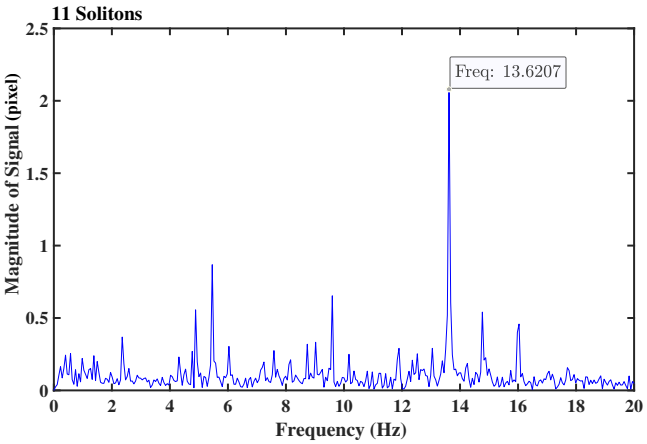

(c) Power spectrum, till 11 solitons fade away

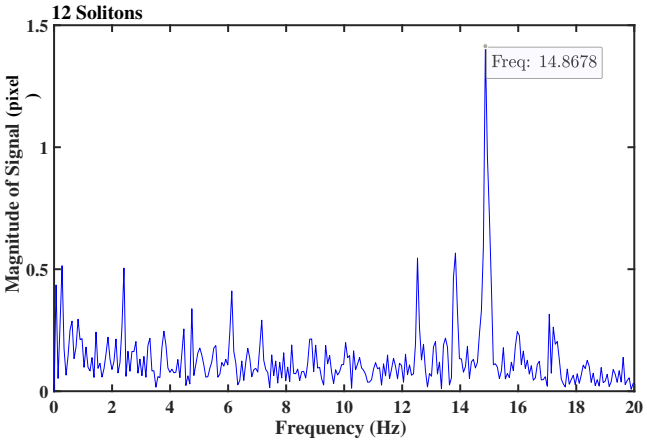

(d) Power spectrum for 12 solitons

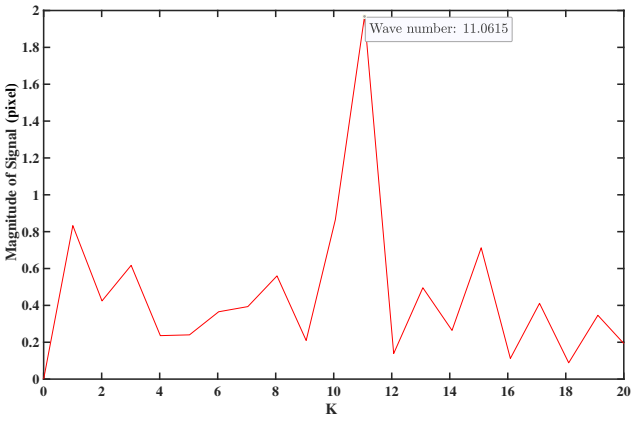

(e) Wave number for 11 symmetrical solitons

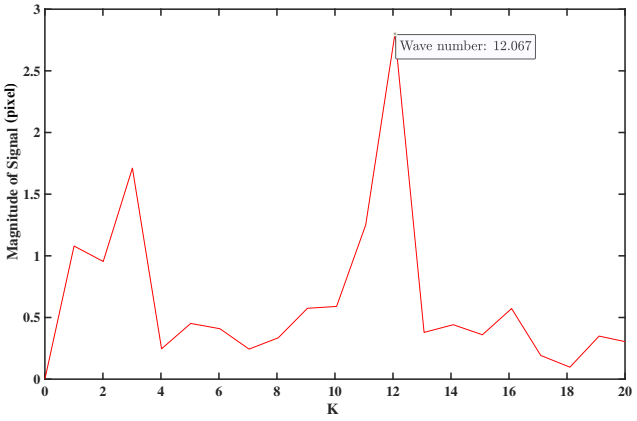

(f) Wave number for 12 symmetrical solitons

Figure 32: FFT analysis for 125 rpm to 143 rpm after an abrupt velocity decrement

5 Conclusions

The main focus of this thesis has been on the findings and development of solitons in spindle oil vortices. The tests were conducted inside a stationary cylinder with a rotating disk on the bottom. The effects of a precipitous change in disk velocity in both increasing and decreasing sequences were investigated. It was observed that an abrupt change in the angular velocity could also lead to the discovery of new Kelvin equilibrium states. Also, it was verified that an instantaneous change in the disk speed, possess a considerable effect in the inception of solitons. This conclusion was taken to use in an increment of the speed, even in the spin-down sequence. When changing the angular velocity in several tests, solitary waves were rotating around the pattern non-symmetrically in the transition between the two soliton states. Eventually, solitons form, disappear, and transit into each other without following a specific rule. The creation of a group of solitons is not simultaneously for every one of them.

The solitons frequency and disk angular velocity ratio ($\frac{\omega_s}{\omega_d}$) was not necessarily constant for each group of solitons, independent of boundary conditions. For instance, 13 symmetric solitons in the ascending sequence had a different ratio in the descending sequence with a different boundary condition. It was seen that the stable non-symmetric solitons compared to other experiments under the same boundary condition, did not have the same frequency ratio either. It can be argued that those non-symmetric solitons are multiple groups of solitons rotating together instead of a pack of solitons. As an exemplification, instead of two solitons rotating, they could have been two groups of one separate soliton; or two groups of two solitons instead of four. Much of these results are drawn to the FFT analysis on the power spectrum and wavenumber plots. It was observed that stable solitons in the same experiment state (when they transform into each other in the same boundary condition) have the same velocity. Nevertheless, the solitons which appear during the transient regions have a different angular velocity. The frequency ratio in experiments are the same for each group of solitons, and this is a way to find out how the pattern of our soliton group is.

The superposition of the results for all the tests in terms of $\frac{\omega_s}{\omega_d}$ versus Weber number is shown in Figure 35. The Weber number is calculated in two ways to compare the frequency ratio in terms of the speed of the disk and the soliton angular velocity. The Weber number, frequency ratio, and the number of solitons existed are also mentioned for each data on the plot. The Weber number formulas in respect to the frequencies are:

Weber number in respect to the disk angular velocity = $\frac{\rho(R_d\omega_d)^2 h_0}{\sigma}$

Weber number in respect to the soliton angular velocity = $\frac{\rho(R_d\omega_s)^2 h_0}{\sigma}$

It can be verified from the plot in Figure 34, that the mean for the $\frac{\omega_s}{\omega_d}$=0.558 and the standard deviation is 0.03049. Also, it is investigated that smaller velocity ratio leads to the higher number of solitons observed. It is identified that the soliton frequency and disk speed ratio is between 0.5 and 0.6 with respect to the statistical analysis. It can be argued that the solitons existed from disk speed ranging from 115 to 145 rpm.

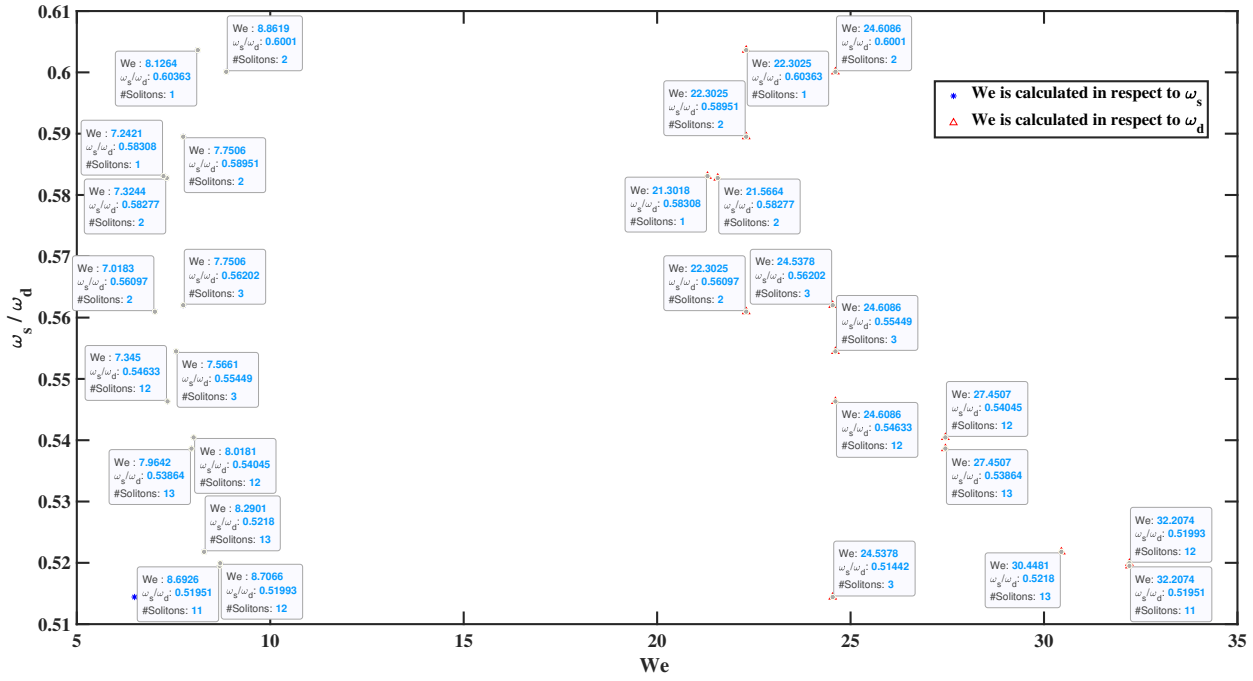

Figure 33: Superposition of ratio of Soliton frequency to disk's speed versus Weber number

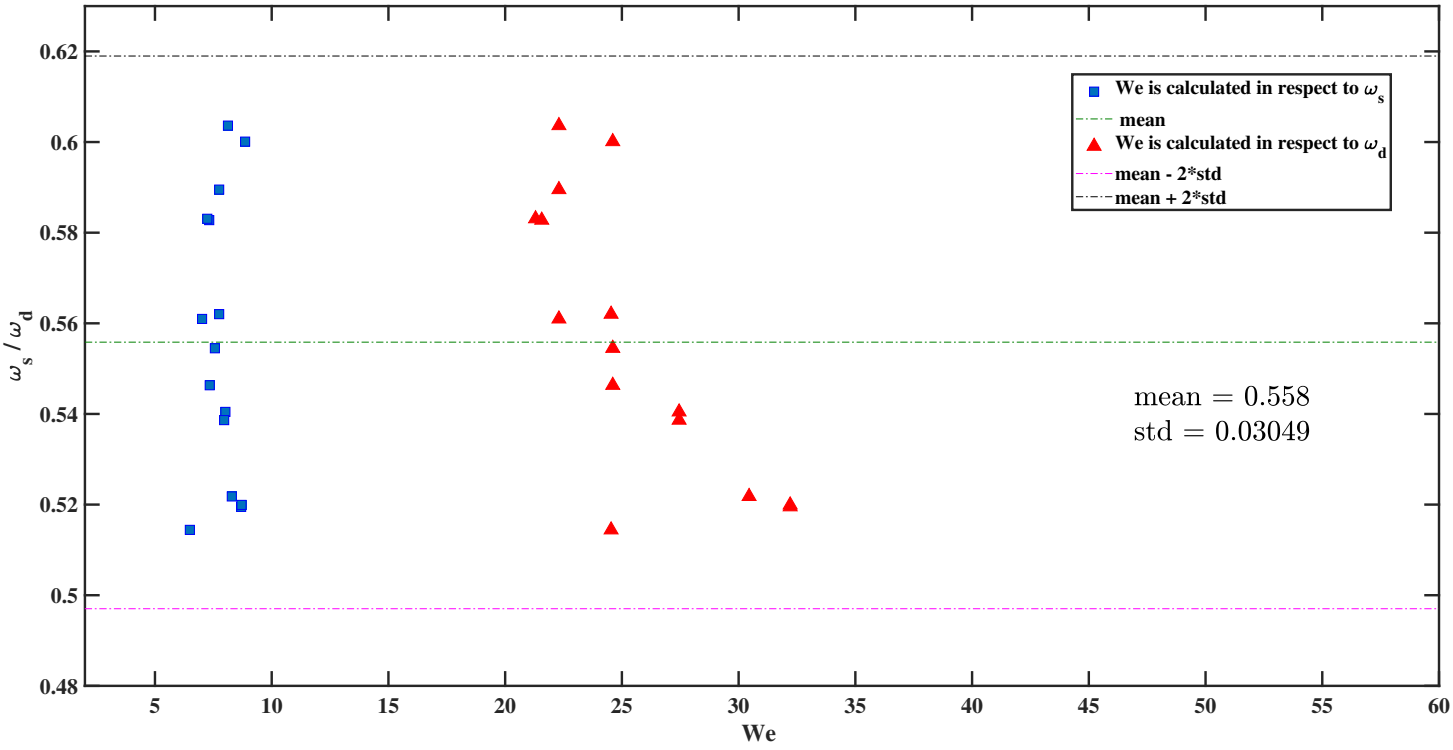

Figure 34: Statistical analysis of the speed ratio versus Weber number

6 Future studies

The present thesis has introduced a new method not only to observe the behavior of solitary waves (particularly solitons) but also has conducted a new process to create them. This new method, an abrupt change in the disk speed, can be useful to others who wish to contribute to experiments associated with solitary waves with different fluids possessing various viscosities. Besides, the influence of pulsating and wobbling variables in the formation of solitons may be addressed.

Future experiments may include disks of different sized, more initial liquid heights, and even PIV analysis to discern frequencies more precisely.

Numerical investigation and mathematical interpretation of the results would lead to a significant discovery of new formulas.

References

[1] Reynold Alleyne Nicholson. *The Mathnawi of Jalalu'ddin Rumi*. Luzac, 1926.

[2] C. Rasinariu. Solitons of kdv equation, Department of Science and Mathematics, Maple Document, Columbia College, 600 S. Michigan Ave, Chicago, IL 60605, USA, Nov 20, 2001.

[3] Pooya Soltanian Sedeh. *Exploratory Experiments on Oil Vortices Produced Inside a Cylindrical Container*. PhD thesis, Concordia University Montreal, Quebec, Canada, 2017.

[4] Lord Kelvin. I880 vibrations of a columnar vortex. *Phil. Mag*, 10:155.

[5] William Thomson. Xxiv. vibrations of a columnar vortex. *The London, Edinburgh, and Dublin Philosophical Magazine and Journal of Science*, 10(61):155–168, 1880.

[6] William Thomson. 4. on vortex atoms. *Proceedings of the Royal Society of Edinburgh*, 6:94–105, 1869.

[7] Albert A Michelson and Edward W Morley. On the relative motion of the earth and of the luminiferous ether. *Sidereal Messenger, vol. 6, pp. 306-310*, 6:306–310, 1887.

[8] GH Vatistas, J Wang, and S Lin. Experiments on waves induced in the hollow core of vortices. *Experiments in fluids*, 13(6):377–385, 1992.

[9] Albert Einstein et al. On the electrodynamics of moving bodies. *Annalen der physik*, 17(10):891–921, 1905.

[10] Georgios H Vatistas. A note on liquid vortex sloshing and kelvin's equilibria. *Journal of Fluid Mechanics*, 217:241–248, 1990.

[11] GH Vatistas, J Wang, and S Lin. Recent findings on kelvin's equilibria. *Acta mechanica*, 103(1-4):89–102, 1994.

[12] SF van der Laan. The vortex theory of atoms-pinnacle of classical physics. Master's thesis, 2013.

[13] Georgios Vatistas, Nabil Esmail, and Costas Ravanis. Wave development in disk-like nearly inviscid liquid vortices. In *39th Aerospace Sciences Meeting and Exhibit*, page 158, 2001.

[14] Harald Hanche-Olsen. Buckingham's pi-theorem. *NTNU: http://www.math.ntnu.no/~ hanche/notes/buckingham/buckingham-a4.pdf*, 2004.

[15] Georgios H Vatistas, Hamid A Abderrahmane, and MH Kamran Siddiqui. Experimental confirmation of kelvin's equilibria. *Physical review letters*, 100(17):174503, 2008.

[16] Willy Hereman. Shallow water waves and solitary waves. *Mathematics of complexity and dynamical systems*, pages 1520–1532, 2011.

[17] J Scott Russel. Report of the 14th meeting of the british association for the advancement of science, 1844.

[18] Joseph Boussinesq. Théorie de l'intumescence liquide appelée onde solitaire ou de translation se propageant dans un canal rectangulaire. *CR Acad. Sci. Paris*, 72(755–759), 1871.

[19] M Peyrard and Th Dauxois. Physics of solitons, 2006.

[20] Roger K Dodd, Hedley C Morris, JC Eilbeck, and JD Gibbon. Soliton and nonlinear wave equations. *London and New York, Academic Press, 1982, 640 p.*, 1982.

[21] Ramamurti Rajaraman. Solitons and instantons. 1982.

[22] Norman J Zabusky and Martin D Kruskal. Interaction of" solitons" in a collisionless plasma and the recurrence of initial states. *Physical review letters*, 15(6):240, 1965.

[23] Peter S Lomdahl. What is a soliton. *Los Alamos Science*, 10:27–31, 1984.

[24] T Maxworthy. Experiments on collisions between solitary waves. *Journal of Fluid Mechanics*, 76(1):177–186, 1976.

[25] TD Lee. Particle physics and introduction to field theory. *Contemp. Concepts Phys.*, 1:1–865, 1981.

[26] Philip G Drazin and Robin S Johnson. *Solitons: an introduction*, volume 2. Cambridge university press, 1989.

[27] Noel De Nevers and Ragnar Grahn. *Fluid mechanics for chemical engineers*. McGraw-Hill New York, 1991.

[28] Hamid Ait Abderrahmane. *Two cases of symmetry breaking of free surface flows*. PhD thesis, Concordia University, 2008.

[29] Harry Nyquist. Certain topics in telegraph transmission theory. *Transactions of the American Institute of Electrical Engineers*, 47(2):617–644, 1928.

7 appendix

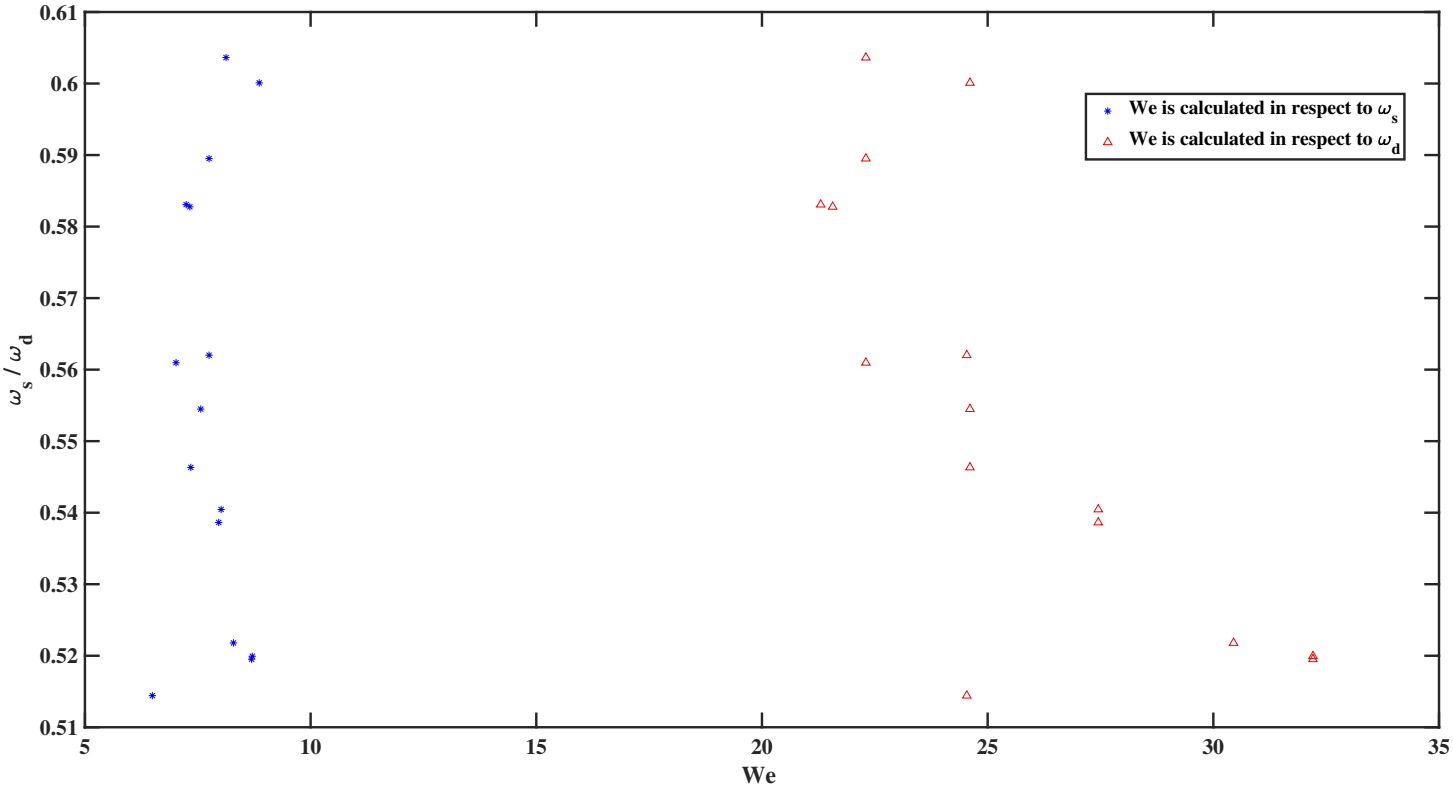

Figure 35: Raw plot for the superposition of ratio of Soliton frequency to disk's speed versus Weber number

```
close all;
clear;
clc;

tic;
%{
 n is the number of images processed for the desirable result
which depends
 on the experiment. In other words, each experiment has its own
n.
%}
n = 8432;

FONTS = 18;
FONTW = 'normal';
FONTA = 'normal';

%Preallocation
section==================================================

X = cell(n,1);
XX = cell (n,1);
fname = zeros(1,19);
fname1 = zeros(1,13);
angle0 = zeros(360,n);
angle1 = zeros(360,n);
st0 = zeros(360,n);
st1 = zeros(360,n);
x0 = zeros(1,n);
x1 = zeros(1,n);
y0 = zeros(1,n);
y1 = zeros(1,n);
Degrees = (1:360)';
maxamp = NaN(1,n);
maxamplpad = NaN(1,n);
Radius_max =225;
Radius_min =185 ;

%Plots and figures template=============-=====================
for ii= 1:n

    fname= sprintf('1and2solitons_%04d.tif',ii);
    im = imread(fname);
    im = im(70:570,70:580);                % Frame size

    h = fspecial('gaussian',21,5);         % Filtering
    bim = imfilter(im,h,'replicate');      % Filtering
```

```
bim = imbinarize(bim);
bim = ~bim;

figure(1);          % Sketching the raw and filtered images.

set(figure(1),'visible', 'on');
subplot(121),imshow(im),title('Original Image');
subplot(122),imshow(bim),title('Output of gaussian filter');
folder = 'Path';
FileName = sprintf('testImage%04d',ii);
fullFileName = fullfile(folder, FileName);
saveas(gcf,fullFileName,'fig');

B0 = boundaries(bim);  %Finding the boundaries of the image.
d = cellfun('length',B0);
[max_d,k] = max(d);
b0 = B0{k};
[M,N] = size(bim);     % M=length and N=width of the image.
a1 = ones(1,10)/10;    % 10 points averaging filter
b0 = filtfilt(a1,1,b0);

[st0(:,ii),angle0(:,ii),x0(ii),y0(ii)] = signature(b0);
% To draw the contour=======================================
    for j=1:max(size(b0))

        b0(j,1) = b0(j,1) - x0(ii);
        b0(j,2) = b0(j,2) - y0(ii);

    end
[st1(:,ii),angle1(:,ii),x1(ii),y1(ii)] = signature(b0);
contx=b0(:,1)-x1(ii);              %Contour x coordinate
conty=b0(:,2)-y1(ii);              %Contour y coordinate

figure(2);

plot(contx,conty,'LineWidth',3,'MarkerSize',8);
axis equal;

plot(contx,conty,'LineWidth',2,'MarkerSize',MyMarkerSize);
axis equal;
xlabel('Radius','Interpreter','latex',...
       'FontName','Times','FontSize',FONTS);
ylabel('Radius','Interpreter','latex',...
       'FontName','Times','FontSize',FONTS);
title('Contour');
set(gca,'FontName','Times','FontSize',FONTS,'LineWidth',2);
folder = 'Path';
```

```
    FileName = sprintf('Contour_image_no%04d',ii);
    fullFileName = fullfile(folder, FileName);
    saveas(gcf,fullFileName,'fig');

%=================================================================
end

% FFT application on time section================================
for k=1:360

        X{k} = st1(k,:);
        X{k} = X{k} - mean(X{k}); %get rid of the DC component

        Fs = 250;              % Camera frequency added manually
        L = length(X{k});

        T_inc = 1/Fs;          % Time increment for fft plot
        Tf = T_inc*n;                    % Final time
        time = 0:T_inc:Tf-T_inc;          % Time vector

        signal_FFT = fft(X{k},L)/L;      % Modified fft output
        amplitude = 2*abs(signal_FFT(1:ceil(L/2)));
        frequency = Fs/2*linspace(0,1,ceil(L/2));

        conv = 19;        %Raduis is in pixels;to convert...
                          %... it into cm (manually)
        figure(3);        % Plotting the power spectrum

        set(figure(3), 'Visible', 'on');
        plot (frequency,amplitude,'red')
        title ('Signal-Sided Amplitude Spectrum')
        xlabel('Frequency (Hz) ','Interpreter','latex',...
              'FontName','Times','FontSize',FONTS);
        ylabel('Magnitude of Signal','Interpreter','latex',...
              'FontName','Times','FontSize',FONTS);

set(gca,'FontName','Times','FontSize',FONTS,'LineWidth',2);
        xlim([0 20])

        folder = 'Path';
        figFileName = sprintf('FFT_for_deg_no_%03d',k);
        fullFileName = fullfile(folder, figFileName);
        saveas(gcf,fullFileName,'fig');

        figure(4);                    % Plotting the signal radius

        set(figure(4), 'Visible', 'on');
```

```
        plot(time(:),st1(k,:)/conv,'b');

        title('Simulated Signal of Radii');
        xlabel('Time (s)','Interpreter','latex',...
              'FontName','Times','FontSize',FONTS);
        ylabel('Radius (cm)','Interpreter','latex',...
              'FontName','Times','FontSize',FONTS);

set(gca,'FontName','Times','FontSize',FONTS,'LineWidth',2);
        set(gcf, 'Position', get(0, 'Screensize'));

        folder = 'Path';
        figFileName = sprintf('Radii at %03d Degrees',k);
        fullFileName = fullfile(folder, figFileName);

        saveas(gcf,fullFileName,'fig');

end
% Plotting the wave number via fft application==================
for kk=1:n

        XX{kk} = st1(:,kk);
        XX{kk} = XX{kk} - mean(XX{kk});  % remove the DC element

        FS = 1;                          % sampling fquency(degree)

        signal_FFTK = fft(XX{kk},360)/360; % Normalized fft
        amplitudeK = 2*abs(signal_FFTK(1:ceil(360/2)));
        frequencyK = FS/2*linspace(0,1,ceil(360/2));

        [max_amp,idx] = max(amplitudeK);

        figure(5);

        set(figure(5), 'Visible', 'on');
        plot (frequencyK*360,amplitudeK,'red')
                                  %1/deg->dimensionless number.

        title ('Signal-Sided Amplitude Spectrum')
        legend (sprintf('Wave no = %0.f ',frequencyK(idx)*360))
        xlabel('K ','Interpreter','latex',...
              'FontName','Times','FontSize',FONTS);
        ylabel('Magnitude of Signal','Interpreter','latex',...
              'FontName','Times','FontSize',FONTS);

set(gca,'FontName','Times','FontSize',FONTS,'LineWidth',2);
        xlim([0 20])
```

```
        folder = 'Path';
        figFileName = sprintf('FFT_on_image_no_%04d',kk);
        fullFileName = fullfile(folder, figFileName);
        saveas(gcf,fullFileName,'fig');

        figure(6);   % Plotting the graph signal for each image.

        set(figure(6), 'Visible', 'on');
        plot(Degrees(:),st1(:,kk)/conv,'b','LineWidth',2);
        title('Simulated Signal of Radii');
        xlabel('Degree','Interpreter','latex',...
              'FontName','Times','FontSize',FONTS);
        ylabel('Radius (cm)','Interpreter','latex',...
              'FontName','Times','FontSize',FONTS);

set(gca,'FontName','Times','FontSize',FONTS,'LineWidth',2);
        set(gcf, 'Position', get(0, 'Screensize'));

        folder = 'Path';
        figFileName = sprintf('Radius at each degree in image no
%04d',kk);
        fullFileName = fullfile(folder, figFileName);
        saveas(gcf,fullFileName,'fig');

end
%{
 To wind up the graph signal around a circle, in order to
correspond the solitons to the image and contour.
%}
A = zeros(1,360);
Xc = zeros(1,360);
Yc = zeros(1,360);

for index = 1:10:n

    A = st1(:,index);
    Xc = A.*cos((Degrees*(pi/180)));
    Yc = A.*sin((Degrees*(pi/180)));

    figure(7);            % Plotting the signal radius.

    set(figure(7), 'Visible', 'on');
    plot(Xc,Yc,'red','LineWidth',2);
    axis equal;

    title('Radii plot around the center');
    xlabel('Radius ','Interpreter','latex',...
```

```
        'FontName','Times','FontSize',FONTS);
    ylabel('Radius ','Interpreter','latex',...
        'FontName','Times','FontSize',FONTS);
    set(gca,'FontName','Times','FontSize',FONTS,'LineWidth',2);
    set(gcf, 'Position', get(0, 'Screensize'));

    folder = 'Path';
    figFileName = sprintf('Circular radii (img%04d',index);
    fullFileName = fullfile(folder, figFileName);
    saveas(gcf,fullFileName,'fig');

end

toc;
```

```
function [st, angle, x0, y0] = signature(b, varargin)
%SIGNATURE Computes the signature of a boundary.
%   [ST, ANGLE, X0, Y0] = SIGNATURE(B) computes the
signature of a
%   given boundary, B, where B is an np-by-2 array (np
> 2)
%   containing the (x, y) coordinates of the boundary
ordered in a
%   clockwise or counterclockwise direction. The
amplitude of the
%   signature as a function of increasing ANGLE is
output in
%   ST. (X0,Y0) are the coordinates of the centroid of
the
%   boundary. The maximum size of arrays ST and ANGLE
is 360-by-1,
%   indicating a maximum resolution of one degree. The
input must be
%   a one-pixel-thick boundary obtained, for example,
by using the
%   function boundaries. By definition, a boundary is a
closed
%   curve.
%
%   [ST, ANGLE, X0, Y0] = SIGNATURE(B) computes the
signature, using
%   the centroid as the origin of the signature vector.
%
%   [ST, ANGLE, X0, Y0] = SIGNATURE(B, X0, Y0) computes
the boundary
%   using the specified (X0, Y0) as the origin of the
signature
%   vector.

%   Copyright 2002-2004 R. C. Gonzalez, R. E. Woods, &
S. L. Eddins
%   Digital Image Processing Using MATLAB, Prentice-
Hall, 2004
%   $Revision: 1.6 $  $Date: 2003/11/21 14:46:47 $

% Check dimensions of b.
```

```
[np, nc] = size(b);
if (np < nc || nc ~= 2)
   error('B must be of size np-by-2.');
end

% Some boundary tracing programs, such as boundaries.m,
end where
% they started, resulting in a sequence in which the
coordinates
% of the first and last points are the same. If this is
the case,
% in b, eliminate the last point.
if isequal(b(1, :), b(np, :))
   b = b(1:np - 1, :);
   np = np - 1;
end

% Compute parameters.
if nargin == 1
   x0 = round(sum(b(:, 1))/np); % Coordinates of the
centroid.
   y0 = round(sum(b(:, 2))/np);
elseif nargin == 3
   x0 = varargin{1};
   y0 = varargin{2};
else
   error('Incorrect number of inputs.');
end

% Shift origin of coord system to (x0, y0)).
b(:, 1) = b(:, 1) - x0;
b(:, 2) = b(:, 2) - y0;

% Convert the coordinates to polar.  But first have to
convert the
% given image coordinates, (x, y), to the coordinate
system used by
% MATLAB for conversion between Cartesian and polar
cordinates.
% Designate these coordinates by (xc, yc). The two
coordinate systems
```

```
% are related as follows:  xc = y and yc = -x.
xc = b(:, 2);
yc = -b(:, 1);
[theta, rho] = cart2pol(xc, yc);

% Convert angles to degrees.
theta = theta.*(180/pi);

% Convert to all nonnegative angles.
j = theta == 0; % Store the indices of theta = 0 for
use below.
theta = theta.*(0.5*abs(1 + sign(theta)))...
        - 0.5*(-1 + sign(theta)).*(360 + theta);
theta(j) = 0; % To preserve the 0 values.

temp = theta;
% Order temp so that sequence starts with the smallest
angle.
% This will be used below in a check for monotonicity.
I = find(temp == min(temp));

% Scroll up so that sequence starts with the smallest
angle.
% Use I(1) in case the min is not unique (in this case
the
% sequence will not be monotonic anyway).
temp = circshift(temp, [-(I(1) - 1), 0]);

% Check for monotonicity, and issue a warning if
sequence
% is not monotonic. First determine if sequence is
% cw or ccw.
k1 = abs(temp(1) - temp(2));
k2 = abs(temp(1) - temp(3));
if k2 > k1
   sense = 1; % ccw
elseif k2 < k1
   sense = -1; % cw
else
   warning(['The first 3 points in B do not form a
monotonic ' ...
```

```
            'sequence.']);
end
% Check the rest of the sequence for monotonicity.
Because
% the angles are rounded to the nearest integer later
in the
% program, only differences greater than 0.5 degrees
are
% considered in the test for monotonicity in the rest
of
% the sequence.
flag = 0;
for k = 3:length(temp) - 1
   diff = sense*(temp(k + 1) - temp(k));
   if diff < -.5
      flag = 1;
   end
end
if flag
   warning('Angles do not form a monotonic sequence.');
end

% Round theta to 1 degree increments.
theta = round(theta);

% Keep theta and rho together.
tr = [theta, rho];

% Delete duplicate angles.  The unique operation
% also sorts the input in ascending order.
[~, u, ~] = unique(tr(:, 1));
tr = tr(u,:); % u identifies the rows kept by unique.

% If the last angle equals 360 degrees plus the first
% angle, delete the last angle.
if tr(end, 1) == tr(1) + 360
   tr = tr(1:end - 1, :);
end

% Output the angle values.
angle = tr(:, 1);
```

```
% The signature is the set of values of rho
corresponding
% to the angle values.
st = tr(:, 2);
%=========================================================

 function B = boundaries(BW, conn, dir)
%BOUNDARIES Trace object boundaries.
%   B = BOUNDARIES(BW) traces the exterior boundaries
of objects in
%   the binary image BW.  B is a P-by-1 cell array,
where P is the
%   number of objects in the image. Each cell contains
a Q-by-2
%   matrix, each row of which contains the row and
column coordinates
%   of a boundary pixel.  Q is the number of boundary
pixels for the
%   corresponding object.  Object boundaries are traced
in the
%   clockwise direction.
%
%   B = BOUNDARIES(BW, CONN) specifies the connectivity
to use when
%   tracing boundaries.  CONN may be either 8 or 4.
The default
%   value for CONN is 8.
%
%   B = BOUNDARIES(BW, CONN, DIR) specifies the
direction used for
%   tracing boundaries.  DIR should be either 'cw'
(trace boundaries
%   clockwise) or 'ccw' (trace boundaries
counterclockwise).  If DIR
%   is omitted BOUNDARIES traces in the clockwise
direction.

%   Copyright 2002-2004 R. C. Gonzalez, R. E. Woods, &
S. L. Eddins
```

```
%   Digital Image Processing Using MATLAB, Prentice-
Hall, 2004
%   $Revision: 1.6 $  $Date: 2003/11/21 14:22:07 $

if nargin < 3
   dir = 'cw';
end

if nargin < 2
   conn = 8;
end

L = bwlabel(BW, conn);

% The number of objects is the maximum value of L.
Initialize the
% cell array B so that each cell initially contains a
0-by-2 matrix.
numObjects = max(L(:));
if numObjects > 0
   B = {zeros(0, 2)};
   B = repmat(B, numObjects, 1);
else
   B = {};
end

% Pad label matrix with zeros.  This lets us write the
% boundary-following loop without worrying about going
off the edge
% of the image.
Lp = padarray(L, [1 1], 0, 'both');

% Compute the linear indexing offsets to take us from a
pixel to its
% neighbors.
M = size(Lp, 1);
if conn == 8
   % Order is N NE E SE S SW W NW.
   offsets = [-1, M - 1, M, M + 1, 1, -M + 1, -M, -M-
1];
else
```

```
    % Order is N E S W.
    offsets = [-1, M, 1, -M];
end

% next_search_direction_lut is a lookup table.  Given
the direction
% from pixel k to pixel k+1, what is the direction to
start with when
% examining the neighborhood of pixel k+1?
if conn == 8
    next_search_direction_lut = [8 8 2 2 4 4 6 6];
else
    next_search_direction_lut = [4 1 2 3];
end

% next_direction_lut is a lookup table.  Given that we
just looked at
% neighbor in a given direction, which neighbor do we
look at next?
if conn == 8
    next_direction_lut = [2 3 4 5 6 7 8 1];
else
    next_direction_lut = [2 3 4 1];
end

% Values used for marking the starting and boundary
pixels.
START    = -1;
BOUNDARY = -2;

% Initialize scratch space in which to record the
boundary pixels as
% well as follow the boundary.
scratch = zeros(100, 1);

% Find candidate starting locations for boundaries.
[rr, cc] = find((Lp(2:end-1, :) > 0) & (Lp(1:end-2, :)
== 0));
rr = rr + 1;

for k = 1:length(rr)
```

```
   r = rr(k);
   c = cc(k);
   if (Lp(r,c) > 0) && (Lp(r - 1, c) == 0) &&
isempty(B{Lp(r, c)})

      % We've found the start of the next boundary.
Compute its
      % linear offset, record which boundary it is,
mark it, and
      % initialize the counter for the number of
boundary pixels.
      idx = (c-1)*size(Lp, 1) + r;
      which = Lp(idx);

      scratch(1) = idx;
      Lp(idx) = START;
      numPixels = 1;
      currentPixel = idx;
      initial_departure_direction = [];

      done = 0;
      next_search_direction = 2;
      while ~done
         % Find the next boundary pixel.
         direction = next_search_direction;
         found_next_pixel = 0;
         for k = 1:length(offsets)
            neighbor = currentPixel +
offsets(direction);
            if Lp(neighbor) ~= 0
               % Found the next boundary pixel.

               if (Lp(currentPixel) == START) && ...

isempty(initial_departure_direction)
                  % We are making the initial departure
from
                  % the starting pixel.
                  initial_departure_direction =
direction;
```

```
            elseif (Lp(currentPixel) == START) &&
           (initial_departure_direction == direction)
                % We are about to retrace our path.
                % That means we're done.
                done = 1;
                found_next_pixel = 1;
                break;
            end

            % Take the next step along the boundary.
            next_search_direction = ...

next_search_direction_lut(direction);
            found_next_pixel = 1;
            numPixels = numPixels + 1;
            if numPixels > size(scratch, 1)
               % Double the scratch space.
               scratch(2*size(scratch, 1)) = 0;
            end
            scratch(numPixels) = neighbor;

            if Lp(neighbor) ~= START
               Lp(neighbor) = BOUNDARY;
            end

            currentPixel = neighbor;
            break;
         end

         direction = next_direction_lut(direction);
      end

      if ~found_next_pixel
         % If there is no next neighbor, the object
must just
         % have a single pixel.
         numPixels = 2;
         scratch(2) = scratch(1);
         done = 1;
      end
   end
```

```
      % Convert linear indices to row-column
coordinates and save
      % in the output cell array.
      [row, col] = ind2sub(size(Lp),
scratch(1:numPixels));
      B{which} = [row - 1, col - 1];
   end
end

if strcmp(dir, 'ccw')
   for k = 1:length(B)
      B{k} = B{k}(end:-1:1, :);
   end
end
```